

INFORMATION TO USERS

This manuscript has been reproduced from the microfilm master. UMI films the text directly from the original or copy submitted. Thus, some thesis and dissertation copies are in typewriter face, while others may be from any type of computer printer.

The quality of this reproduction is dependent upon the quality of the copy submitted. Broken or indistinct print, colored or poor quality illustrations and photographs, print bleedthrough, substandard margins, and improper alignment can adversely affect reproduction.

In the unlikely event that the author did not send UMI a complete manuscript and there are missing pages, these will be noted. Also, if unauthorized copyright material had to be removed, a note will indicate the deletion.

Oversize materials (e.g., maps, drawings, charts) are reproduced by sectioning the original, beginning at the upper left-hand corner and continuing from left to right in equal sections with small overlaps.

Photographs included in the original manuscript have been reproduced xerographically in this copy. Higher quality 6" x 9" black and white photographic prints are available for any photographs or illustrations appearing in this copy for an additional charge. Contact UMI directly to order.

**Bell & Howell Information and Learning
300 North Zeeb Road, Ann Arbor, MI 48106-1346 USA
800-521-0600**

UMI[®]

HAPTIC DISPLAY
FOR
TELE-ROBOTICS AND VIRTUAL REALITY

Scott L. Springer

A dissertation submitted in partial fulfillment of the requirements for the degree of

Doctor of Philosophy

(Mechanical Engineering)

at the

UNIVERSITY OF WISCONSIN-MADISON

2000

UMI Number: 9972914

**Copyright 2000 by
Springer, Scott Lawrence**

All rights reserved.

UMI[®]

UMI Microform 9972914

Copyright 2000 by Bell & Howell Information and Learning Company.

**All rights reserved. This microform edition is protected against
unauthorized copying under Title 17, United States Code.**

**Bell & Howell Information and Learning Company
300 North Zeeb Road
P.O. Box 1346
Ann Arbor, MI 48106-1346**

**© Copyright by Scott L. Springer 2000
All Rights Reserved**

A dissertation entitled

**HAPTIC DISPLAY
FOR
TELE-ROBOTICS AND VIRTUAL REALITY**


Submitted to the Graduate School of the
University of Wisconsin-Madison
in partial fulfillment of the requirements for the
degree of Doctor of Philosophy


by
Scott L. Springer


Date of Final Oral Examination: February 18, 2000

Month and Year Degree to be awarded: **MAY 2000**

.....
Approval Signatures of Dissertation Readers:







Signature, Dean of Graduate School



Table of Contents

Preface: Terminology and Organization of this Document	iii
List of Symbols	xi
Thesis Statement	xvi
Abstract	xvii
Chapter 1	
Introduction and Overview of Present State of the Art in Haptic Display	
1.1 Introduction	1
1.2 Performance Measures	11
1.3 Interface Applications	19
1.4 Conclusions of Haptic Display State of the Art	23
Chapter 2	
Analysis of Dynamics of Contact with Rigid Bodies in Tele-operation	
2.1 Introduction	26
2.2 Human Contact with Real Rigid Surface	31
2.3 Contact Simulation of Traditional Haptic Displays	36
2.4 Contact Simulation of Proposed Haptic Display	40
2.5 Generalization to Multi-Degree of Freedom Systems	43
2.6 Simulation of Results	46
2.7 Conclusions and System Requirements for Rigid Surface Display	52
Chapter 3	
Description of Proposed System for Haptic Display	
3.1 Introduction	54
3.2 Mechanical Systems	55
3.3 Electrical Systems	63
3.4 Control Software	66
3.5 Slave Simulation Test Bed for Virtual Finger	73
3.6 Conclusions of Proposed System Description	75

Chapter 4**Human Performance Experiments**

4.1 Introduction	78
4.2 Experimental Procedures	80
4.3 Experimental Results	86
4.3.1 Perceptual Comparison to Real Surfaces	86
4.3.2 Haptic Perceptual Accuracy in Location of Surface Boundaries	89
4.3.3 Stability and Oscillation Amplitudes	95
4.3.4 Effects of Pre-Contact Velocity on Perceptual Accuracy	98
4.3.5 Statistical Analysis of Accuracy Experiments	100
4.3.6 Statistical Analysis of Amplitude Experiments	109
4.4 Conclusions of Experimental Investigation	114

Chapter 5**Contributions, Extensions, and Conclusions**

5.1 Introduction	116
5.2 Applications and Extensions of the Research	120
5.2.1 Reducing Computation Load for VR Applications	121
5.2.2 Application of DECAFF to General Haptic Interface Design	127
5.3 Contributions of the Research	137
5.4 Conclusions	139
References	142

Preface:

Terminology and Organization of this Document

This document presents the methodologies and results of an extensive research program into the design of haptic interfaces for application in virtual reality computer interfaces and tele-operation robotic control. The area of haptic interface research is very much a cross disciplinary field. Research includes disciplines such as Control Theory, Robotics, Computer Science, Mechanical Engineering, Electrical Engineering, and Psychology. Because of the wide range of topics in this area, a common language for haptics research is emerging utilizing terms historically associated with these fields, with many terms following those commonly used in control theory. While every attempt to utilize terminology consistent with that emerging within the haptics field has been used in the preparation of this document, for clarity some of the key phrases and words used in this document are clearly defined in this section. The main topic of this research is force reflecting haptic interfaces, devices that typically perform two functions; to measure the human operator's motion (usually by position at discrete time intervals), and to display a resistance to motion or force to the operator. The measured human positions of the haptic interface, often called the master are generally used to control the positions of a remote device commonly called the slave. The slave may be a physical robotic device, such as a portion of a robotic manipulator system, or may be a computer

pointer used for interaction with a computer program. Some common computer pointers include a cross hair (typically in CAD systems), an arrow (typically in MS-Windows applications), and a rendering of a human hand (often utilized in virtual reality simulation programs). In virtual reality applications the computer pointer is frequently referred to as a virtual slave. To implement the second primary function of force display, forces of contact between the slave pointer or device are either calculated (for computer pointers) or measured (for robotic devices) within the slave environment and used as an input signal to the haptic interface. The haptic interface then acts upon the input force signal to present a proportional resistance to motion (or force) to the human operator. Hence the term force reflection is often used for haptic interfaces that display a force to the operator. Often the term force feedback is used in place of force reflection. The traditional design approach used for force reflecting haptic interfaces employs one or more actuators that are, by design, in continuous direct physical contact (or mechanically coupled) with the person at all times of operation with the device. In this document actuators are defined as devices that convert an electric signal representing the force of the slave contact into a display force. Thus when using a traditional design haptic interface, the operator will drive the actuator (which is not provided with an input signal) for any motion wherein the slave is not in contact with an entity within the slave environment. This is often called “back driving” the actuator during free or unobstructed motion. In order to determine the magnitude of the force signal that should be delivered to the operator via the haptic interface when the slave is a virtual slave, computer surfaces are traditionally defined

by spring constants and damping coefficients. Then the force to be delivered is calculated as the sum of an elastic term and a damping term. The elastic term is the product of the spring constant and the interference distance between the virtual slave pointer and a computer surface (also called a penetration distance). The damping term is calculated as the product of the damping coefficient and the velocity of the virtual slave pointer. Because the motion is sampled at the master and displayed in the computer via discrete time positions, there exists a time lag between the operator's (master) position and the slave position. Further there exists a second time lag between the time at which an electric signal is sent to the actuator and the time at which the actuator delivers the prescribed force. A result of these time lags is that when interacting with rigid surfaces that are defined by a high spring constant and a high damping coefficient, oscillatory motion at the haptic interface can result. This oscillatory motion is often called instability.

In this report a new approach to the design and control methods for force reflecting haptic interfaces is presented. The new design calls for actuators that are not in continuous physical contact with the operator while the interface is in use, but rather the design calls for actuators that can selectively assume a contacting or a non-contacting condition. In this document the use of an actuator in this manner is referred to as a de-coupled actuator, or de-coupled actuation. Thus the proposed method for design of haptic interfaces utilizes actuators that are not in direct physical contact (or mechanically coupled) with the person at all times of operation with the device. In order to control the actuator that is de-coupled from the operator, information

regarding the relative positions between the slave pointer or manipulator and entities within the slave environment is used. The distance information is used to calculate an appropriate position for the actuator in the event that the pointer should move toward a nearby slave object in the future. The use of this anticipatory information regarding relative positions of the pointer and slave entities (also called pre-contact distance) to control the actuator position is called feed forward control in this document. This terminology is used because information about a future event is used for control purposes. The proposed approach for design and control of haptic interfaces also employs control of the *position* of the actuator during simulated contact with a slave entity that results in a maximum actuator force command upon contact. Such a slave entity is called a rigid surface or a non-deformable body as the haptic interface is commanded to deliver the maximum force upon simulated contact with this entity. Slave entities that do not result in a maximum force command under the contact conditions are called deformable entities, or non-rigid bodies. In the proposed approach, upon contact with a deformable entity a variable resistance to motion (or force) is delivered to the operator, proportional to the force command of the slave pointer or manipulator. The new approach for design and control of force reflecting haptic interfaces is called DECAFF, as an acronym for DE-Coupled Actuator and Feed-Forward control, emphasizing the features present in the proposed approach and lacking in traditional design and control of haptic interfaces.

Following this preface, a list of symbols is provided. The symbols used and their common meanings are listed by chapter in their order of appearance. The symbols

were chosen as those commonly used in the literature to describe the represented quantity. For equations taken from referenced articles or texts, the original notation is used where practical, permitting easy cross-reference between this dissertation and the cited article. The deficit of this approach is that the same symbol may be used in different chapters to represent different quantities (e.g. β in chapters 3 and 5 represents an angular position, and β in chapter 4 is the common symbol for probability of a Type II error in hypothesis testing). To alleviate any confusion with the nomenclature, in addition to the sequential list of symbols, each symbol is defined in the text when it is introduced in an equation.

An overview of the organization of this document is outlined in the following section. In Chapter I an introduction to the field is presented that includes background information on the various modalities of haptic senses that interfaces have been designed for, and the degree of performance offered by prior works is reviewed. In this chapter it is determined that the haptics field could benefit from the introduction of a multi-finger interface capable of full finger motion range measurement and force display. It is also determined that for many robotic and virtual reality simulations it is most beneficial and practical for forces to be displayed in a direction that is substantially normal to the distal finger phalange. Several metrics for haptic interface performance are discussed, and opportunities for improvement, given the present state of the art are identified. Of these opportunities for improvement, one key issue applicable to all haptic interface configurations is identified. This key issue is the ability to overcome instabilities in haptic interfaces due to computation and actuator

response time lags, and due to interference (penetration) between virtual surfaces and virtual pointers required for prior haptic interface design and control paradigms.

In Chapter 2 the physics involved during initial contact between a haptic interface controlled slave pointer and a slave object are analyzed for three cases of interest. The first case involves mathematical modeling of real contact between a human and a real object. In the second case, the dynamics of initial contact are modeled for the simulation of contact as occurs when a human operator of a traditionally designed haptic interface interacts with a slave object. The third case of analysis involves simulation of initial contact as it would occur if a new haptic interface design and control approach were implemented wherein the force providing actuator is selectively de-coupled from the operator. From the analysis, simulations are developed in order to predict the stability and positional accuracy conditions of contact for the first two cases. This is done with the implication that the third case will closely resemble that of the first case, or the proposed new design method will provide a human perception very similar to that of real world contact between the operator and actual physical objects.

In Chapter 3 a detailed design description of one physical embodiment of the general DECAFF design and control method developed in Chapter 2 is presented. The detailed design not only implements the method for improved representation of initial contact in tele-presence systems, but includes additional performance enhancing features when compared to prior designs in finger bend haptic interfaces for grasp task simulation and control. In this chapter the design of a four bar serial chain is

introduced that when worn on the operator's hand forms a six bar closed loop kinematic chain. This mechanical configuration and is capable of both representation of the finger position as a single variable and presentation of forces substantially normal to the finger distal phalange, while permitting both position measurement apparatus and force display apparatus to be located remote from the operator. Also presented here is the design of electrical systems and a detailed discussion of the control algorithm used to take advantage of the de-coupled actuator included in the DECAFF design method. This control algorithm is used to provide human perceptual improvements while performing tele-operation within the realm of human hand grasping tasks. The algorithms associated with a virtual reality test bed program are also presented, resulting in specification of a complete haptic display system design. A prototype of the design given in Chapter 3 is used for human perceptual experiments that are discussed in Chapter 4. The experiments are designed to verify the predictions derived in Chapter 2. The experimentation performed utilizes side by side comparisons of the proposed new DECAFF design and control methods with traditional design and control methods. In the experiments, subjects found that in a virtual simulation the new system provided a haptic sensation more like one they expect in a real fingertip surface contact. The improvements in haptic sensation and performance are measured by three separate experimental responses, each in a factorial experimental design. The three responses measured are: (i) subjects' perception of which control method feels more like a real surface in a forced choice response, (ii) the amplitude of oscillations developed during contact with a virtual

slave surface, and (iii) the accuracy at which the subjects perceive the initial contact position with slave surfaces during tele-operation. The results of these experiments are analyzed by statistical methods to provide a scientific basis for performance expectations with implementations of the proposed DECAFF system. The results indicated an improvement in all response areas measured. For numerical response measurements of oscillation amplitudes and accuracy of perception, the new control method demonstrated an improvement significant beyond a 99.9% confidence interval. In Chapter 5 extensions of the work performed to date are discussed in terms of further detailed implementations and applications of the results to other classes of haptic interface designs. Some fundamental and specific application contributions to the field of haptics research derived from the research program are delineated. Conclusions of the research and investigation are also summarized in this chapter.

List of Symbols

Chapter 1

F_k force driving a haptic interface

K simulation wall stiffness

x_k haptic interface position

x_{wall} simulation wall position

B simulation damping coefficient

x_k' haptic interface velocity

$t_0, t_1, \text{ etc}$ time step 0, time step 1, etc.

V finger velocity

x finger position

$x_0, x_1, \text{ etc.}$ finger position at time 0, position at time 1, etc.

F force delivered by haptic interface

Chapter 2

m mass

x'' acceleration

f_h hand force

b_e equivalent damping coefficient

x' velocity

k_e equivalent spring constant

x position

f_k active component of hand force

k_p potential energy constant

k_v damping constant

T sample period

x_{k-1} position at previous time step

k_{pulse} braking pulse constant

b haptic interface internal damping

K maximum achievable simulation stiffness

B maximum achievable simulation damping
F(t) time dependent force
 m_f finger mass coefficient
 b_f finger damping coefficient
 k_f finger spring constant
 x_f'' finger acceleration
 x_f' finger velocity
 x_f finger position
 $t_1, t_2, \text{ etc.}$ time step 1, time step 2, etc.
E energy
 U_{12} work done between time step 1 and time step 2
 x_{f+s}'' acceleration variable lumped for finger and simulation
 x_{f+s}' velocity variable lumped for finger and simulation
 x_{f+s} position variable lumped for finger and simulation
 b_{eq} equivalent damping coefficient for lumped model
 k_{eq} equivalent spring constant for lumped model
 b_s simulation damping coefficient
 k_s simulation spring constant
 x_s'' simulation acceleration
 x_s' simulation velocity
 x_s simulation position
 $q''(t)$ spatial acceleration
 $q'(t)$ spatial velocity
 $q(t)$ spatial position
I(t) impulse
B(t) damping
K(t) potential
F force vector
M mass matrix
q position vector
q' velocity vector

\mathbf{q}'' acceleration vector
 $\mathbf{B}(\mathbf{q}, \mathbf{q}')$ damping force vector
 $\mathbf{P}(\mathbf{q})$ potential force vector

Chapter 3

T torque
 F_i force of i^{th} finger
 β_i finger bend angle of i^{th} finger
read_volt voltage reading of finger bend potentiometer
pos_low lowest voltage reading of finger bend potentiometer
pos_high highest voltage reading of finger bend potentiometer
 α_i pre-contact distance for i^{th} finger (angular)
 γ_i contact drum position for i^{th} finger (angular)
 α^* constant offset distance for pre-contact condition (angular)
 γ_i^* proximity contact drum position (angular)
a, b, c, d, e linear distances
 α_{max} maximum pre-contact distance (angular)
K spring constant
B damping constant
 Φ proportion of motor torque

Chapter 4

F force
K spring constant
B damping constant
S communication rate
 K^+ , k^+ high level for spring constant
 K^- , k^- low level for spring constant
 B^+ , b^+ high level for damping constant
 B^- , b^- low level for damping constant
 S^+ , s^+ high level for communication rate

S -, s - low level for communication rate
 σ_m mean standard deviation
 N number of higher order effects to be neglected
 n number of experimental tests conducted
 y_i response data of experiment
 y_m mean of response data of experiment
 $E(i)$ effect estimate attributable to variable i
 x_j experiment variable
 s.e. standard error of experiment
 μ_{Ei} true mean effect
 $r_{.j}$ low value of variable j
 $r_{.j}$ high value of variable j
 α probability of erroneously rejecting the null hypothesis
 β probability of failing to reject the null hypothesis when it is false
 δ difference between the true mean hypothesis mean to be considered of interest
 σ population standard deviation
 s_p pooled sample standard deviation
 s_p^2 pooled sample variance
 Z percentage point of the standard normal distribution
 Φ cumulative distribution function of the standard normal distribution
 s sample standard deviation
 s^2 sample standard variance

Chapter 5

F force

K, k spring constant

B damping constant

x position

x' velocity

x'' acceleration

α^* constant angular distance of pre-contact condition

γ angular position variable of actuator
 β angular position variable of pointer
 α_{\max} maximum angular distance of pre-contact condition (constant)
 γ^* fixed contact drum position (angular)
 β' pointer velocity
 δ maximum contact drum positional error (angular)
 T sample period
 G_x motor drive position (linear)
 B_x pointer position (linear)
 d_{xA}, d_{xB} linear pre-contact distance
 d linear distance
 D_x linear distance
 α_A, α_B angular pre-contact distance
 δ angular distance constant
 θ angular distance constant
 β angular position variable of pointer
 x, y, z position in three dimensional cartesian coordinate system
 dx, dy, dz change in position in three dimensional cartesian coordinate system
 r_1, r_2 link lengths
 ϵ allowable position error

Thesis Statement

Human haptic perception in tele-operation with force reflecting haptic interfaces can be improved when the haptic interface employs means for selective physical contact between the operator and an actuation device. The actuation device being controlled to assume: a position dictated by anticipated contact information prior to simulation initial contact, a contact position during simulation of contact with rigid surfaces, and otherwise controlled to provide a variable resistance to motion during simulation of contact with deformable, non-rigid surfaces.

**HAPTIC DISPLAY FOR
TELE-ROBOTICS AND VIRTUAL REALITY**

Scott L. Springer

Under the supervision of Assistant Professor Nicola J. Ferrier

At the University of Wisconsin-Madison

Abstract

Haptic display is an emerging technology wherein a person's sensation of touch is used to interface with machines. This research is directed toward the development of force reflecting haptic display systems suitable for use in virtual reality environments and robotic tele-operation. One promising application of haptic display systems is human-computer interaction wherein the operator's body positions are measured and used to control corresponding computer pointer positions and force of contact between the computer pointer and other computer objects are reflected back to the human operator. A detailed literature review classifies prior research in the development of haptic displays by modality within the haptics realm. Performance measures of haptic displays are discussed. A new design for a haptic display representing grasping tasks is introduced, analyzed, constructed and tested for performance. The proposed design is portable and provides a single degree of freedom per finger, fingertip force modality that demonstrates potential for increased performance in several areas. Traditional design of haptic interfaces calls for force providing actuators that are mechanically

coupled to the operator during use and often produce instability when modeling interaction with rigid objects. The rigid body simulation problem is addressed by implementation of an actuator that is not mechanically coupled to the person, the actuator being initially position controlled by *a priori* determination of distance to contact. The proposed approach for design of haptic display devices is called DECAFF as an acronym for DE-Coupled Actuator and Feed Forward control. After initial contact, variable force control is provided. Although developed for fingertip force display, the general DECAFF design and control method can be applied to any force reflecting haptic interface configuration. In this report dynamic mathematical models of the virtual wall problem are presented, through which the present approach is shown to provide superior performance to previous haptic displays. The effectiveness of the proposed DECAFF approach is verified through experimental human perception studies wherein performance comparisons are made between the proposed approach and a traditional haptic interface design paradigm.

Chapter 1

Introduction and Overview of Present State of the Art in Haptic Display

1.1 Introduction

Haptic display or haptic feedback refers to a method of human-machine interaction that provides the user with a sense of touch. According to Howe and Lederman (1996):

“Research has shown that touch information is essential both for perception and for motor control in everyday tasks. More recently it has been demonstrated that touch can be equally important for controlling remote manipulators teleoperationally and for interacting with computer models in virtual environments.”

In the literature, haptic display is often defined as display of a sense of touch to include two categories of force display and tactile display. Tactile display generally refers to touch sensations applied to the skin, at a smaller more localized level than those of force display. Tactile information is sensed by high bandwidth receptors (50-350 Hz) placed close to the skin. The highest density of these receptors are found in the human hand, and they are associated with the perception of initial contact with the environment, local surface geometry, temperature and slipping. Force display differs from tactile display in that force display restricts operator motion while tactile display

does not (Burdea, 1996). Forces are sensed by lower bandwidth receptors typically located on bone/muscle attachments and joints. Two main application domains for haptic display include tele-operation and virtual reality (FIG. 1.1).

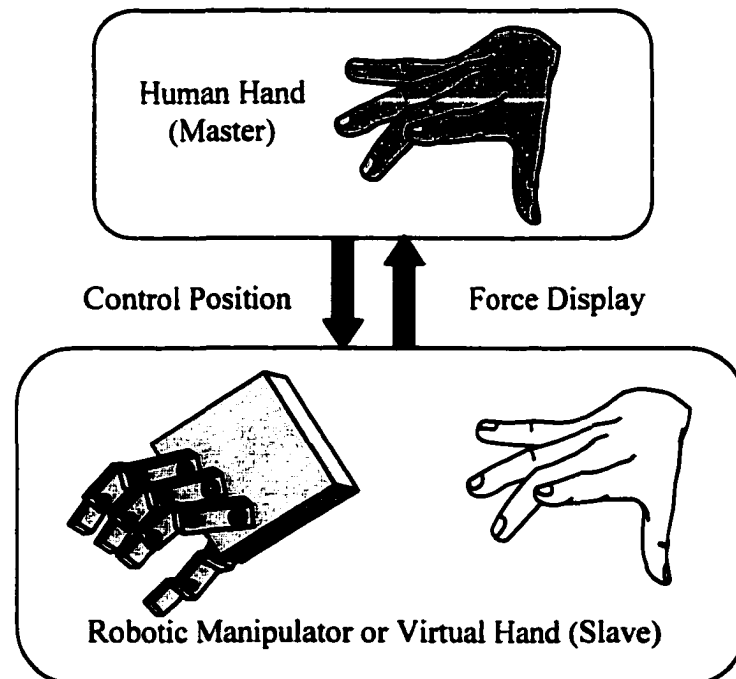


Figure 1.1 - Haptic Interface Application Domains

In tele-operation, a slave robotic manipulator is controlled by a remotely located master robotic device. A common use is to have the slave motions imitated by the master device, wherein the slave is placed in some hazardous location while the operator remains in a more protected environment. The forces of contact experienced by the slave manipulator are often displayed to the human operator through the master haptic interface. Because of this, the process is often referred to in the literature as “force feedback” or “force reflection”. Classic examples include space missions,

under water operations, and toxic environments. The value of haptic display in tele-operation is that for very dexterous tasks, human operators can use their highly developed natural motor control skills to very precisely control the slave manipulator, if the human operators are provided with the sensory (force and tactile) information relevant to the task.

In the virtual reality (VR) domain, the slave hand is a computer generated image, similar to a solid model of the hand as would be seen in a solid modeling computer aided design (CAD) software package. VR is generally characterized as a three-dimensional, interactive, computer-generated, multi-sensory synthetic environment. VR is used for simulation of physical events, training, and mechanical design. A VR system for mechanical design and creation of a CAD model is under development at the ICARVE Lab., at the University of Wisconsin Madison (Dani and Gadh, 1997, Chu, et. al., 1997). The large screen display is viewed while wearing stereographic shutter glasses and produces a large semi-immersive three-dimensional graphic display. Hand position and orientation information is determined through Flock of Birds magnetic tracking device (Ascension 1998). Presently finger bend information is provided by a position sensing glove, 5th Glove (Fifth Dimension, 1998). A detailed discussion of the state of the art in VR and haptic display hardware is given by Springer and Gadh (1996). A conclusion from that research was that haptic display devices would be beneficial in VR applications such as CAD, but the current technology is lacking in available devices. When a representation of the operator's hand is utilized in VR environments, controlled so as to follow the operator's real

hand, haptic display to present contact forces of the simulation to the operator can increase the sense of immersion in the virtual world. Many advantages and applications of haptic display for mechanical design in a VR domain are cited by Springer and Gadh (1997).

1.2 Background

The approaches to haptic feedback that have been proposed to date, can be categorized by the modalities of feedback they provide. In Figure 1.2 the modalities are first subdivided by provision of feedback lumped to a hand vs. provision of feedback to individual fingers. This distinction is made as feedback lumped to the hand provides no means for natural grasp of an object, a very desirable and often necessary feature for tele-operation and VR applications. In contrast, feedback to local finger tips can support grasping applications. Those modalities previously explored for provision of output to the individual fingers are further subdivided by functional modality of tactile vs. force feedback.

Pen based devices have been developed by Massie and Salisbury (1994), Iwata (1993), and Buttolo and Hannaford (1995). Arm exoskeleton devices have been proposed by Ephanov and Hurmuzlu (1996), which generally consist of structure for controlling resistance to shoulder, elbow, and wrist motion. Haptic displays that employ a handle grip operator interface have been reported by Millman, et. al. (1993) and Brooks, et. al. (1990). Many joystick devices have been developed (Berkelman et. al., 1996), (Salcudean and Vlaar, 1994), (Adlestein et. al., 1996). One example of a mouse device for haptic feedback is given by Kelley and Salcudean (1994).

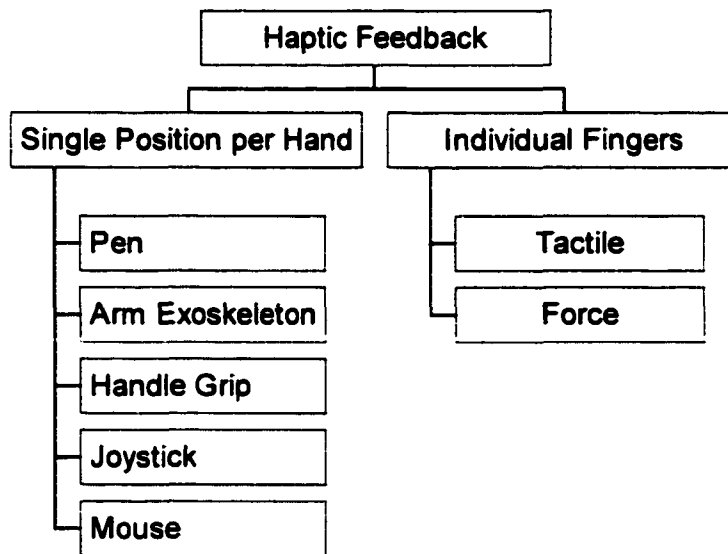


Figure 1.2 – General Approaches to Haptic Display

A partial listing of the many approaches to tactile feedback for individual fingers is given in the first column of FIG. 1.3. A detailed literature review of technologies employed is given by Shimoga (1993b). The pressure approach generally utilizes an air bladder that presses against the skin when inflated (Stone, 1991). Pin arrays can be employed to represent sharp corners and edges, or to provide high frequency vibrations simulating surface textures (Kontarinis and Howe, 1993). Air jets have been proposed as another modality to provide touch sensation. Vibration applied to areas of the hands has been implemented in the form of voice coils (Shimoga, 1993b) and electro-mechanical actuators (CyberTouch, 1996). Thermal conductivity has also been considered as a mode of interaction with virtual objects. Electrotactile stimulation has also been explored, but is currently not widely accepted in VR and tele-operation areas. Presentation of slip has been investigated by Chen and Marcus (1994), in the form of a small rotating cylinder mounted to the fingertip.

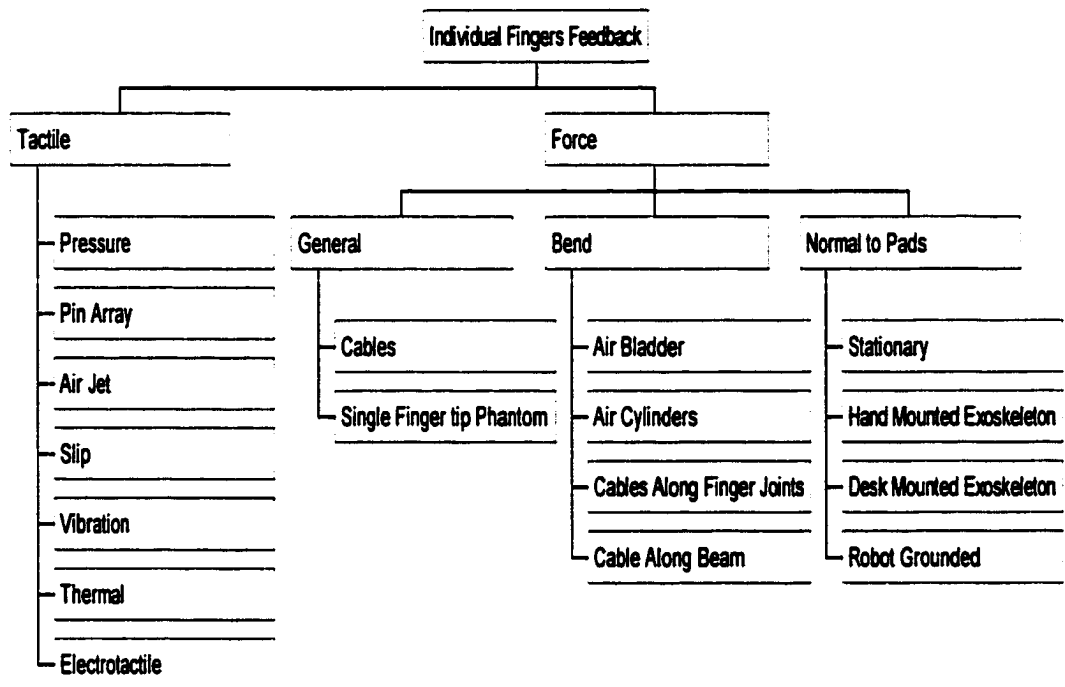


Figure 1.3 - Individual Finger Haptic Feedback

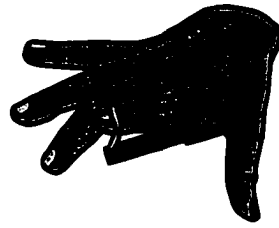
The present research addresses the area of force display to individual fingers. It is believed that providing the human operator with a sensation of the forces exerted by the slave fingers would positively enhance the operator's abilities (Shimoga, 1993a). It will be shown later that one aspect of tactile display is also addressed by the present research because real time initial contact with an object sensed by high bandwidth (tactile) receptors is provided. Application of force to the fingertips can be divided into three approaches, (i) general direction force between fingertip and earth, (ii) finger bend as a single DOF, and (iii) forces to multiple finger pads on each finger. The present research addresses area (ii) of representing the force resisting finger bend as a single degree of freedom, the force being applied to the distal finger pad.

Two approaches have been explored for provision of a general direction force to the user's finger tips. The first approach employs several cables that can generate a force vector to the user's fingertip (Ishii and Sato, 1994). The benefit of this approach is that each finger may have a general direction vector and the force is applied without reaction "ghost" forces applied to the operator. The Phantom device, by Massie and Salisbury (1994), is also capable of application of a force of general direction to the fingertip. The deficit of these two methods is that the workspace is somewhat limited, and that complexity and cost rise quickly if we attempt to provide feedback for numerous fingers and represent general grasping operations.

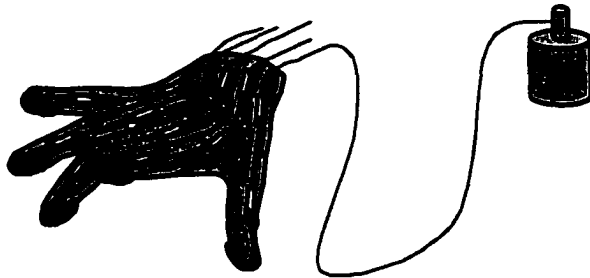
Another force application mode is to restrict the bend or curl of the user's finger(s). An early approach first developed in the mid 1960's for tele-operation robotic control by Jones and Thousand (1966) is shown in figure 1.4(a). The early development employed an air bladder attached to a glove, such that the bladder pressure corresponded to the robotic gripper force, and resulted in resistance to finger bend. The glove included position measurement, and thus was remarkably similar in function to haptic display devices emerging in the 1990's. The main problem with this approach is that the bladder construction requires relatively thick material that interferes with natural hand closing. Another air powered approach was developed by Burdea (1996) and Gomez et. al. (1995) as shown in figure 1.4(b). This device called the Rutgers Master I (1992 version) and Rutgers Master II (1994-5 version) utilizes air cylinders mounted between palm, the thumb and three fingers. Burdea's approach is well suited for many grasping tasks. Because the cylinders are mounted to the palm



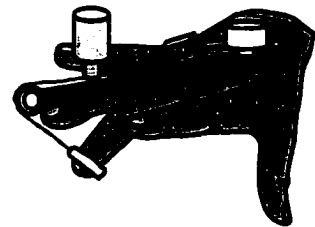
1.4(a) Air Bladder



1.4(b) Air Cylinder



1.4(c) Tendons



1.4(d) Cable/Beam

Figure 1.4 – Prior Approaches to Single DOF per Finger Force Display

this device distributes reaction forces to the palm for *all* grasp tasks. This is undesirable for many precision grasp tasks, wherein real forces are present at the fingertips *only* hence palm reaction forces are “ghost” forces that exist in the simulation, but do not exist in real tasks. Furthermore, with this approach, when the fingers are near a fully extended position, the angle between the cylinder and the finger becomes very small. Consequently a large portion of the cylinder force is directed along the finger longitudinal axis, while only a small portion is correctly directed perpendicular to the finger longitudinal axis (in the normal direction). A normal direction force is assumed to be the primary force direction during grasp tasks,

neglecting the tangential forces due to friction. A second drawback is the somewhat limited range of motion (40-90 degrees) provided by this approach Burdea (1996).

Another approach of providing resistance to finger bend was proposed in a patent by Kramer (1993), filed in 1990. This approach shown in FIG. 1.4(c) calls for cables routed along the surfaces of the finger such that when a cable is pulled resistance to finger bend is provided to the fingertip. This approach suffers in that the friction of the cable becomes very significant as the finger approaches full curl, and thus the cable force must be relatively large. Further this method is lacking in that with high cable forces, it is increasingly difficult to maintain the cable in its desired position, along the outer most surface of the finger joints. Seven years after filing the initial patent Virtual Technologies, Inc. (1997) introduced the CYBERGRASP haptic display, based on the 1990 concept of Kramer, but equipped with "moment arms" that eliminated the aforementioned problems (Kramer, 1997). The 1997 device is available to purchase for a list price of \$39,000, including CYBERGLOVE position measurement glove. While the CYBERGRASP product is effective in displaying forces normal to the fingertip, this approach also provides "ghost" forces to the outer surface of the finger secondary link.

A similar cable based approach shown in FIG. 1.4(d) was developed by Iwata (1992), except that the cable extends the length of a beam element rigidly attached to the user's hand and travels through a pulley to apply a force to the operators fingertip. One problem with this approach is that the angle of applied force varies greatly as the finger bend angle exceeds 60 degrees, assuming a value almost entirely tangential at

180 degree finger bend. Another draw back of this device is that the actuator and position measurement components are mounted directly to the operator's hand, which may result in discomfort due to excess weight and bulk.

Finger pad force application devices are shown in the left most column of FIG. 1.3. This class of devices provides a force to each of three pads on the inner surface of each finger phalange. The three finger pad devices that are earth grounded have been proposed by Zarudiansky, Hashimoto, [see Burdea (1996) pp7-9 and 94-95] and Leucke et. al. (1996). The Zarudiansky and Hashimoto devices are conceptually desk mounted and thus have a small range of motion for the hand. The Leucke device uses an industrial robot to position and apply force between the ground and magnetic finger interface. This approach is novel in that there is no mechanical connection between the user and the robot, but rather the connection is via magnetic fields. The Leucke approach however, carries a burden of the high cost of an industrial robot as part of the system. Other approaches by LRP, EXOS, ARTS [see Burdea (1996) pp 120-124, 259] provide a system of finger pad force presentation, utilizing a portion of the operator's body for grounding the applied forces. These devices may be well suited for VR in that they are portable, do not undermine the workspace, and are capable of representing grasp forces. The drawback of these approaches however is that the cost is high. The costs for these devices range from \$50,000 to \$100,000+ per hand. All of the finger pad devices control multiple active degrees of freedom for each finger, leaving concern for the ability to represent all five fingers, at a sufficient processing and display speed.

1.3 Performance Measures

In evaluating the state of the art in haptic interfaces, it is useful to consider measures of performance for those devices for which this data has been published. A table of such data for hand worn devices (hand masters), of the class under consideration in the present research is shown in Table 1 below.

Name	DOF	Force output	Work space	Bandwidth
Iwata	2/finger	20 N	normal	Not Available
LRP Hand master	15	11N-m	normal	Not Available
ARTS Lab.	12/4 fingers	1 N/phalanx	normal	Not Available
EXOS SAFIRE I	5/2 fingers	0.2 N-m	90°	30 Hz
EXOS SAFIRE II	8/3 fingers	0.2 N-m	90°	30 Hz
Rutgers Master I	4/4 fingers	4 N	40-90°	11 Hz
Rutgers Master II	4/4 fingers	16.4 N	50-90°	15 Hz
CYBERGRASP	5/5 fingers	12 N	normal	50 Hz

Table 1.1 - Performance Measures of Hand Worn Haptic Display Devices

Several papers have been published that discuss desirable features of haptic interfaces, interested readers are referred to Hasser (1995), Ellis, et.al. (1993), Shimoga (1993a) (1993b). The intent of this section is to outline those features frequently reported.

1. MOBILITY

Range of motion should be consistent with task to be modeled. For finger bend, 0 to 180 degrees/finger is most desirable, this can be met by implementing kinematic constraints consistent with those of the human. For general manipulation, 6 DOF free hand motion in large workspace is desirable, although as mentioned earlier, tele-robotics can be accomplished as long the slave robot motion can be mapped to corresponding hand motion.

2. TRANSPARENCY

A haptic interface should be highly transparent to the operator during unobstructed motion. Light weight, low inertia, and low friction are desirable characteristics. In actuator selection, a low back drive friction is required for traditional design with direct physical coupling between the operator and the actuator.

3. SIGNAL

The haptic device should provide a signal to the operator close to the real signal experienced in the task being simulated. For precision, highly dexterous grasping tasks, normal forces to fingertip are a primary signal. Minimal ghost forces should be presented to the user. Control speed should be fast enough to represent the operator's perception of "real time" interaction. For force presentation while in contact with an object, a bandwidth of 20-30 Hz is reasonably well accepted as meeting this criteria. However for initial contact, 300-350 Hz has been repeatedly cited (Kazerooni, 1993, Shimoga, 1993a, Brooks, 1990).

4. SAFETY

Safety to the operator must not be sacrificed. It is useful to employ a kill switch that permits all force display to be deactivated. Another useful safety feature is to limit motion with mechanical stops, to not exceed that of the human joints under haptic display.

5. COST

Cost should be as low as possible and must be less than the value derived from the application. If cost exceeds value, the solution is not economically viable, and thus not really a solution. Thus a high cost leads to a very small field of application. For many robotic tele-manipulation applications, cost is a lesser constraint, while for many VR applications, cost is a much greater constraint.

The above criteria apply to all classes of haptic interfaces as defined in the preceding sections. One key area of the “signal” feature described above that has not been adequately addressed by all classes of haptic devices presented in the literature is the problem of representation of initial contact between the slave or virtual hand and the object to be manipulated. The problem is especially important for representation of rigid objects or those with high stiffness, known as “virtual walls”. The problem of haptic representation of initial contact, particularly pronounced when interacting with rigid objects, is well known in the haptics research community. According to Burdea (1996) [p192]:

“A real wall does not deform under impact (except for very high forces) and produces an instantaneous and very large increase in the contact force. Creating such a force is problematic given the current state of haptic interface technology. If a simple Hooke’s law (spring) model is used then present achievable stiffnesses of 2000-10000 N/m cannot reproduce metal on metal or other hard contact sensations”

Colgate et.al. (1993) studied this problem in light of the “typical” implementation of a virtual wall. This “common approach” is to model the wall with a virtual stiffness K ,

and a virtual damping coefficient B , whereby the haptic sensation to be presented to the operator is a force given by:

$$F_k = K(x_k - x_{wall}) - Bx'_k \quad [1.1]$$

Where F_k is the force driving the interface, x_k is the position of the interface, x_{wall} is the wall position, K is the wall stiffness, B is the virtual damping coefficient, and x'_k is the interface velocity. Colgate and his associates discuss how virtual walls modeled without damping exhibit a property of generating energy due to discrete time modeling, and subsequently they develop a stability criterion for virtual walls requiring that they be passive elements. The passivity requirement is met only when the device damping is greater than zero and permits a greater margin when device damping and sampling rate are increased. Rosenberg and Adelstein (1993) concluded that damping was also beneficial for the operator's perception of initial contact with rigid surfaces. Salcudean and Vlaar (1994) argue that the major limitation in representing initial contact with virtual walls with direct drive haptic interfaces is due to the time delays present in data acquisition and control. Ellis, et.al (1997) propose better estimates of force values as a method to alleviate the "important problem of haptic rendering of contact". In tele-operation tasks, this problem is usually addressed by having the human operator perform grasp operations very slowly, thus reducing the initial force of contact between the slave manipulator and the object of interest. For example, Shimoga et. al. (1996) studies a tele-operation grasping task using binary tactile display and reports time to complete a three finger grasp in excess of 20 seconds. By comparison, Klatzky et. al. (1996) report human grasp with real objects

having a duration of approximately 100 milliseconds, 200 times faster than that reported in the Shimoga study. The aforementioned research indicates there is agreement within the haptics community that haptic display of initial contact with rigid objects is a significant problem.

In order to better understand the problems associated with haptic display of initial contact it is useful to consider a time snapshot sequence of the functions taking place during teleoperation. Upon review of the events in sequence, as shown in figure 1.5, one can begin to identify precise causes and (hopefully) conceptual solutions to the problems associated with stability of rigid body haptic display. From the figure it is apparent that there exist two types of errors due to the time delays in relaying the information from one coordinate frame to another. The first delay results in a slave position error, while the second delay results in human perception of position and forces errors. The first type of error requires that human body positions must be measured at the human, sent to the virtual reality computer and then displayed. The time required for this task is relatively low (when compared to human vision processing speed), and thus the virtual position error usually does not appear to the operator. In robotic tele-operation, the slave positioning delay is more significant as mechanical actuators must respond to the position control signals sent by the master.

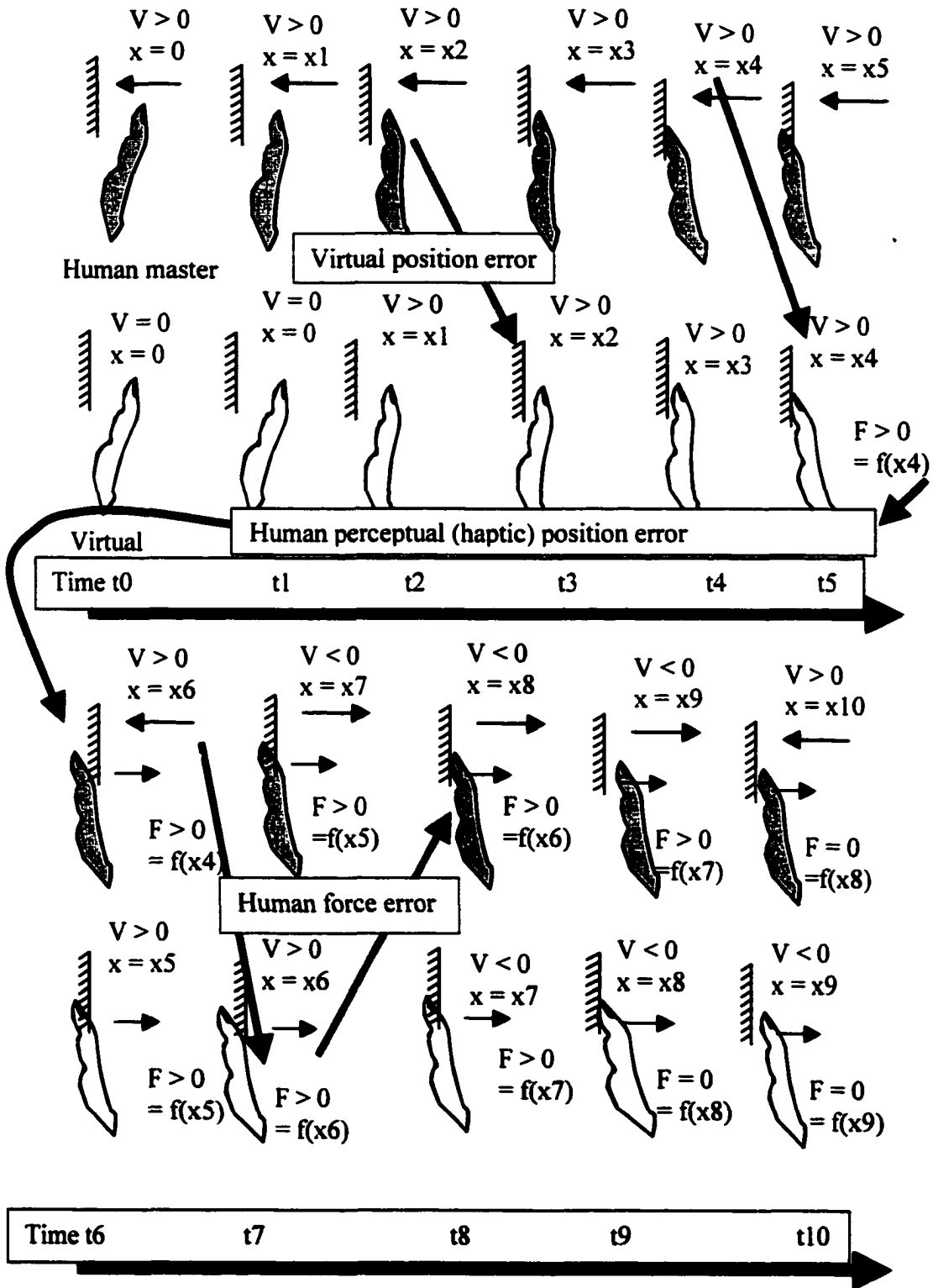


Figure 1.5 Sequential Master and Slave Positions and Forces

Human force and position perception errors are apparent for both robotic and virtual applications. The force error is often observed as an oscillatory instability when attempting to model highly rigid objects in a virtual slave environment. For rigid object simulations, a high stiffness and/or damping coefficient is used to define the virtual surface force of contact. This results in a very abrupt change in the magnitude of force commanded to be delivered by the actuator, often changing from 0 to 100% in a single calculation cycle. The rapid application of force appears to the human operator at a time following actual crossing of the object surface boundary. The total time offset or delay in force presentation includes the virtual display time discussed above in addition to the time elapsed from virtual environment receiving the positional data to human reception and recognition of the force signal.

The time to calculate a force within the virtual environment, send it to the haptic controller, determine a signal to send to the actuator, have the actuator respond to the signal, and deliver a force can be significant for both virtual and robotic tele-operation. This time delay is largely attributable to the haptic interface actuator response time. The limitation here is of more long-term concern than those due to computation requirements, because it is expected that trends in increases in computation speed as the technology progresses will continue. However, because actuators represent a more mature technology, significant increases in actuator response time are less likely in the immediately foreseeable future. According to Burdea, (1996) [p. 36], the human finger can apply force and motion commands at only 5-10 Hz, but can sense two distinct separate force signals at up to 320 Hz. In the same reference [p. 73], the

response time for actuators explored for haptic interface applications is reported to range from 0.3 Hz to 100 Hz. Thus signals from even the fastest actuator will only provide less than one third of the speed necessary to exceed the human sensory bandwidth. Therefore we can conclude that limits in actuator response time represent a fundamental limitation in haptic display performance under a traditional design paradigm that calls for the operator to be directly coupled to the haptic display actuator. As shown in the figure 1.5, a large delay (with respect to human sensing capabilities) is most troublesome when applied as the human crosses a virtual object boundary. In this case, the delay in actuator response permits continued human motion beyond the object boundary with respect to the human coordinate system. As can be seen in the figure, the human finger crosses the surface boundary at time (t_4), but receives no force of contact until time (t_6). Even then the force received is that due to the position (x_4) at time (t_4). As the force is a function of previous human positions, the force continues to be applied even after the finger has moved away from and is no longer in contact with the surface. The result of these delays is that the contact may become oscillatory or unstable (especially for rigid surfaces). Another potential problem that has received little attention in the literature is that the contact is perceived by the human to be at a different position in the human coordinate reference frame than that of the slave environment reference frame. The difference in slave position and master position relative to their respective frames of reference (or positional inaccuracy) prohibits direct positional control of the slave. In virtual reality slave environments the positional inaccuracy may be addressed by providing a

graphical display that prohibits virtual surface penetration for rigid objects, thus convincing the operator via visual information that no penetration has taken place. In robotic applications, a system imposed velocity limitation is sometimes used to prevent positional inaccuracy from causing excess forces to occur at the robotic manipulator. In other cases deformable manipulator force sensors are used to help accomplish this task.

1.4 Interface Applications

One of the primary benefits we hope to derive from haptic feedback is the ability to realistically grasp virtual objects and display the forces of contact between the virtual hand and the virtual object as shown in FIG. 1.6, or between the robotic hand and a real object.

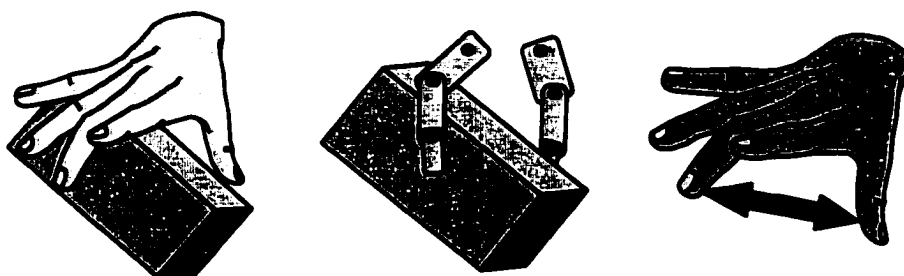


Figure 1.6 - Grasping Task for Direct Manipulation

To simulate this most fundamental task, typical VR systems employ hand tracking with a solid model of a human hand as an interactive interface element. The position and orientation of the hand can be provided by tracking devices such as Flock of Birds Ascension (1998), or Polhemus (1998). The finger bend information can be provided

by 5th Glove by Fifth Dimension (1998), Cyberglove by Virtual Technologies (1997), pinch gloves, etc.

While this approach is a significant improvement over the traditional menu mouse system, there remains several shortcomings when haptic display is omitted: (i) the human operator when grasping an object will be easily able to penetrate the grasped object as no contact forces are represented, (ii) accuracy of manipulating a component's shape suffers from lack of a natural stiffness display interaction, and (iii) the ability to grasp through the object without contact force representation can be disorienting to some operators. These shortcomings may be overcome with haptic display to represent contact forces to the operator's fingertips. The fingertips are chosen since most dexterous manipulation is performed with only this area of the hand in contact with the object (Cutkosky and Howe, 1990).

In tele-manipulation systems, the virtual hand is replaced by a slave robot end effector, and is moved into the desired position and orientation via a general robotic device, typically a multi-degree of freedom serial arm robot. Many of the same parameters hold in both the virtual and tele-manipulation applications. The human hand is connected to the master haptic interface and the slave (virtual or robotic) motion is controlled by the human hand. The haptic interface will at least provide some position and/or force measurement, and if also a haptic display, it provides a method to display touch sensations, mimicking those experienced by the slave. Most commonly force is the touch sensation that is displayed, although position display has been proposed (Kazerooni, 1993) and tactile display has been tested (Shimoga, et. al., 1996). The

master haptic interface may have position and orientation information measured by the same tracking device commonly used in virtual environments, or in some applications includes a complete duplicate (or scaled version) of the slave robot. When the robot is duplicated, the slave can be programmed to precisely duplicate the joint angle values read from the master. In either the virtual or tele-manipulation application domains, the same desirable system features or requirements, as discussed earlier are present.

Another very important task for VR simulations is the representation of contact force during elastic and plastic deformation of virtual objects, (Springer and Gadh, 1997).

In the mechanical design application area it is desirable to provide a haptic feedback to aid in the control of plastic deformation of virtual solid bodies (FIG. 1.7). This type of operation is similar to that of molding clay from an initial shape (i.e. cuboid) into a final desired shape of the design artifact while maintaining a constant volume of material.



Figure 1.7
Shape Deformation

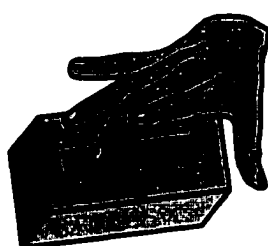


Figure 1.8
Virtual Clay Sculpting

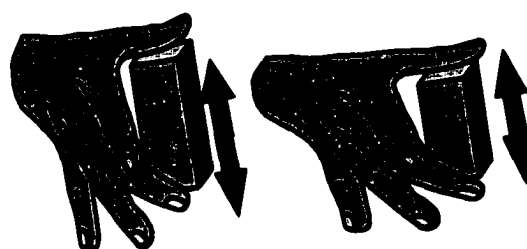


Figure 1.9
Force-Deflection

A related area involving free form shape creation, is the sculpting operation, shown in FIG. 1.8. In sculpting, material is removed from an initial virtual body, by chipping it away with the fingertips. A higher applied force corresponds to a larger removal chip,

whereas smaller magnitude forces are used for finer detail definition of the shape under consideration. Similar to material removal from free form shapes, one can utilize haptic display to improve control and thus efficiency in changing a single dimension of a three dimensional object, such as shown in FIG. 1.9. As shown in this example, the length of the object is being altered while all other dimensions remain constant. The magnitude of change in length is displayed to the user as a magnitude in change of force, however as this is a plastic mode of shape deformation, removal of the grasp forces results in the body remaining at the deformed shape.

Another area of free form deformation, which provides benefits in the understanding of designs created, is the elastic deformation of design artifacts created with materials of different elastic moduli. This type of information in design review is currently only available through separate analysis or by building physical prototypes, can become available to virtual prototypes, through implementation of haptic feedback in VR-CAD. The above characteristics for shape modification in a VR-CAD system constitute a new and powerful method for creation of and interaction with virtual prototypes.

In tele-manipulation the ability to present the user with forces of contact is even more readily appreciated. In this application the human operator is charged with the task of precisely controlling the remote manipulator. When provided a sense of the forces of contact, (actual or scaled forces) the operator can more readily control the slave robot manipulator. This becomes even more relevant when the manipulation tasks are those requiring a human's unique ability to precisely manipulate objects within their grasp.

According to Shimoga et. al. (1996), such an ability becomes crucial when handling delicate objects. Some application examples include handling fragile or explosive devices, and manipulating radioactive materials or other toxic substances. For example, when an object held in the grasp of the robot, collides with the surrounding environment, the forces measured at the robot hand will vary accordingly, and display of these forces can aid in the manipulation control, especially when a portion of the grasp object is not visible. When no visual display is available in tele-manipulation, the value of force display to the fingers can be further appreciated in identification of objects to be manipulated. Force display can aid in the discrimination of the size and the force deflection characteristics of the object being grasped by the robot.

1.5 Conclusions of Haptic Display State of the Art

In this chapter definitions regarding the terminology commonly used in haptic interface research have been discussed. The present state of the art in the development of human computer interfaces for haptic display has been reviewed. From this review it has been shown that the present state of development leaves several opportunities for improvement in the following areas:

1. For grasp task tele-operation, the field could benefit by development of a system capable of full range of finger motion and presentation of grasp resisting forces in a direction normal to the distal finger phalange at all positions of finger bend.
2. The general design paradigm for previous force display haptic interface design calls for direct physical coupling between the human operator and the force providing actuator.

3. **Fundamental limits exist in actuator response time. Because actuators represent a relatively mature technology, it is unlikely that the response time will be significantly reduced in the near future.**
4. **Prior haptic device development efforts have repeatedly demonstrated a problem with the display of initial contact with surfaces. This problem is most evident as instability when the initial contact is with rigid surfaces defined by a high stiffness and/or damping coefficient.**
5. **Prior haptic interface designs have an inherent positional inaccuracy due to time lags between master position, slave position, and force reflection from the slave to the master. This topic has received little attention in the literature, but the result prevents direct master-slave position control during initial contact.**
6. **One can describe the performance of haptic interfaces in terms of operational characteristics such as mobility, transparency, and signal. Because of the high levels of energy transfer between the interface and an operator safety is of utmost concern in the design of haptic interfaces. As in all machine development a true solution is one for which the cost falls below the value of its application.**

The desired outcome of the present research is to systematically address the fore-mentioned issues in development of a new approach to haptic interface design and control. A new design is to be directed specifically toward representation of common and highly dexterous tasks involving finger tip manipulation and grasping of objects through tele-operation where a human operator wears a master haptic interface, through which human finger positions control a slave device modeled after the human

hand. Forces of contact that occur between the slave human hand model and slave environment objects are to be reflected to the haptic master and in turn to the operator in a real time fashion so as to permit exploitation of the highly developed human control capabilities in dexterous manipulation.

Chapter 2

Analysis of Dynamics of Contact in Tele-operation

2.1 Introduction

In this chapter mathematical models of the dynamics of various contact situations are developed. The models are used to compare the results of real finger (or hand) contact with a real wall, with those obtained by simulations resulting from prior haptic interface designs, as well as those resulting from a novel haptic interface design proposed in this dissertation. Simulations of the equations of motion that describe the kinematics and kinetics involved during initial contact are presented in order to predict errors in forces of contact experienced by haptic interface operators in comparison to forces experienced during contact with real objects.

One key area of haptic simulation is the ability to present to the operator the sensation of initial contact with rigid objects or virtual walls. As identified in Chapter 1, this problem may be largely attributable to time delays in a traditional closed loop control system including those due to actuator response time. Many researchers have reported undesirable vibration when attempting to simulate stiff surfaces. Kazerooni (1993) analyzed the stability of a position controlled (joystick type) haptic interface, coupled to the human operator. In his report, analysis of the closed loop dynamics is represented by traditional control theory transfer functions. The time delay between input force

sensed at the controller and hand controller position response results in oscillatory hand controller motion due to “limit cycle instability”. To address this problem, Kazerooni recommends a sampling time smaller than 0.003 seconds. Salcudean and Vlaar (1994) model a hand held joystick interacting with a stiff wall as:

$$\begin{aligned} mx'' &= f_h - b_e x' - k_e x && \text{if } x \leq 0 \\ &= f_h && \text{if } x > 0 \end{aligned} \quad [2.1]$$

where x is the position, b_e is the equivalent damping coefficient and k_e is the equivalent spring constant. The hand force f_h is considered to have an active component depending on mass and operator applied force (f_k), and passive component, depending on the position and impedance of the operator. For a constant actuation force between samples (f_k) the stiff wall component of the above equation when implemented in a discrete time PD controller, using a first order finite difference approximation of the velocity term is given by:

$$\hat{f}_k = -k_p x_{k-1} - (k_v/T) (x_{k-1} - x_{k-2}) \quad [2.2]$$

In EQ. [2.2], k_p is the potential energy constant, k_v is the damping (velocity dependant) constant, and T is the sample period. By examination of the roots of the closed loop characteristic polynomial (using $m = 0.7$ kg, $1/T = 200$ Hz), Salcudean and Vlaar found the maximum k_p to be 3900 N/m and the maximum k_v to be 60 N/(m/s). They further comment that such an implementation would lead to a “marginally stable system” and

recommend that a braking pulse (described by k_{pulse} , below) be implemented. This would provide a very high damping upon wall penetration such that:

$$\hat{f}_k = -(k_{\text{pulse}} + k_v/\Gamma)(x_{k-1} - x_{k-2}) \quad \text{if } x_{k-2} > 0 \text{ and } x_{k-1} \leq 0 \quad [2.3]$$

$$\hat{f}_k = -k_p x_{k-1} - (k_v/\Gamma)(x_{k-1} - x_{k-2}) \quad \text{otherwise}$$

Some problems remain when implementing the braking pulse recommend here. The first problem is that the force presented to the operator lags the position of wall penetration by at least one computation cycle, and further, the force magnitude is based on the average velocity during the period two cycles prior to force display time. Therefore, one could anticipate significant errors if the deceleration is high, or the velocity is rapidly decreasing, which is exactly what the velocity is expected to be when contacting a wall.

Love and Book (1995) also analyze the contact stability of virtual walls utilizing Jury's test to evaluate the bounds of the parameters of the system's characteristic equation. Their analysis shows that stability can be lost by increasing stiffness for a given sampling rate and damping, or can also be lost by employing a simulation damping that is either too small or too large for a given stiffness and sampling rate. They also show that for a given damping and stiffness, increasing the sampling rate can restore stability of contact with virtual walls. Colgate, et.al.(1993) also analyze the stability of contact with virtual walls through evaluation of control theory block diagrams and transfer functions. Their analysis focuses on maintaining stability by maintaining passivity of the wall. They develop the midpoint impedance principle:

$$b > KT/2 + B$$

[2.4]

where b is the haptic interface internal damping, K is the maximum achievable simulation stiffness, B is the maximum achievable damping that can be produced, and T is the sample time period. The main problem with implementation of this approach is that increasing sampling (smaller T) results in higher errors for velocity estimation, since velocity is estimated based on previous position data as is done by Sacludean and Vlaar, above.

Ellis, et.al. (1997) also studied the rendering of contact, particularly with stiff surfaces and develop numerical methods to reduce the error in force values presented to the operator. Their estimation of the force to be presented is based on the slope of the force/time curve between the prior two force values. The analysis consists of lagrangian dynamic modeling of the haptic interface. In the present analysis, the general analysis approach of Ellis et.al. is followed, with the exception that our analysis considers three situations: (i) the operator, in combination with a real wall, (ii) a traditional virtual wall simulation, and (iii) the wall simulation rendered by the proposed de-coupled actuator design with a position switching to force control paradigm (called DECAFF).

Upon review of the literature in the area of rendering and stable control of haptic interfaces for the simulation of stiff surfaces, we can draw the following conclusions:

- (1) The rendering of stiff walls remains problematic given the present state of the art in haptic interface design.

- (2) By sophisticated and rigorous control system analysis, prior research has been able to identify methods to maintain stability, but still surface penetration is required for the simulation. For the methods recommended in previous research, stability can only be guaranteed for a specific combination (or range) of the stiffness, damping, and sampling variables. Furthermore the ranges tend to limit either the maximum stiffness and/or the transparency, or require sampling at rates higher than practical given the present state of technology.
- (3) For all methods of stable rendering, higher sampling rates are recommended and provide a more convincing representation.
- (4) Because there exists a finite delay between the time the slave or virtual fingers (or hand) contacts the object of interest and the time at which force is displayed to the operator, there is *always* an error in the controllable position of the slave or virtual fingers for traditional direct coupled haptic interface designs.

It is proposed that the DECAFF haptic interface design and control method specified in this research report advances the state of the art in the rendering of contact with stiff surfaces. This is done by reducing the time delay between slave finger/object contact and force display to the operator to zero, thereby eliminating slave position errors, and permitting precise control of tele-manipulation, and virtual interaction. The slave position error is eliminated by the addition of a feed forward control variable, measurement of the distance to contact, before contact between the slave and the object has occurred. The use of a distance sensor to better control contact between a robot and

an object, was proposed by Li (1996), but for application to multi-phase control, not human controlled tele-manipulation. No articles in the literature describing a distance before contact control strategy for human haptic display have been found. A de-coupled actuator is proposed, that operates on the distance information to properly control the location of the master contact sensed by the operator, before the actual contact has occurred, as is described in detail in chapter 3 of this report. For this analysis, traditional mass/spring/damper models are considered for the following cases: (i) contact between a real (human) finger and a real physical wall, (ii) contact simulation modeling provided by traditional haptic displays, and (iii) contact simulation modeling provided by the haptic display of the present research. For each of the three models, the force experienced by the operator and the energy transfer is considered in evaluating how closely simulation cases (ii) and (iii) resemble real contact of case (i).

2.2 Human Contact with Real Surface

First considering the case of real contact between a human finger (or other body part) and a real wall, we model the finger as a mass, spring, damper system that interacts with a non-movable wall entity. The single DOF, linear displacement model is later generalized to a multi-DOF, spatial model. The finger mass is denoted by m_f , while the spring rate and damping are denoted by k_f , and b_f , respectively, as shown in FIG. 2.1. The finger initially in a position just before contact, at time t_1 , has a velocity V_1 , and

after contact (force transients have settled to a steady state value) at time t_2 the velocity is zero.

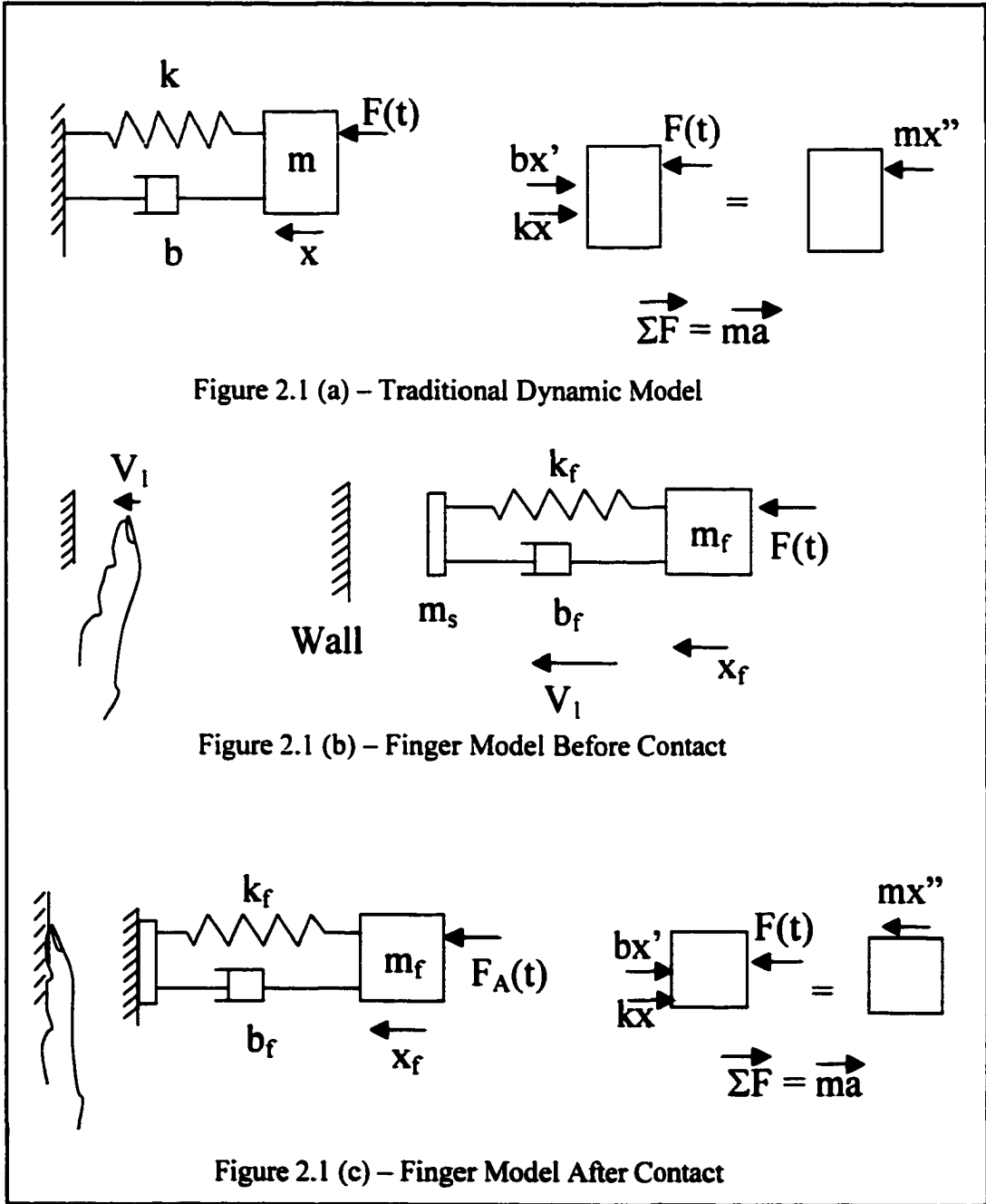


Figure 2.1 - Human Finger Contacting Real Wall

Our goal in this analysis is to describe a force experienced by a person during the initial contact event. A traditional dynamic model of a vibrating system is shown in figure 2.1(a). Providing this system with a positive displacement and giving it a positive velocity (see Shigley and Uicker, 1995), results in a free body diagram shown in the right side of figure 2.1(a). Subsequent application of the vector form of Newton's second law to the free body diagram yields an equation of motion:

$$F(t) - b x' - k x = m x''$$

$$\text{Or } F(t) = m x'' + b x' + k x \quad [2.5a]$$

Where $F(t)$ is an applied time varying force in the same direction as the displacement coordinate x . The stiffness of the system is denoted by k , b is the damping coefficient, and m is the system mass. The position is x , the velocity is x' (the time derivative of position) and the acceleration is x'' (the second time derivative of position).

A similar type of analysis is used to describe the initial contact between a real human finger, initially in motion, and a stationary rigid surface or wall. Prior to contact with the wall we have a finger model as shown in figure 2.1(b), moving at a pre-contact velocity of V_1 in the positive x direction. In this model the skin surface is denoted by m_s , which has a mass magnitude assumed to be negligible when compared with the overall finger mass (m_f). The position of the finger skin surface is indicated by m_s while m_f is indicative of the finger bone position.

After contact between the finger and the rigid surface has been made, the skin is assumed to remain in contact with the surface, resulting in a model depicted in figure 2.1(c), which is now the same as the model of figure 2.1(a). Application of Newton's second law to the free body diagram given here results in:

$$F(t) - b_f \dot{x}_f - k_f x_f = m_f \ddot{x}_f \quad [2.5b]$$

which can be rearranged to:

$$F(t) = m_f \ddot{x}_f + k_f x_f + b_f \dot{x}_f \quad [2.5c]$$

Our goal of the analysis is to describe the force experienced or perceived by the human and we now assume that the force sensed by the person is of equal magnitude and opposite direction as that applied by the person. Then the force just before contact will be given by the product of the mass and acceleration, while after contact, the force will be given by:

$$F(t_2) = m_f \ddot{x}_f(t_2) + b_f \dot{x}_f(t_2) + k_f x_f(t_2) \quad [2.6]$$

However at time t_2 , the contact phase is complete and the force has settled to a steady state value, resulting in an acceleration and velocity that are approximately equal to zero, yielding a final force of:

$$F(t_2) = k_f x_f(t_2) \quad [2.7]$$

In evaluating this force, first we consider the magnitude of $x_f(t_2)$, which is of a small value due to the limited deflection of the fingertip touch pad (on the order of 4 mm).

Secondly, considering the k value of the finger, which has been shown by others [Hajian and Howe (1994), and Karson and Srinivasan (1995)] to assume a value proportional to the force applied, is also very small, when the subject applies a small force to the wall after initial contact. In such cases, which are most pronounced when subjects “tap” a wall, Lawrence, et.al. (1996), the force at time (t_2) is quite small. Should the subject apply a high force after contact, the finger deflection remains relatively constant, and thus the k_f value increases proportionately. When we consider an energy balance between time (t_1) and time (t_2), we have:

$$E(t_1) = E(t_2) - U_{1-2} \quad [2.8]$$

The energy of time (t_1) in EQ. 2.8 is completely kinetic, while that of time (t_2) is completely potential, and the work done between time (t_1) and time (t_2) is that absorbed predominantly by the damping of the human finger. Substitution of the appropriate terms into EQ. 2.8 yields:

$$(1/2)m_f x_f'(t_1)^2 = (1/2)k_f x_f(t_2)^2 + b_f (1/2)(x_f'(t_1) - x_f'(t_2)) x_f(t_2) \quad [2.9]$$

Again upon evaluation of the terms, we find that while the subject maintains a low contact force after initial contact, k_f is small and $x_f(t_2)$ is small, from which we can conclude that U_{1-2} is large, or most of the kinetic energy of the finger is absorbed by the internal damping in the finger. It should be noted here that $x_f'(t_2)$, the final velocity is zero after the contact phase with a real wall and the force has settled to a steady state value.

2.3 Contact Simulation of Traditional Haptic Displays

Secondly we consider a two mass, spring damper system as shown in FIG. 2.2, as a model of the typical simulation of contact between virtual finger and a virtual wall, or contact between a slave manipulator and a rigid body, as felt by the operator. The model includes a simulation mass, spring and damper, and a finger mass, spring and damper, as well as positional changes for each mass, denoted as x_s , and x_f , respectively. Following the analysis of equations 2.5a – 2.5c and utilizing a lumped parameter model [Norton (1999)], the dynamic system can be evaluated by the model given in FIG. 2.2. For this system, the contact force experienced by the person is as follows:

$$F(t) = m\ddot{x}_{f+s} + b_{eq}\dot{x}_{f+s} + k_{eq}x_{f+s} \quad [2.10]$$

Where

$$b_{eq} = (b_s b_f) / (b_s + b_f) \text{ and } k_{eq} = (k_s k_f) / (k_s + k_f) \quad [2.11]$$

Both the equivalent damping coefficient and the equivalent spring constant for the EQ. [2.10] and EQ. [2.11] assume a value close to the smaller of the two input terms, for wide variation between the finger and the simulation. Thus if k_f is very small and k_s is very large, k_{eq} will be approximated by k_f . However, if the two values are reasonably close in magnitude, the equivalent k approaches one half the magnitude of each k_s , and k_f . The other possible combination is that k_s is small while k_f is large, for which k_{eq} is approximated by k_s . Because of this relationship, simulation stiffness must necessarily be

chosen much larger than finger stiffness to achieve an equivalent stiffness close to that of the finger alone (on the order of $k_s = 10 k_f$ for a 9% error $k_{eq} = 0.91 k_f$).

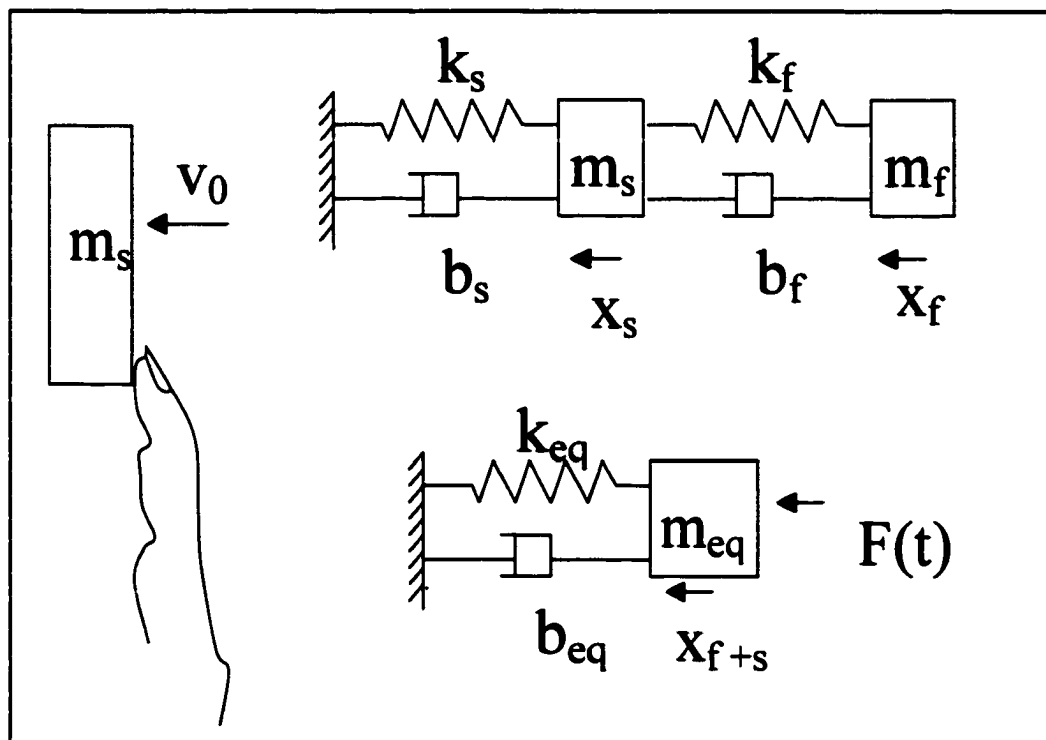


Figure 2.2 - Human Finger Contacting Simulated Wall

Similarly the equivalent damping will assume a value approximated by the smaller of the simulation and finger values, or when b_s is very small and b_f is very large, b_{eq} will be approximated by b_s . Again as b_s approaches the magnitude of b_f , the equivalent damping will be approximated by one half of the finger damping value. In evaluating the force and the energy balance as was done for the actual finger wall model, we see that the both the force and the energy of time (t_2) is generally higher for the simulated virtual wall, since the magnitude of $x_{s+f}(t_2)$ is always greater than $x_f(t_2)$. Assuming the

simulation has stopped penetration motion at time (t_2) and the force has reached a stable steady state value, and thus the velocity and acceleration are zero, the force experienced by the person is given as follows:

$$F(t_2) = k_f x_{f+s}(t_2) \quad \text{for } k_s \gg k_f \quad [2.12]$$

The error is then given by the difference between the simulation force and the real wall contact force.

$$\begin{aligned} \text{Force Error} &= F(t_2)_{\text{simulation}} - F(t_2)_{\text{real}} \\ &= k_f x_{f+s}(t_2) - k_f x_f(t_2) = k_f x_s(t_2) \end{aligned} \quad [2.13]$$

Assuming $x_{f+s}(t_2)$ is equal to $x_f(t_2) + x_s(t_2)$, the error reduces to $k_f x_s(t_2)$. We find similar results upon consideration of the energy balance as was done for the real wall. For the typical case where the simulation damping and stiffness are significantly higher than that of the finger, we have:

$$\begin{aligned} E &= (1/2)mx'(t_1)^2 \\ &= (1/2)k x(t_2)^2 + b(1/2)[x'(t_1) - x'(t_2)] x(t_2) \end{aligned} \quad [2.14]$$

$$\begin{aligned} E(t_2)_{\text{simulation}} - E(t_2)_{\text{real}} &= (1/2)k_{eq} x_{f+s}(t_2)^2 + b_{eq}(1/2)x'(t_1) x_{f+s}(t_2) \\ &\quad - [(1/2)k_f x_f(t_2)^2 + b_f(1/2)x'(t_1) x_f(t_2)] \end{aligned} \quad [2.15]$$

which yields:

$$\begin{aligned}
 & E(t_2)_{\text{simulation}} - E(t_2)_{\text{real}} \\
 &= (1/2)k_f [x_f(t_2) + x_s(t_2)]^2 + b_f (1/2)x'(t_1)[x_f(t_2) + x_s(t_2)] \\
 &\quad - [(1/2)k_f x_f(t_2)^2 + b_f (1/2)x'(t_1)x_f(t_2)] \quad [2.16]
 \end{aligned}$$

For $k_s \gg k_f$, and $b_s \gg b_f$, this reduces to an error in energy of

$$\begin{aligned}
 & E(t_2)_{\text{simulation}} - E(t_2)_{\text{real}} \\
 &= k_f x_s(t_2) x_f(t_2) + (1/2) k_f x_s(t_2)^2 + b_f (1/2) x'(t_1) x_s(t_2) \quad [2.17]
 \end{aligned}$$

The above relationship shows that the energy error assumes a value increasing quadratically in simulation penetration distance $x_s(t_2)$, which upon real wall contact would be zero. The penetration distance depends on the system bandwidth, and is a result of both a time delay between the time of virtual hand crossing the wall edge and force output, and the wall dynamic model described in EQ. [1.1]. A force and energy of an excess magnitude would be consistent with the typical description of the feeling of a virtual wall as “lively” or “active” Colgate et.al. (1993). To increase the accuracy, of course, the sampling period can be decreased, resulting in a decreased simulation penetration distance for a given initial velocity. However the delay for actuator response still permits a penetration into the slave surface (x_s) and there still exists some error due to the *required* penetration distance (due to the wall dynamic model) for prior rigid body contact simulations in VR applications. Thus, regardless of how fast the

sampling is, there is still a resulting error attributable to the penetration distance of the simulation x_s , which is not zero, as it is in a real wall contact. In a tele-manipulation robotic application, it is the delay error rather than penetration distance that can cause problems. In this application, the robot position response is presumably slower than that of a VR slave due to the need to position the robot. The result of a slower robot response is that the robot is commanded to proceed to a position *inside* of a target object before contact between the robot and the slave target occurs. Prior to robotic contact, the force sensed and reflected to the master is of zero magnitude. Therefore master finger position proceeds beyond that of the slave target. If the robotic gripper fingers are rigid and the grasped object is rigid, the robot will impact the target object resulting in very high forces of contact between the slave fingers and the object. This may result in damage to either the robotic hand, or the object being grasped, hence to prevent high contact forces, present tele-manipulation systems require a slow grasp speed.

2.4 Contact Simulation of Proposed Haptic Display

Finally we consider a dynamic model of the proposed de-coupled actuator under position control paradigm, as shown in FIG. 2.3. Where the simulation positions x_s , is assumed to be constant during the initial contact event. In chapter 3 a design is presented that satisfies this assumption.

In mathematical terms,

$$x_s(t_1) = x_s(t_2) \quad [2.18]$$

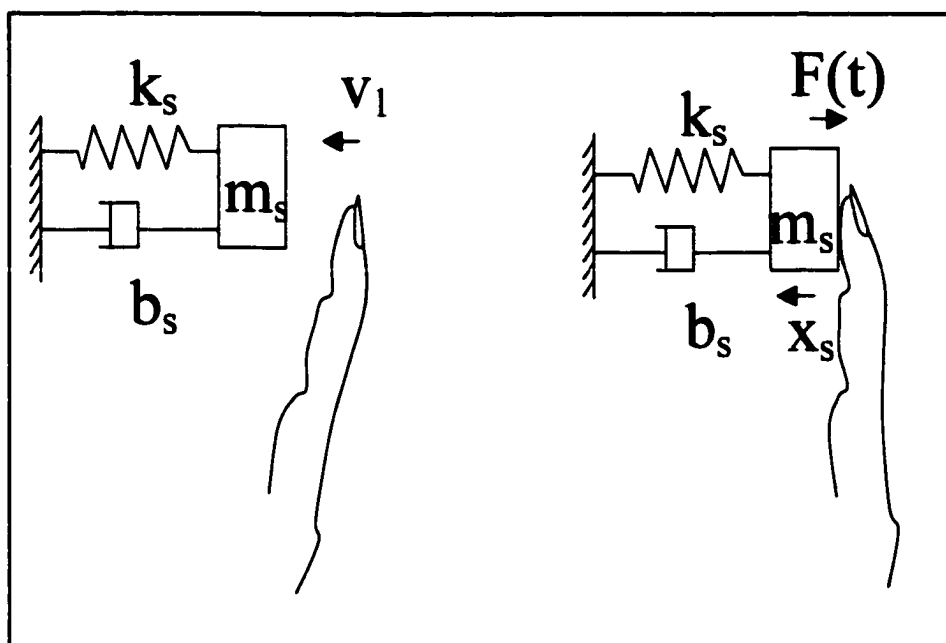


Figure 2.3 - Finger Contacting Simulated Wall with Proposed Haptic Display

For the simulation position change of zero, the force during contact $F(t)$, is function only of the finger mass, spring rate, damping, and position, which is an exact match of the controlling parameters during real contact with a real wall. Thus, the highly transient force experienced by the operator, will be extremely close to that of the real experience, and certainly much more accurate than that possible with the traditional modeling of haptic sensations while contacting virtual walls. While the initial contact control is by position, forces of the slave hand, (in a robotic tele-manipulation application) are still measured. Once the force values return to a near steady-state magnitude, position control is disabled, and force control is re-established, permitting accurate representation of both the initial contact with the object, and subsequent force controlled manipulation of the object. In VR simulations, the position control is

maintained when interacting with rigid bodies (eg. $F= 100\%$ upon contact), while force control is used when interacting with deformable bodies (eg. $0\% < F < 100\%$), permitting accurate simulations for both types of bodies.

One problem associated with discrete time controlled simulations, common to all systems controlled by a sample hold digital data processing, is that the output data is delayed by a small amount of time from the input data. Additionally, actuators require some time to respond to the output data. This time delay results in some inherent error in the output forces. The traditional approach to address this delay error is to utilize high technology, high-speed signal processing equipment in combination with fast response actuators. While this approach provides reasonable force displays for many force control tasks, the speed at which initial contact is sensed exceeds actuator, signal processing, and computation limits of today's technology. Although there is not wide acceptance of required display update rates, (often called system bandwidth), it generally agreed that force control tasks require bandwidths in the range of 10-30Hz, while initial contact, sensed by tactile sensors requires bandwidth of 300-350 Hz to exceed that of the human receptors. Presently technology in haptic displays has reached the 10-30 Hz mark, but falls far short of the 300-350 Hz target for initial contact (see device performance table 1.1). Recognizing this pitfall, Ellis et.al (1997), developed a set of tools to address the estimation of forces, in an attempt to provide a more realistic representation of initial contact, especially with highly rigid objects.

2.5 Generalization to Multi-Degree of Freedom Systems

Following the method of Ellis and his colleges (1997), the models presented above can be represented by lagrangian equations of motion, yielding solutions for forces at discrete time steps. Although the method presented here follows that of the Ellis paper, several important differentiations are made in the following analysis:

The forces due to damping and spring deflection in the following analysis are not ignored or assumed to be zero.

Both the human finger and haptic interface mass, spring and damping are included in the present model.

Time delays due to system control bandwidth are eliminated for many grasp tasks due to the de-coupled actuator and feed forward distance to contact control method.

The lagrangian formulation of EQ. 2.5 is given by replacing linear displacement, velocity, and acceleration with spatial generalized coordinates as follows:

$$F(t) = mq''(t) + bq'(t) + kq(t) \quad [2.19]$$

This equation can be analyzed term by term, as has been done for the linear displacement models, applying boundary conditions of $q(t_1) = 0$, $q'(t_2) = 0$, and $q''(t_2) = 0$. When this is done, we obtain the same conclusions of the real finger real wall model above, in that the final steady state force is small, and the kinetic energy of the finger in motion before contact is primarily consumed by internal finger damping. If we further

evaluate the equation of motion to determine impulse and energy in the form of Ellis,

we can describe the motion as follows:

$$q'(t_1) = \int q''(t) dt = 1/m \int F(t) dt + 1/m \int (b q'(t) + k q(t)) dt \quad [2.20]$$

$$q(t_2) = \int q'(t) dt \quad [2.21]$$

for limits of integration from t_1 to t_2 . Defining shorthand for impulse, damping, and potential

$$\text{Impulse} = I(t_1) = \int F(t) dt \quad [2.22]$$

$$\text{Damping} = B(t_1) = \int b q'(t) dt \quad [2.23]$$

$$\text{Potential} = K(t_1) = \int k q(t) dt \quad [2.24]$$

We can rewrite EQ. [2.20] as:

$$q'(t_1) = (1/m) (I(t_1) + B(t_1) + K(t_1)) \quad [2.25]$$

Noting that we have deviated slightly from that shorthand notation of Ellis by defining separately the damping and potential terms, since we will not be assuming these terms to be zero, we can evaluate the kinetic energy at time t_1 as:

$$\begin{aligned}
E(t_1) &= (1/2) m \dot{q}(t_1)^2 = \\
&= (1/2m) I(t_1)^2 + B(t_1)^2 + K(t_1)^2 + 2 I(t_1)B(t_1) \\
&\quad + 2I(t_1) K(t_1) + 2B(t_1) K(t_1) \quad [2.26]
\end{aligned}$$

From which we can conclude, as did Ellis, that errors in estimating the impulse term magnify the apparent energy quadratically. However, since damping and potential terms are also considered, we can comment on the quadratic effect of errors in these terms in the energy transfer. Since real human fingers (or hand) and haptic interfaces are often multi-degree of freedom mechanisms, the lagrangian model can be further generalized into matrix form, as a vector form of EQ. [2.19]:

$$\mathbf{F} = \mathbf{M}(\mathbf{q})\ddot{\mathbf{q}} + \mathbf{B}(\mathbf{q}, \dot{\mathbf{q}})\dot{\mathbf{q}} + \mathbf{P}(\mathbf{q}) \quad [2.27]$$

Where \mathbf{M} is a mass matrix, \mathbf{q} is a vector of position variables, $\mathbf{B}(\mathbf{q}, \dot{\mathbf{q}})$ is the vector of damping forces, and $\mathbf{P}(\mathbf{q})$ is the vector of potential terms. The energy values are found by integrating the vector form of EQ. [2.20], where division by m is replaced by multiplication by the inverse of the mass matrix \mathbf{M} . The quadratic relationship will still hold, subject to the position dependent mass matrix.

2.6 Simulation of Results

Equations [2.2] through [2.17] can be better understood by examination of a sample case of “typical” finger contacting a wall trajectory, and determining the resulting force vs. time $F(t)$ response. Then equations [2.19] through [2.27] will be apparent as applications of the simulations presented in this section. It should be noted that the selection of a typical position vs. time $x(t)$ operator input is quite arbitrary, since this is controlled by the human operator, and thus is subject to high variability between operators and for the same operator on different occasions. Although the $x(t)$ is controlled by the operator and likely to be variable, one can make some reasonable assumptions about the trajectory of the finger while in contact with a real wall:

- (i) The starting point of $x = 0$, defined as initial contact position, occurs at time t_1 .
- (ii) At time t_2 , the position x has reached a steady state value, indicative of constant (approximately) grasp force while resting the finger against an object.
- (iii) Between time t_1 and t_2 , the position x remains positive, indicating continuous contact between the finger and object.

Subject to the above assumptions, the $x(t)$ function may assume a value between zero and a maximum value (x_{max}), wherein x_{max} is never less than $x(t_2)$. Subject to the above restrictions, an assumed $x(t)$ is created, and from that differentiated (twice), to yield $x'(t)$, and $x''(t)$. These values are used to compute $F(t)$, for the cases of real wall contact and simulation wall contact of traditional virtual wall models. The $x(t)$ for traditional wall models is assumed to contain an additional magnitude of the simulation object penetration (x_s). Plots for the cases of interest are shown in FIGS. 2.4 - 2.11. On

all simulation plots the horizontal axis indicates time in milliseconds and the vertical axis indicates position in millimeters and force in newtons.

The force plots of FIG. 2.4 through FIG. 2.9 are based on the assumption that there is a high virtual damping and spring constant such that the b_{eq} and k_{eq} are approximated by b_f and k_f respectively. For the simulations b_f is assumed to be 6000 N s/m, k_f is assumed to be 200 N/m, and m_f is assumed to be 0.02 kg, indicating the data found by Hajian and Howe, 1994 for low force application levels. The first simulation is that of a real finger contacting a real wall given in FIG. 2.4. Here it is notable that the force starting at zero climbs quickly and settles to a steady state value while the in contact with the surface. When the finger is moved away from the surface the force briefly drops below zero and then returns to a zero magnitude.

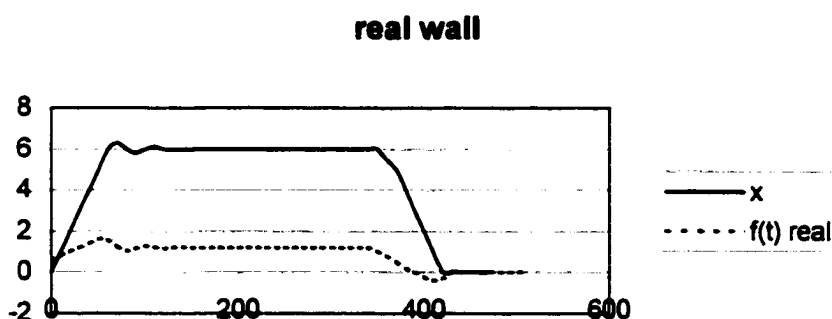


Figure 2.4 Real Wall Model Displacement and Force

FIG. 2.5 shows the simulation position and force that would result if a traditional virtual wall simulation could be performed without time delays in force output. Note that the simulation position includes a wall penetration x_s and a finger deformation x_f . It should be clear from the plot that the steady state force while in contact with the wall is higher

for the simulation due to the wall penetration. In this figure the force is shown to remain greater than zero as the finger is moved away from the surface due to the increased force magnitude from object penetration. FIG. 2.6 shows a closer view of the forces involved for the combined effects of delay and wall penetration. In this figure it should be clear that there is a delay present in the simulation force (shown in dashed line) and that this force also contains more variations in magnitude (oscillation) before reaching steady state. This is the result predicted for a total time delay of 40 milliseconds, which would be present for a system operating at 25 Hz in combination with the effect of surface penetration.

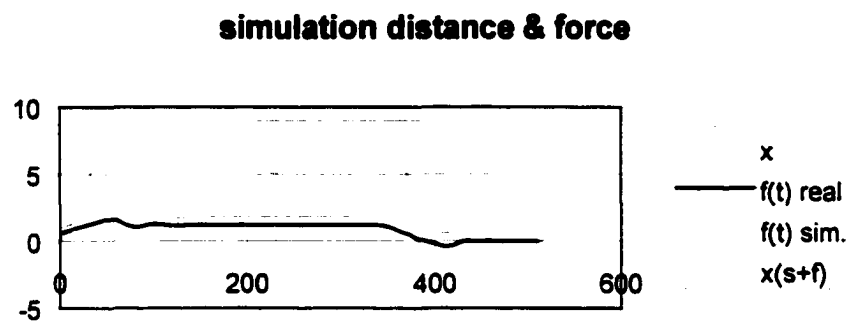


Figure 2.5 Simulation and Real Displacement & Force

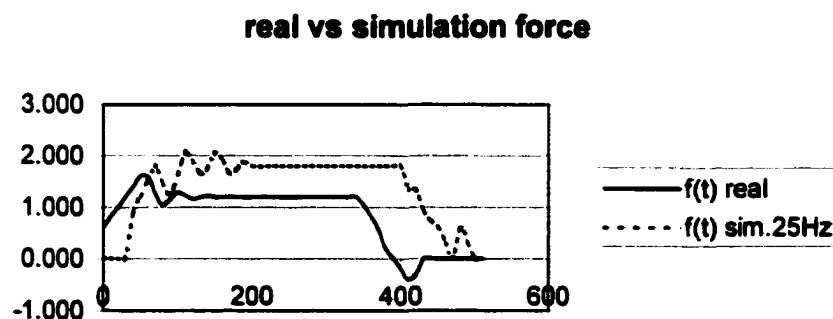


Figure 2.6 Simulation and Real Displacement & Force

In FIG. 2.7, a force response is given for a simulation that only includes a delay of 40 milliseconds and no effect of wall penetration. The force data presented here are calculated from the real wall position data and the force equation [2.5], except that each force data point is based on position, velocity, and acceleration delayed by 40 ms. One observation from this figure is that the delay results in a force being applied to the operator after contact with the object has been lost. Another observation is that the delay results in a correct steady state force, but the delay alone causes significant increases in the oscillations during all force transients.

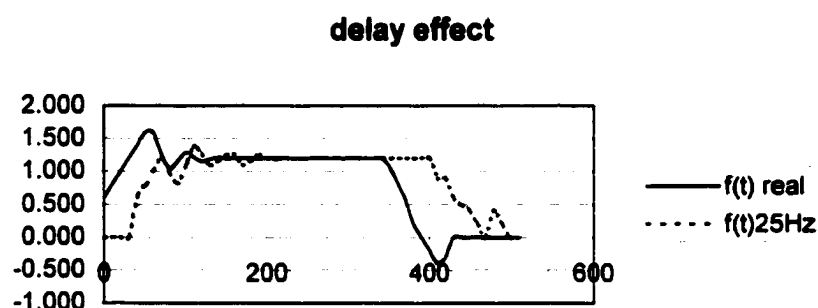


Figure 2.7 Simulation and Real Displacement & Force: Delay Effect

The effect of only the virtual wall penetration distance and no delay effect is shown in FIG. 2.8. Here the force experienced by the operator demonstrates an error of excess magnitude, and in duration extending beyond contact. Note that the penetration effect produces a larger magnitude force at all times. Both of the effects of FIGS. 2.7 and 2.8 are shown together in FIG. 2.6, would likely lead to a “lively” wall perception for the operator.

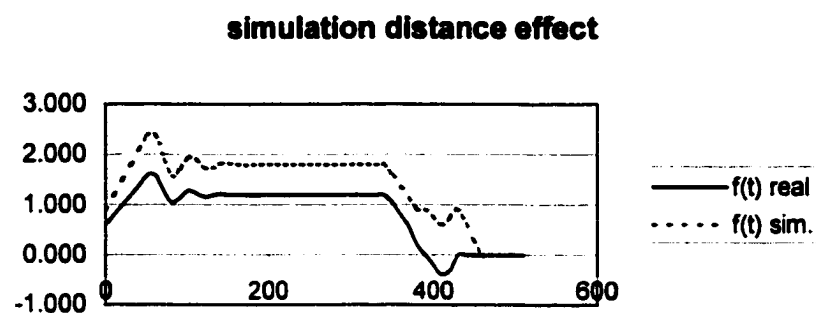


Figure 2.8 Simulation and Real Displacement & Force: Distance Effect

A simulation of the problem of instability between the operator and a haptic interface is shown in FIG. 2.9. Here the position of the simulation has been modeled so as to include an operator's response to the prior force output, as might occur when a high magnitude force is applied to the operator's finger. This is done by subtracting the force of the previous time step (multiplied by a constant) from the x_{s+f} data. One can see in this figure that the model is truly unstable, with increasing magnitude of both force and position deviations from that which would be felt while interacting with a real wall.

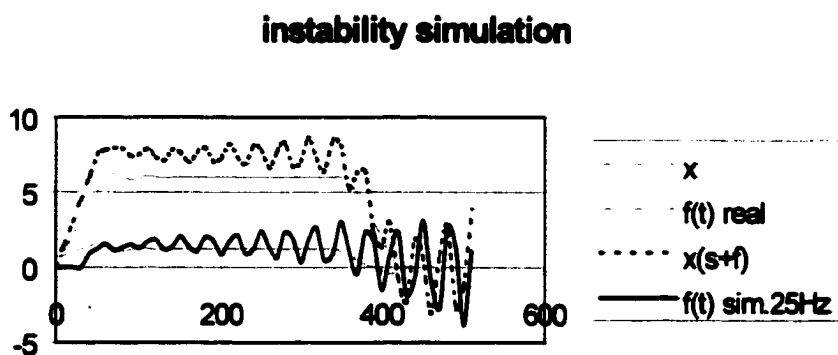


Figure 2.9 Simulation and Real Displacement & Force: Instability Model

The effect of having a simulation spring constant that was not significantly larger than that provided by the operator is shown in the model of FIG 2.10. Here it is assumed that k_{eq} is given by $k_f/2$ (100 N/m), as one would see if the simulation spring constant and the human operator's spring constant were both of the same value (eg. $k_f = k_s$ 200 N/m). It is clear that this low spring constant in combination with the other simulation effects tends to decrease the magnitude of the steady state force, subject to the assumed finger trajectory.

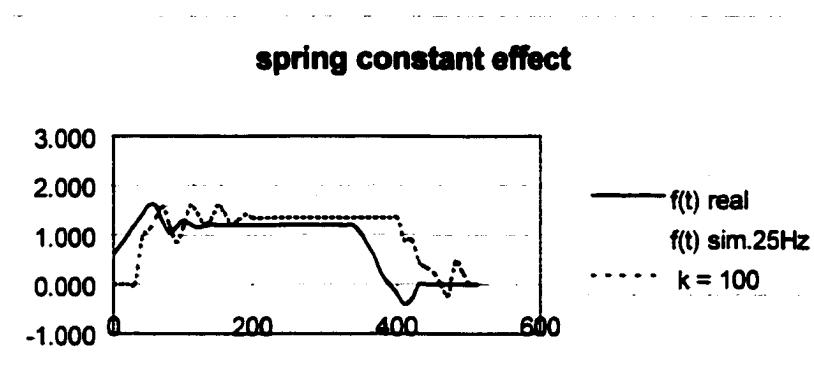


Figure 2.10 Simulation and Real Displacement & Force: Spring Constant Effect

In FIG. 2.11, the results of a similar investigation are shown. Here instead of varying the spring constant, the damping constant is varied for the simulation force output. For this study, the simulation damping constant b_s was given a value of 1.2 N s/m, which results in a b_{eq} of 1 N s/m. For a damping coefficient that is low, we observe that the force rises more slowly, and retains a high value longer after contact is lost than that of the matching $b_{eq} = b_f$ and $k_{eq} = k_f$ simulation.

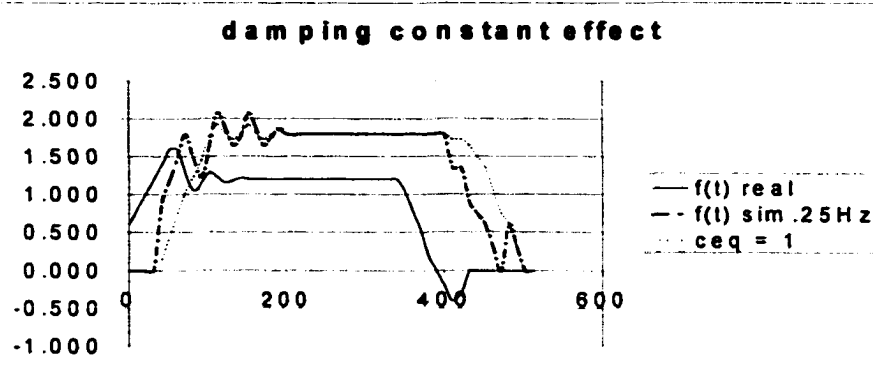


Figure 2.11 Simulation and Real Displacement & Force: Damping Constant Effect

2.7 Conclusions and System Requirements for Rigid Surface Display

Through the analysis of the preceding models of human contact with real and simulated surfaces, several conclusions can be drawn. First it has been shown that instabilities and active walls frequently reported in the literature, can be predicted by comparison of the force-time plot of human contact with a rigid surface in the real world with the force-time plot of haptic simulations provided by a traditional design and control method. One can also conclude that penetration into a virtual rigid surface (defined by high stiffness and/or damping) is a direct factor in producing the instabilities and “lively” sensations often reported. This penetration results in a step response of the actuator from a zero force level to a very high magnitude force application, with the magnitude of the force being dependent upon the penetration distance and surface stiffness and damping characteristics. It has also been shown that the stiffness and damping values of a traditional haptic simulation must be significantly greater than those of the human in order to produce a sensation resembling that experienced during real world contact with rigid bodies. Further the analysis and simulations presented in this chapter confirm (as pointed out in the literature review) that reduction or elimination of the time delay

between human position and contact force reflection will also improve stability. Also pointed out in the literature review was that due to actuator technology limitations, the reduction in delay can not be satisfactorily met through the use of presently available high-speed actuators.

One conclusion drawn from this chapter is that elimination or minimization of penetration distance will improve stability of haptic rendering of initial contact with rigid surfaces. A second conclusion is that the elimination or minimization of apparent system time delay will also improve the haptic sensation. It follows from the above conclusions that if a method can be developed wherein the surface *position* is controlled *prior to* and *during* initial contact, a more realistic haptic rendering of rigid surfaces will be apparent. Although surface position control can achieve the desired stability of rigid surfaces, means for force control is required to enable haptic force display of less rigid, deformable surfaces.

In the next chapter a system is described that through the use of a de-coupled actuator and a feed forward control algorithm, provides reductions in both the penetration distance and the delay in force reflection. The system also provides an automatic switching between position and force control algorithms permitting improved haptic display of surfaces with a wide range of stiffness and damping values. In Chapter 4 it will be shown that the proposed new system provides a haptic sensation that operators perceive to be more like that of a real surface when compared to haptic renderings of surfaces presented by traditional haptic interface design and control methods.

Chapter 3

Description of a Proposed System for Haptic Display

3.1 Introduction

In this chapter a detailed description of one embodiment of the DECAFF system for haptic display is presented. Section 3.1 provides a general introduction and overview of the overall system design while a more detailed description of the various systems is given in the following sections. Section 3.2 includes a description of the design of the mechanical systems. A description of the electrical schematic is presented in section 3.3. Computer algorithms used to control the haptic display are specified in sections 3.4 and 3.5. Finally in section 3.6 the conclusions of this chapter are presented. A prototype of this embodiment, designed for utilization in grasping tasks, was constructed and used in formal human perception experiments described in chapter 4.

The specific embodiment of the general DECAFF system for haptic display developed and tested in this research project was designed for representation of human grasp tasks. The design goals and performance measures detailed in chapter 1 can be summarized as:

1. **Provide a large workspace and represent complete 180° motion of fingers.**
2. **Provide high transparency during “free” motion simulation.**
3. **Provide a normal force to the fingertips, with an apparent real time simulation of**

contact.

4. Provide a system that offers a high degree of safety for operators.
5. Provide a system meeting the above criteria at an acceptable cost.

The haptic display system developed to meet the above criteria utilizes a planar serial linkage attached between the operator's fingertip and back of hand to transmit fingertip motion to a remote position sensing and force provision apparatus. The configuration of the remote force provision mechanism provides a means for de-coupled actuation, that results in several advantages discussed in this chapter. A feed forward position switching to force control system is implemented that capitalizes on the de-coupled actuation to provide perceptual improvement over the traditional approaches to haptic display design. A distributed computation scheme is implemented to permit the haptic display to be utilized with VR and robotic control computers. A test bed VR program is presented that provides a graphical display of a virtual finger motion that traces the operator's finger positions in real time. The test bed VR program also permits haptic evaluation of surfaces defined by a wide variety of stiffness and damping parameters. Additionally, for comparative testing purposes, a traditional haptic display control algorithm is implemented. The details of these systems are presented in the following sections of this chapter.

3.2 Mechanical Systems

To implement a grasping mode of display with a large workspace, a portable haptic

display mechanism with reaction forces grounded to the operator's body, in a location near the fingertips was developed. The outer surface of the hand opposite the palm is the area in close proximity to the finger tips that has been shown to be least sensitive to force application (14 g/mm^2) Woodworth (1938). Based on this result the back of the hand was selected as the mounting location for a hand to finger tip force display mechanism. The advantages of a portable device include lack of mechanical structure inertia to be carried by the operator in changing hand positions, lack of hand workspace limitations, and the ability to develop a simple, lightweight structure for contact force display. The disadvantage of this approach is that global force to the hand as described above can not be truly represented unless the haptic interface is attached to a master robot. In this application, it may be desirable to not have the haptic interface contain an earth grounding linkage, so that the hand position and orientation measurement can be attached to a master robot arm of precisely the same kinematic design as the slave robot arm. For VR applications, position and orientation measurement of the hand as a single point is readily available in the form of a magnetic tracker.

An initial design goal for the hand linkage was defined by two primary functions (i) measure the position of the finger as a single degree of freedom (DOF) and (ii) provide a force to the finger perpendicular to the fingertip pad. In the early design stages, it was recognized that while each finger has three DOF along the longitudinal plane, the degrees of freedom are usually not controlled independently by human beings in grasping tasks. The fore-mentioned primary functions of the design are met by a set of linkages mounted between the back of the hand and the fingertip. The interface utilizes

a four link serial planar mechanism for transmitting force resistance to finger bend toward the palm. The same linkage is utilized for transmitting output motion of the finger bend (or position of the fingertip with respect to the back of the hand) to a linear motion of a flexible sheathed cable. The hand mechanism for a single finger is shown in FIG. 3.1, and is provided with three rotational DOF, matching those of the finger in its longitudinal plane. The mechanism is also configured such that position measurement and/or force input to one of the three degrees of freedom is sufficient to represent the natural movement or restriction thereof, during finger bend, at the finger tip position. A single DOF motion representation simplifies both the mechanical structure and the computation requirements of haptic display control, leading toward fulfillment of the objectives of real time response, and low system cost.

When mounted to the hand the haptic mechanism, in combination with the hand, form a six bar closed loop kinematic chain as shown in FIG 3.1.

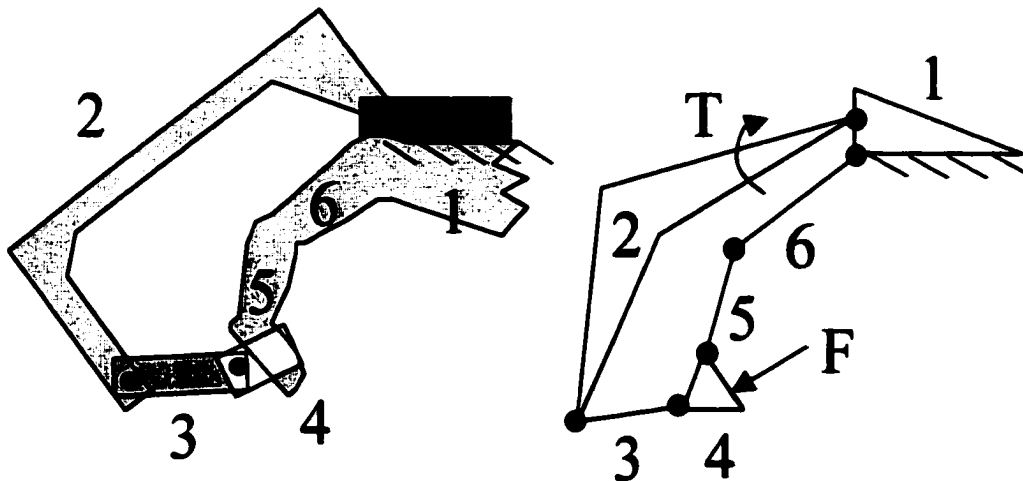


Figure 3.1 - Six Bar Linkage Formed When Operator Wears Haptic Mechanism

The six bar chain consists of the hand outer surface and the hand attachment of the haptic mechanism, which together make up link 1, the ground link. Connected to the ground link is link 2, the inverted “U” shaped link of the haptic device, which is in turn pivotally connected to link 3. Link 3 is pivotally connected to link 4, which comprises the fingertip thimble and the finger distal phalange as a single rigid body while the device is worn. Link 5 forming a pivotal connection with link 4 and link 6, is comprised of the second finger phalange, while link 6 is the proximal finger phalange.

In this linkage design, the driver for clockwise rotation with respect to figure 3.1 is link 2, driven to simulate interference with an object. However, links 4, 5, 6 can also drive the linkage for either clockwise or counter-clockwise rotation. As can be seen from FIG. 3.2, the six bar chain permits an approximate perpendicular angle formation between link 4 and link 3, throughout the range of motion.

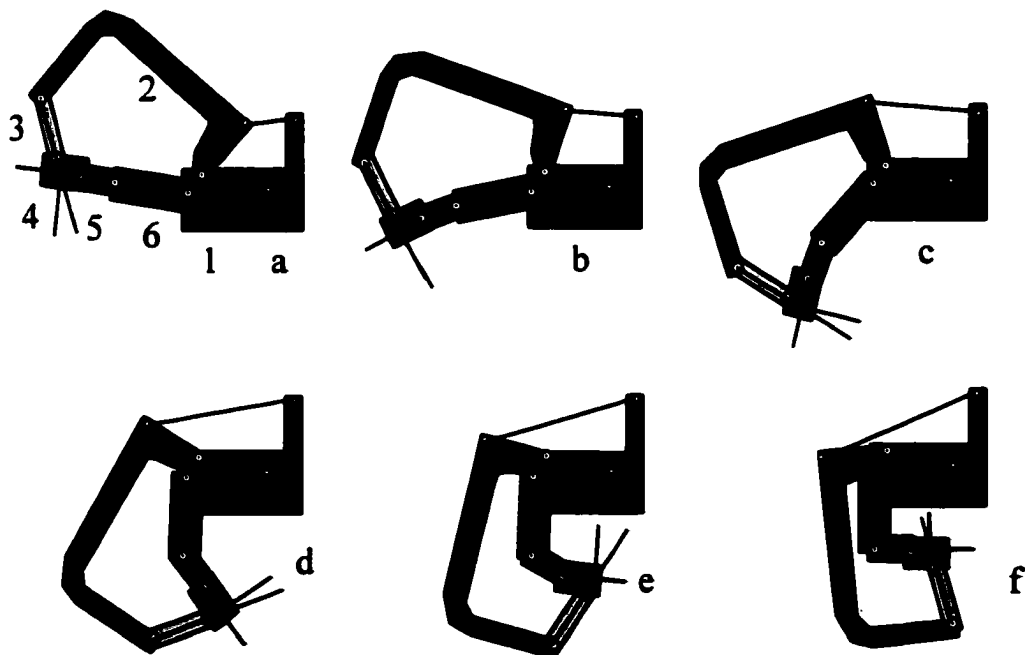


Figure 3.2 Positions of Six Bar Chain During Grasp

Because link 3 is a two force member, the force between links 3 and 4 is directed along a line formed by the two revolute joints of link 3. Considering this line of action for the force presented to the operator, one can evaluate the directional error of the force applied, with respect to normal to the distal phalange (link 4). For the positions shown, the errors (difference between angle and 90°) are as follows: (a) -20° , (b) 0° , (c) $+17^\circ$, (d) $+19^\circ$, (e) $+30^\circ$, (f) -18° . It may appear initially that an error as large as 30° would be problematic, but a closer inspection such as given in FIG. 3.3, demonstrates the quality of human adaptation to the application of the highest directional error of FIG. 3.2e. In FIG. 3.3 it is shown an observed positional adjustment by the operator during a force application, to compensate for an initial force application angle of 30° off perpendicular.

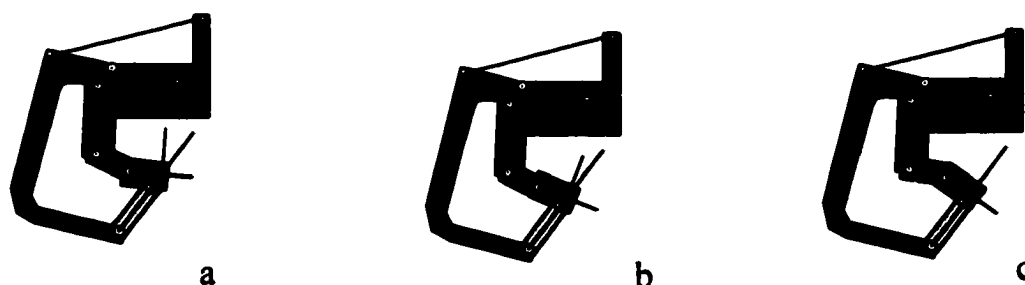


Figure 3.3 - Rotation of Distal Phalange During Force Application

In this type of compensation, it appears from informal self observation, that the operator can choose not to compensate for directional error, or in the absence of a concentrated effort, will automatically compensate for the error. This results in a change of finger joint angles from FIG 3.3a to that of FIG 3.3c, wherein the applied force assumes a normal direction. For situations when the operator does not compensate for off-normal directions, the sensation (for angular errors in the less than 30° range) does not appear

erroneous. This is presumably due to the improved ability to sense relatively large magnitude forces primarily in the normal direction.

The hand mounted mechanism is capable of representing the fingertip position throughout a wide range of grasping motions (FIG. 3.2). The motion of the finger during grasp can be represented as a single variable, indicated by the rotational position of link 2. This single variable representation is not completely unique, since several relative link angles are possible. The range of relative link angles is quite small and thus introduces a small amount of uncertainty in fingertip position. It is argued that in the absence of visual information regarding precise finger phalange rotational positions, the errors will be substantially transparent to the operator. For this argument, we need only consider that in both VR and tele-manipulation tasks, the visual information utilized is that of the virtual hand or slave manipulator, respectively. Additionally, one should consider that the attention level asserted toward the actual operator's finger joint positions, is presumably rather small in a highly over learned task such as grasping.

The hand mounted linkage assembly as described above is successful at representing a three DOF fingertip motion as a one DOF first link rotation motion. Because the motion of each finger is represented by a single degree of freedom (rotation of the hand mounted link is proportional to finger bend angle), the measurement of and resistance to motion can be performed remotely. In our design remote actuation was implemented by using a sheathed cable for motion transmission. With remote position measurement and force application apparatus, the bulk and weight of these systems need not be carried by the operator, leading to increased transparency. Cable transmission has an apparent

disadvantage of high friction, but the cable demonstrates a friction force that is proportional to cable tension. This can be used as an advantage in haptic display, because under conditions of free motion, the cable tension is minimal, and thus the frictional force is also minimal. Conversely, when contact with an object is made the tension in the cable is increased with a corresponding increase in the cable friction. The increased cable friction is in the direction that opposes motion, and thus yields the desirable quality of increasing the force of the operator's finger required to further bend the finger after simulated contact with an object, permitting a magnification of the actuator force to be applied to the operator. Further, if the force on the remote end of the cable is increased, the friction of the cable is increased in a direction opposing motion, thus preventing the perception of fluctuations in forces to the operator's hand, while actuator forces may be fluctuating.

Attached to the remote end of the cable is a pivotal link called the replicated finger, as shown in FIG. 3.4. The replicated finger pivots on the input shaft of the position measurement potentiometer that converts the motion of the replicated finger, which is proportional to the operator's finger bend, into an analog voltage signal. The voltage signal is read into the haptic control PC, by a single ended analog input of the DAQ board. The analog voltage signal is converted to a digital value for use in controlling the slave finger positions and in control calculations as described in the following sections. The replicated finger described above is also used to present forces to the fingertip, which resist finger inward bend. This is possible because the replicated finger as described above accurately reflects the motion of the operator's finger as a single

degree of freedom pivoting link, and resistance to motion of the replicated finger provides a proportional resistance to the operator's finger.

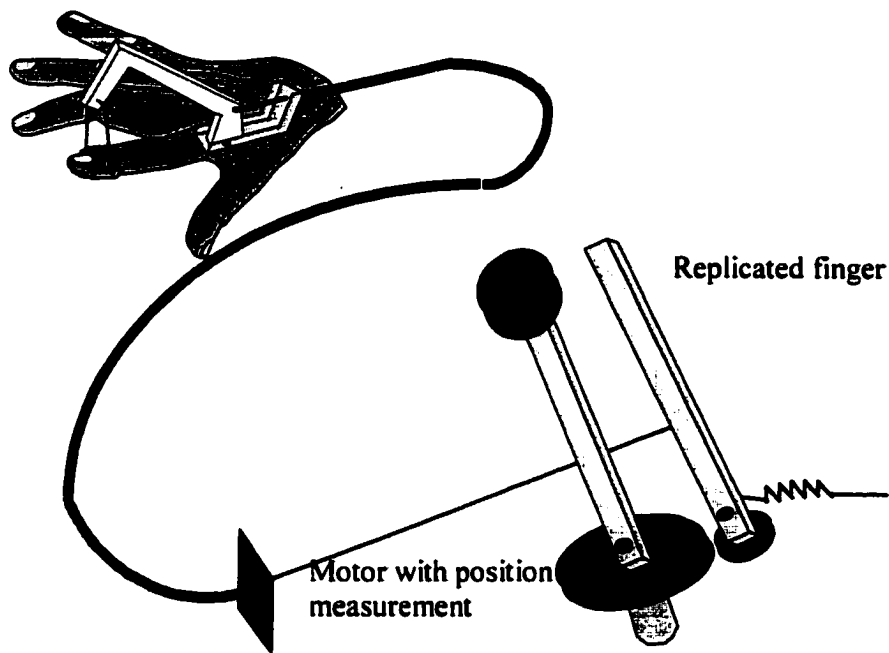


Figure 3.4 - Hand Mounted Mechanism, Measurement & Force Display

The resistance to replicated finger motion is provided by the contact drum, which is capable of occupying a position that under control of the computer selectively interferes with replicated finger rotation. After initial contact the force available at the contact drum can be controlled by PWM through the haptic control PC. PWM control permits the contact force to be lowered as a percentage of the maximum force, F , to correspond with either a scaled force sensed by the robot, or a calculated virtual contact force.

With the system described above, a design has been developed of a mechanical system capable of transmitting finger position, selectively assuming an interfering and non-interfering position, and displaying a variable and controllable stiffness. This is done while requiring only minimal control I/O of replicated finger position measurement, motor position measurement, and digital motor output. The number of control parameters is very important, because the cost and computer execution time both increase with the number of control parameters.

3.3 Electrical Systems

The electrical system includes two main circuits, as shown in the schematic of FIG. 3.5. A first circuit is for driving the 12 VDC motor and the second circuit is provided for reading replicated finger and motor positions, and communicating with the control PC. The motor driving circuit includes a 120 V primary, 14V secondary, 120 VA transformer for providing a 14 volt AC supply from a readily available 120 VAC standard outlet. The 14 volt AC supply at the transformer secondary winding is converted to a DC signal by the bridge rectifier. As some power is dissipated in this conversion, the DC voltage available at the bridge rectifier is approximately 12.5 volts. The positive side of the 12.5 VDC supply is protected by a 3 amp circuit breaker. Normally open limit switch LS1 is provided along the positive line, permitting motor operation only when the operator steps on the foot switch. This is included to insure complete safety for the operator, as they may instantaneously stop all force display by lifting their foot from the switch. Solid state relay R1 is used to control the power supply to the motor. The coil side of this relay appears in the second PC control circuit.

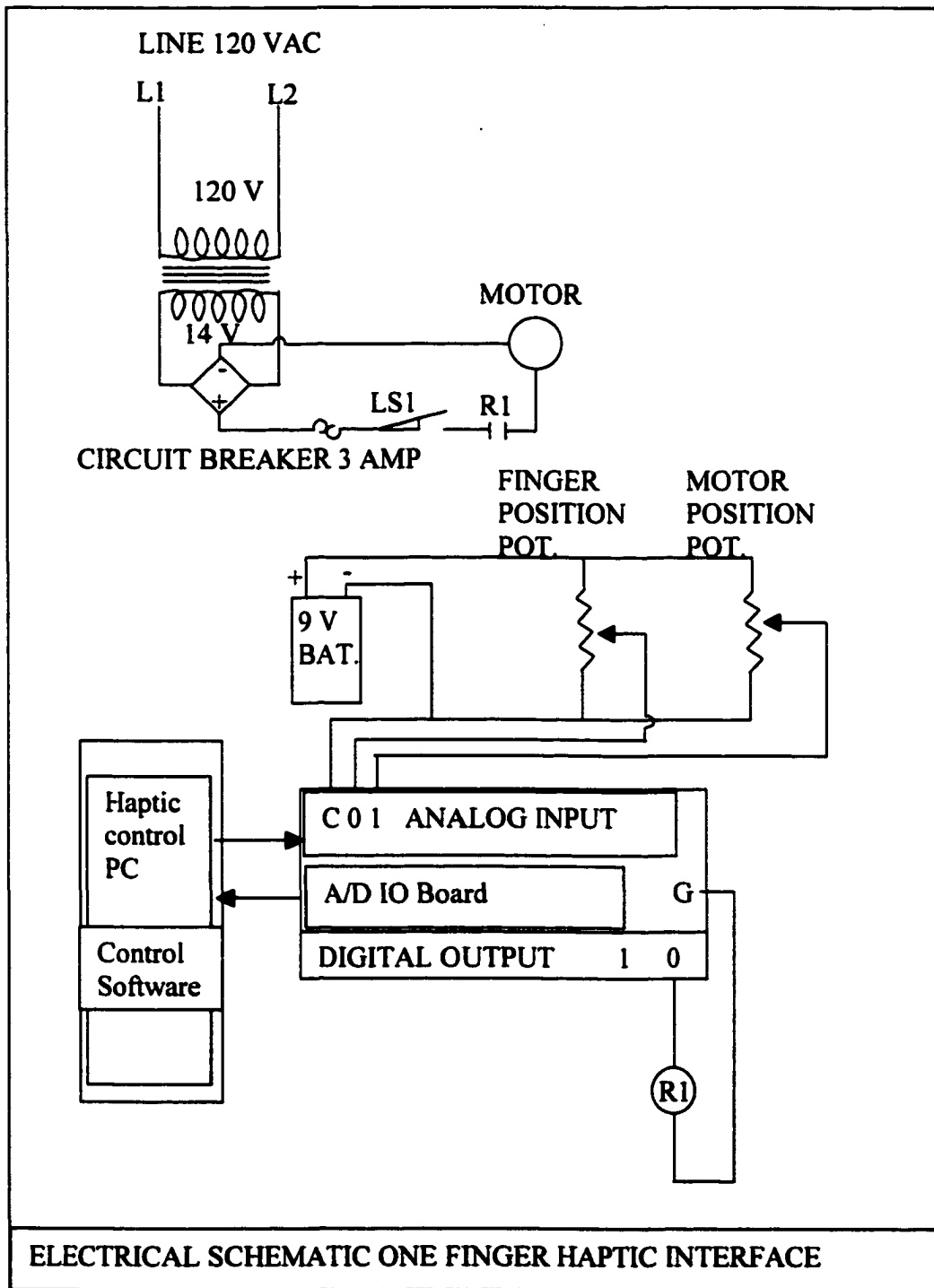


Figure 3.5 - Electrical Schematic

Although shown in the schematic as electro-mechanical relays, the solid state relays do not employ a traditional coil and contact arrangement, but rather utilize opto-isolated transistor based switching, which can very quickly respond to the input signal. These output modules which require specific positive and negative load connections, can respond in approximately 75 μ sec and permits digital logic TTL level inputs to switch up to 2 amps of DC load current.

The PC control circuit receives external power from a standard 9 V battery. The battery provides power for two potentiometers per finger, used in the measurement of the finger bend position and the motor position. The potentiometers are also single ended connected to the A/D multi-function I/O board. Single ended connections were used since a total of 16 single ended inputs are available on the specified board (compared with 8 differential inputs), which will be needed if additional finger force displays are implemented. For single ended connection, the negative lead of the potentiometers must be connected to the reference voltage input of the A/D board, indicated by C on the schematic.

The A/D board utilized in this project is distributed by Intelligent Instrumentation Co., model number PCI-20498, which has general specifications of 16 channel single ended 100 kHz A/D, 12 bit, 2 D/A channels, 16 Digital I/O channels, clock and rate generator functions. The board is supported by Visual Designer icon-function block programming language, and C, C++ drivers available from the board manufacturer. This model has a terminal board that plugs into the A/D board at the back of the control PC, through which field wiring is connected. The PC control circuit also contains a

relay coil symbol, representing the solid state relay type output module. The output module is connected between the board ground and a digital output terminal. The input to the output module is polarity sensitive, and thus care must be taken to connect the sourcing lead to the positive pin, or sinking lead to the negative pin. Thus in the present design, R1 which controls the motor is controlled by digital output port 1, bit 0, while port1, bits 1,2,3, etc. can be used for motors to provide force to additional fingers.

3.4 Control Software

The control system includes a distributed computing platform as has been utilized extensively in the haptics field. The present platform consists of a haptic control PC for execution of all haptic device data acquisition and control algorithms, connected by a standard RS-232 serial cable (null modem cable) to either a slave manipulator control computer, or a virtual reality simulation computer. The haptic control PC software is implemented in C++ language. The haptic control code has three main algorithms: (1) configure multi-function I/O board and calibrate for the individual user finger motion, (2) contact position control for initial contact with virtual objects, (3) variable magnitude force display control. The configuration and calibration algorithm performs DAQ board initialization functions and a user calibration routine. The calibration routine requests the operator to fully extend and retract their fingers, during which the program records the minimum and maximum voltage signal delivered by the finger bend potentiometers. Subsequently, the finger bend angle (β) for finger (i) is then calculated by:

$$\beta[i] = 180 * (\text{read_volt}[i] - \text{pos_low}[i]) / (\text{pos_high}[i] - \text{pos_low}[i]) \quad [3.1]$$

Where $read_volt[i]$ is the current voltage of finger bend potentiometer for finger (i), $pos_low[i]$ and $pos_high[i]$ are the lowest and highest values of the potentiometer voltage recorded during calibration, reflecting a voltage associated with a fully extended and a fully retracted finger, respectively. Equation [3.1] delivers a value of 0 to 180 degrees for the current position of finger (i), wherein 0 degrees corresponds to a fully extended finger and 180 degrees reflects a finger position completely retracted to the palm as shown in figure 3.6.

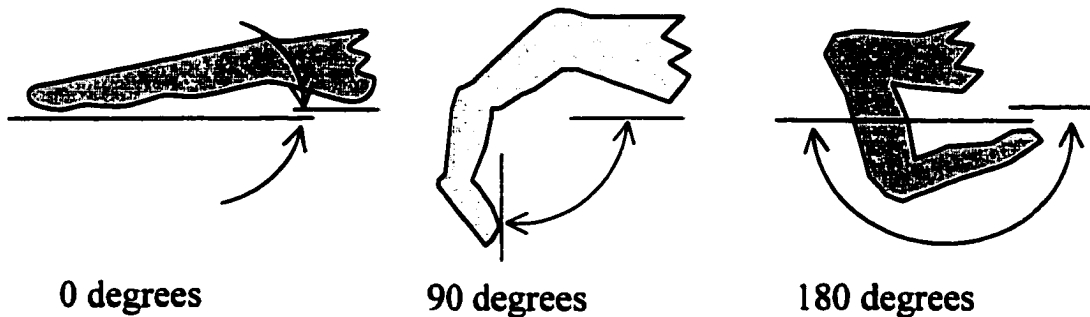


Figure 3.6 – Finger Position Coordinates

In order to calibrate the motor position control, a screen prompt asks the user to fully retract their fingers and allow the contact drum to extend the fingers under a loose grasp. The control algorithm then advances the contact drum, periodically recording the voltage of the motor position potentiometer when the finger bend is at predetermined intervals. This mapping yields a contact drum position accuracy of ± 2 degrees with respect to the replicated finger position for recorded replicated finger position intervals of 20 degrees. For the present implementation test bed, the global position of the hand is not recorded, as the grasp task only is under investigation. Position control variables for each finger,

denoted by subscript i , are shown in FIG. 3.7. The interface between the master and slave controller is shown in FIG. 3.8.

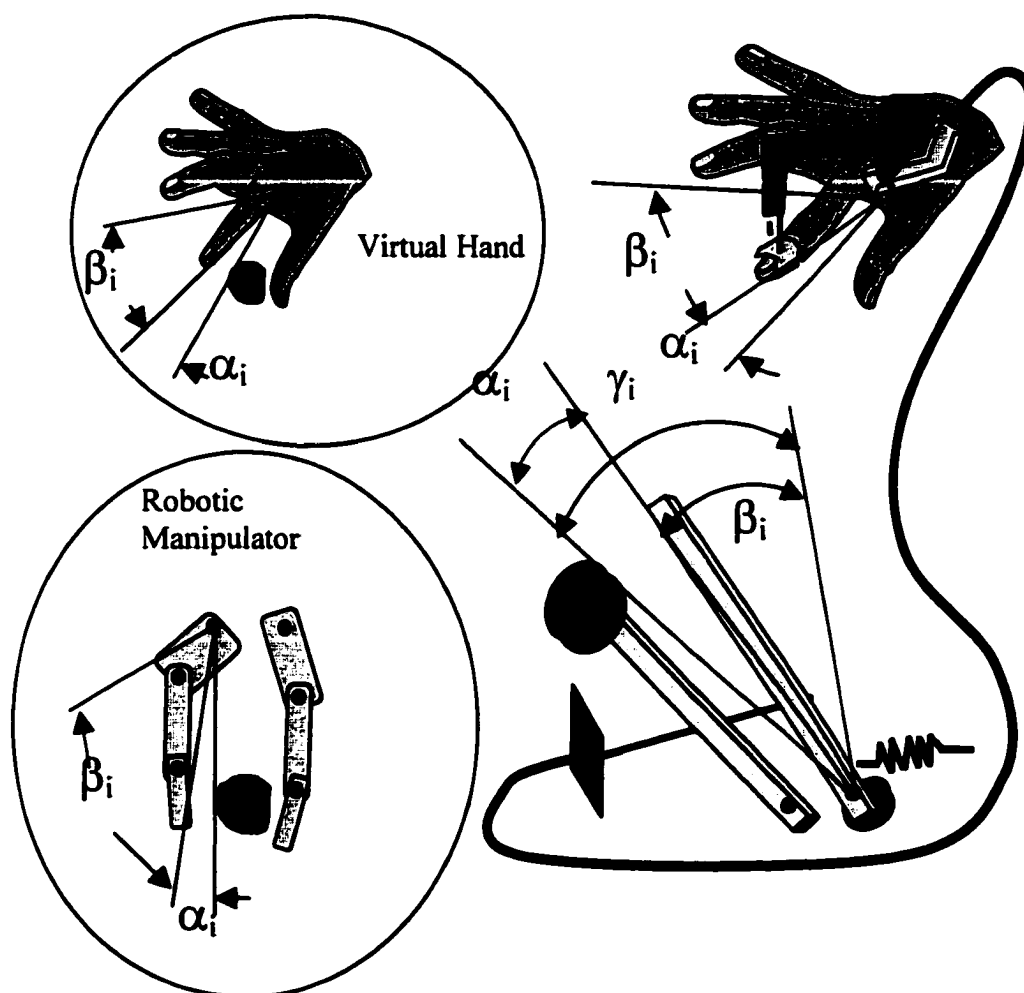


Figure 3.7 – Position Control Variables

Finger bend angle (β) is provided by periodic calls to the finger bend routine described above. Bend angle (β) is measured at the master and sent to the slave to control the position of the slave finger. Pre-contact distance (α) and force magnitude (F) are measured (or calculated) at the slave and sent to the master to control the contact drum position or force. The goal of providing fast response and highly stable contact sensation

display is accomplished by selectively controlling the position or force of the contact drum as follows. Prior to contact between the slave and any slave environment object, the force (F) sent by the slave to the master is zero and the pre-contact distance (α) is greater than zero. In this case, position control is used. If there are no objects within the range of pre-contact distance (α) sensing, the value of α sent by the slave is a maximum range value (α_{max}). If an object is within the range of distance sensing, the measured or calculated value of α and a force (F) of zero is sent by the slave to the master for each finger. The master controller uses the distance value (α_i) to calculate the contact drum position (γ_i) for each finger (i) as follows.

If pre-contact distance (α_i) is greater than a predetermined constant offset distance (α^*), the contact drum for finger (i) is controlled to assume a position (γ_i) as:

$$\gamma_i = \alpha_i + \beta_i \quad \text{for } (\alpha_i > \alpha^*) \quad [3.2]$$

If the operator moves a finger (i) closer toward the palm, so as to cause the slave finger (i) to become closer to an object in the slave environment than the offset distance (α^*), the proximity contact drum position (γ_i^*) is defined as:

$$\gamma_i^* = \alpha_i + \beta_i \quad \text{for } (\alpha_i(t) \leq \alpha^*) \quad [3.3]$$

$$\text{and } (\alpha_i(t-1) > \alpha^*)$$

where $\alpha_i(t)$ is the pre-contact distance of the current calculation cycle and $\alpha_i(t-1)$ is the pre-contact distance of the previous calculation cycle. While the slave finger is closer to an object than the offset distance (α^*), the contact drum is controlled to maintain the proximity position (γ_i^*).

$$\gamma_i = \gamma_i^* \quad \text{for } (\alpha_i \leq \alpha^*) \quad [3.4]$$

If the operator retracts their finger to a position that results in contact between the slave finger and a slave object, the control method used depends on the slave contact force magnitude. For slave objects that are rigid or have a high stiffness (K) and/or high damping (B), the force (F_i) sent to the master by the slave makes an instantaneous step from a value of 0 to 100%. In this case, position control is continued.

$$\gamma_i = \gamma_i^* \quad \text{for } (F_i \geq 100\%) \quad [3.5]$$

For slave objects of lower stiffness and damping, the force will gradually increase with the penetration distance (x) and velocity (x'). With these objects the slave sends a contact force:

$$0 < F_i < 100 \quad [3.6]$$

In this case, the master controller executes the variable magnitude force control algorithm.

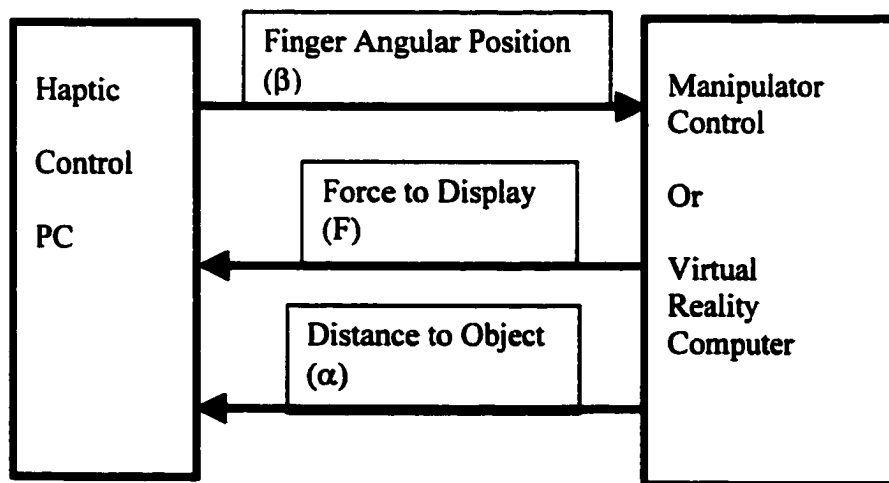


Figure 3.8 - Interface definition

To display a variable magnitude force, the control algorithm uses pulse width modulation (PWM) torque control to the motor driving the contact drum as shown in FIG. 3.9. The force applied to the operator's fingertip is proportional to the motor torque.

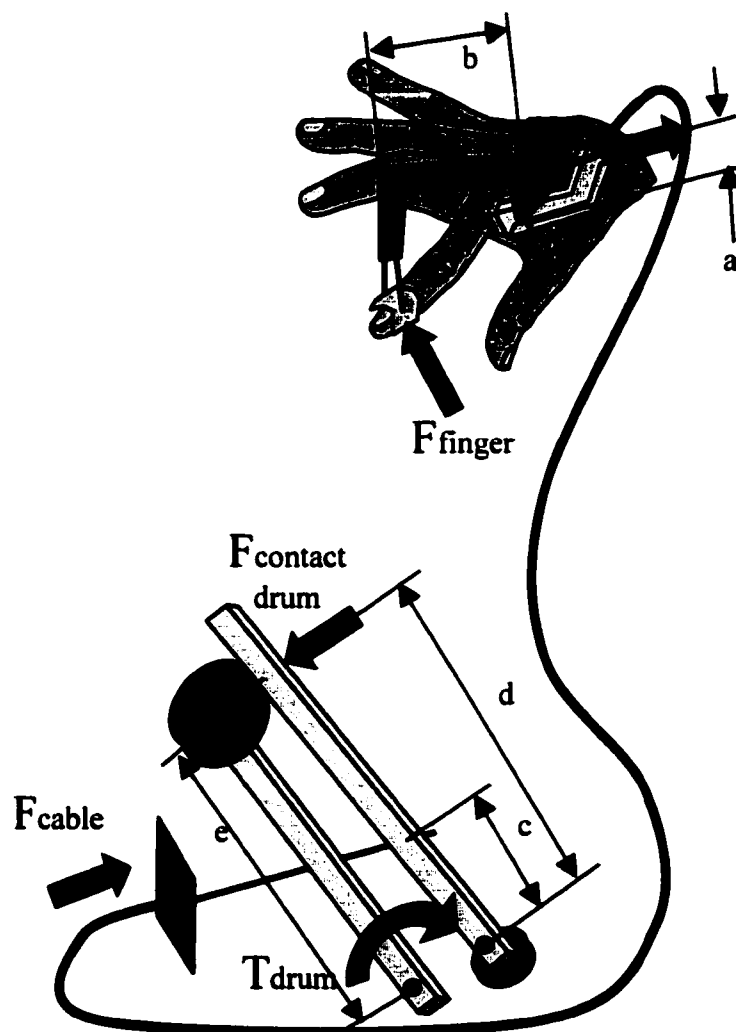


Figure 3.9 – Variable Force Display

Neglecting cable friction, the fingertip force is given by the following geometry based (constant) function of contact drum torque:

$$F_{\text{finger}} = (a/b) * (d/c) * (1/e) * T_{\text{motor}} \quad [3.7]$$

Where lengths a, b, c, d, and e are depicted in FIG. 3.9.

The contact drum is driven by the DC motor (not shown) and thus delivers a torque to the replicated finger that is linearly proportional to the DC motor torque. The torque of the DC motor is linearly proportional to the current supplied, at rated voltage.

Knowing the desired force to be displayed, either by a scale of manipulator force or determined as a function of penetration distance and object stiffness (EQ. 1.1), and by *a priori* measurement of the maximum fingertip force that can be delivered by the system, we can present a PWM ($\Phi = \% \text{ of stall torque}$) controlled force as follows:

$$\Phi = F_{\text{finger}} (\text{desired}) / F_{\text{finger}} (\text{max}) \quad [3.8]$$

The force delivered is dependent on the penetration distance, and as with prior haptic displays, during this mode the penetration distance will be that given by the previous finger bend input and virtual reality environment calculation. To implement PWM force control within the haptic PC, several motor control calculation cycles are required. The basic implementation is such that for a given percentage of maximum force (Φ), the motor digital output is given an “on” signal for a corresponding percentage of calculation cycles followed by an “off” signal for $(1 - \Phi)$ cycles. For example an 80% of stall force ($\Phi = 0.80$) is delivered by giving 4 “on” signals to the motor followed by 1 “off” signal, repeating the sequence. Two nested loops are utilized to provide a continuous variation in Φ between 0 and 1. For example if the value of $\Phi = 0.64$, the inner loop provides an

“on” signal during 2 of 3 iterations, and the outer loop provides an extra “off” signal during every 37th iteration. In this example the value of 64% force is approximated in the present implementation by “on” cycles of $2/3 - 1/37 = 0.6396$.

3.5 Slave Simulation Software Test Bed for Virtual Finger

In order to facilitate testing of the proposed design and control method for haptic interfaces, a test bed software program for graphical display of a slave finger was developed. The VR slave finger test bed software runs on a separate PC as indicated by figure 3.8. In this software, the operator’s finger position is received from the haptic control PC and is used to provide a graphic display of a virtual finger in a position provided by the haptic PC. Thus while both programs are executing, any motion of the operator’s finger is reflected as motion of the virtual finger. Also included in the VR slave test bed program are routines to provide user definable placement of a slave surface, and to define a force developed by contact with the surface, described by EQ. [1.1]. Therefore the VR PC test bed software in combination with the hardware and haptic PC control software described earlier provides a complete prototype of the design and control concepts proposed in this research. The system was implemented for a single finger to permit accurate testing of the performance of the proposed DECAFF haptic interface design and control method.

To operate the VR PC test bed software, the operator is initially provided a text screen menu that allows selection of surface placement, definition of surface stiffness and damping coefficient. The object placement is provided by a value of 0 to 180 degrees

and is taken in with respect to the virtual finger coordinate reference frame. Therefore a virtual surface placement of 0 degrees results in a surface that is at the fully extended finger position, while a surface position value of 90 degrees results in placement of the virtual surface at the midpoint between a fully extended and a fully retracted position. The operator must also select values for the stiffness (K) and damping (B) coefficients of the virtual surface from the initial menu. These values are used in calculation of the force to be displayed while the virtual finger is in contact with the virtual surface. After selection of the above values the VR PC software provides a graphical display of the virtual finger in its present position and the virtual surface.

Should the operator retract their finger to a position beyond the virtual surface position, the VR PC software calculates a force to be displayed based on the magnitude of interference between the virtual finger and surface and the velocity of the virtual finger. This instantaneous force of contact is then sent via serial communication to the haptic control PC for haptic display to the operator. To provide for feed forward control, the VR PC program also calculates the difference between the slave finger position and the virtual surface position. This difference is the pre-contact distance (α). To provide for a faster serial communication between the two PC's, the pre-contact distance and the force to be displayed are sent as a single variable, coded for transmission and decoded by the haptic control PC. The coding permits transmission of both the pre-contact distance and the force information to be represented by 8 bits of data (i.e. an integer between 0 and 255). Values less than 51 are decoded to represent the pre-contact distance as measured in degrees. Values of 51 through 151 are decoded by subtracting

51 from the transmission data to indicate the force (as a percentage of the maximum haptic device output) to be displayed. The communication routine and coding described above is implemented for 9600 baud serial communication through traditional RS-232 ports. This implementation provides satisfactory data transmission speeds for the VR slave test bed, however one could expect to improve the information transmission speed by utilizing other improved technology communication methods such as high-speed ethernet or USB high-speed serial port.

3.6 Conclusions of the Proposed System Description

In this chapter a detailed description of an entire system for haptic display has been presented. The proposed system incorporates a mechanical design that offers two fundamental improvements over previously proposed systems in the haptics research field. First, our design is novel in that it is the first reported de-coupled actuation in the haptic field. This permits selective contact and non-contact conditions to be represented with a large instantaneous difference in the impedance to human motion. Secondly, another novel contribution to the haptic community is the use of feed forward information on impending contact. These novel elements, in combination, permit a computational advantage for any class of force reflecting haptic interface design. The computational advantage is especially relevant for grasp tasks because when grasping an object, people must first move their hand near the object with the fingers forming a pre-grasp shape larger than the object to be grasped, and then bend their fingers toward the palm to grasp the object (Klatzky, et.al., 1996). The use of de-coupled actuation and feed-forward control allows movement of the contact drum to a position such that it will

interfere with finger bend while in the pre-grasp formation, *before* the finger has begun to bend inward to grasp a virtual object. This results in better system response time for grasp tasks. The proposed arrangement compares favorably to directly coupled actuators (employed by all prior haptic interfaces) in that direct-coupled actuators provide a force only *after* virtual finger/virtual object interference. Another advantage is that the actuator need not be driven in contact with the user or be back driven, during free motion in order to appear transparent to the user, and thus permits higher transparency with a lower cost motor. Additionally, the de-coupled actuator provides advantages of increased stability during grasp tasks (since the contact drum is essentially stationary), and the ability to present high stiffness virtual objects.

The feed forward information provides a method to completely eliminate time delays inherent to prior proposed haptic display devices. The time delays in traditional haptic interfaces have resulted in the lack of ability to accurately represent a fundamental entity: rigid surfaces. Prior designs have been plagued with instabilities when programmed to deliver high stiffness surfaces and have thus been forced to resort to display only surfaces of lower stiffness than are present in the real world. Additionally the inherent time delays present in prior designs have resulted in an always-present error in the position of contact provided to the operator compared to that present in the remote environment. This positional error has prevented true master control of slave position during periods of initial contact, thus requiring special exceptions in control algorithms for virtual slaves, causing the graphic display of the slave to not truly represent the position of the master. For robotic slaves, the exception handling requires

system imposed constraints on the human and master velocity to prevent extreme forces of contact due to the lag between slave and master positions. The system imposed velocity constraints prohibit natural motion and thus limit the intended purpose of tele-presence systems, that is to utilize the highly developed (and high speed) motion control skills in humans to control the robot.

The mechanical systems presented in this chapter offer the research field a fresh approach to haptic interfaces specifically designed for grasping tasks. The new approach provides for remote location of position sensing apparatus, through the use of a single mechanism for both human position measurement *and* impedance to motion (force) provision. This approach permits an extremely large workspace with reduced weight and physical connections between the operator's hand and the simulation environment. Also presented is a mechanical linkage design that can represent the finger grasping motion as a single variable while simultaneously permitting a full range of finger motion and providing of forces in a direction substantially normal to the distal finger pad throughout the entire range of motion. This combination of features was not available to the field prior to the present research project. Previous attempts at hand mounted single controlled degree of freedom finger tip force displays have provided forces that vary widely with finger bend angle, and/or are able to represent motion through only a fraction of the 180 degrees of real finger bend motion. Additionally because there are two uncontrolled degrees of freedom, the linkage is effective for a variety of operator's hand sizes, without the need for adjusting link lengths.

Chapter 4

Human Factors Experiments

4.1 Introduction

In order to evaluate the effectiveness of the system described herein, human perception experiments were conducted. The primary goal of the human perception experiments was to provide an indication of the effectiveness of the DECAFF design and control system as compared with that of traditional control. The effectiveness can be measured by several output parameters including, (i) ability to display a surface accurately perceived as a rigid object or “virtual wall”, (ii) stability while contacting the edge of a surface, and (iii) ability to accurately detect initial contact position with the boundary of a surface across a large range of defining surface parameters (i.e. stiffness and damping). Perception of a rigid object can be readily evaluated by performing a side by side comparison of the proposed DECAFF system with that of traditional haptic displays. After a side by side presentation of similar surfaces, subjects can respond to which surface is *feels* more like a wall in a forced choice response experiment. The stability of a surface can be quantifiably measured as an amplitude of oscillation that occurs during contact with the boundary of a virtual surface. While the first two parameters above have been discussed frequently in the literature, the third has received very little attention. This is because traditional control of haptic interfaces require a penetration of a virtual surface by the slave entity in order to display a force of contact, and virtual reality visual outputs can be easily programmed to display no slave/virtual object penetration. In

robotic tele-manipulation applications, auxiliary control algorithms are typically implemented to prevent the robotic manipulator from penetrating a slave environment object of interest. However for both of these applications, the accuracy of perception of initial contact remains an important measure of haptic interface performance. If the field is ever to advance to an ideal system of completely transparent and “real time” tele-operation, a very accurate perception of contact position by the haptic interface user coincidental with the actual contact position of the slave is an absolute system requirement.

Another parameter that gives an indication of improved performance for haptic displays is the ability to provide improvements in any of the above (wall-like perception, stability, or accuracy of boundary detection) while operating at a lower system signal throughput rate (or bandwidth). This final parameter describing the ability to operate with the same or better fidelity while at a lower speed is useful in that the virtual computer is less taxed by the haptic system, freeing more resources for the virtual environment calculations. In physical tele-operation, the ability to operate at a lower speed provides a means to decrease the system imposed delay during grasping tasks, providing a haptic interface rendering that more closely matches the real (high speed) haptic sensations. For both applications, the ability to operate at a lower speed not only overcomes present computing technology speed limitations (which are sure to be reduced as this technology advances), but also provides a permanent solution to actuator response time technology limitations, which are much less likely to be drastically reduced in the near future.

In this chapter the procedures used for the experiments, the results obtained, and a statistical analysis of the results are discussed. The results, as measured by the effectiveness criterion outlined above, demonstrated considerable improvement with the proposed DECAFF system in all areas. Statistical analysis is used to evaluate the variability in results obtained, as well as establish confidence intervals for any conclusions drawn from the experimental data. Additionally the statistical analysis is used to construct predictive models of human haptic performance under test conditions and to evaluate the applicability of results of the 12 subjects tested to the general population. Although human subjects traditionally perform psycho-physical tests with a high degree of variability, as they did in this experiment, overall confidence levels in the performance improvements remained quite high. A 99.9% confidence level for reduced amplitude oscillations and a 95% confidence for improved boundary detection accuracy while using the proposed DECAFF system is indicated by the results. This demonstrates an exceptional degree of confidence in the improved haptic perception provided by the DECAFF design and control method, under the test conditions.

4.2 Experimental Procedures

For the human factors study, twelve subjects were selected. The subjects were graduate students, age 22-40, 7 male and 5 female. The general approach to the study was to have each subject compare the touch sensation of a variety of surface pairs. Before participation in the study subjects were given the following standard introduction to the experiment.

Experiment Introduction

This experiment is designed to help evaluate the human perception of touch sensations of various surface models. The experiment uses a new force reflecting glove, which can present a resistance to finger grasping motion. In general use, the glove measures the operator's finger positions and uses these positions to control the positions of a virtual or robotic slave hand. Forces that are sensed or calculated for the slave hand are presented to the operator as resistance to finger bend.

The test apparatus used in today's experiment utilizes a virtual slave hand, and only the index finger will be used. The virtual finger is programmed to follow the motion of the operator's finger and will reflect forces of contact as the virtual finger enters the virtual object or surface. Several different surface models characterized by the stiffness, damping and display frequency will be presented to each subject for evaluation.

For this experiment there will be 12 trials, each trial consisting of the presentation of two surfaces. For each surface, you will be asked to identify the location of the surface edge. Surfaces will be presented in pairs, and you will be asked to choose which surface is more rigid (or harder), and to comment on or provide a comparison between the pair of surfaces relating to the touch sensation you experience. (ie. What does it feel like?, Which is more comfortable?, etc.)

While you are evaluating the surface pairs, you will not have any visible graphic display of virtual finger positions.

Thank you for participating in this experiment and contributing to the research progress.

Subjects were initially trained in how the system functioned, wearing a single finger mechanism as described in chapter 3. For initial training, subjects could watch a virtual finger motion follow that of their real finger, and could feel the touch sensation as the virtual finger contacted a virtual surface. After the training session, subjects were not permitted to see the virtual finger monitor and thus had to rely solely on the touch sensation to report their perceptual experience.

The experiment was designed as a two level, three variable factorial design, conducted with both a traditional control algorithm and with the proposed DECAFF system described in Chapter 3. As will be discussed later, the experimental design also permits analysis as a two level four variable experiment, considering the control method as the fourth variable. This type of experimental design permits a scientific assessment of the effects of several variables and seeks to randomize all sources of variability and error. The formal analysis of the experimental data that contains multiple measurements for each variable reveals the real effects of the input variables and interactions thereof. These effects can then be evaluated in terms of statistical certainty in order to draw scientific conclusions as to the overall system performance metrics. Several output parameters were recorded as a measure of system effectiveness. A forced choice response as to which of two surfaces felt more like a wall was the first performance measure recorded. A forced choice response was selected to eliminate a potential source of biasing error that can occur when subjects are asked to rate the perception of a numerical scale. Secondly, the accuracy at which the subject could detect initial contact with a surface was recorded. Finally, the amplitude of oscillation immediately preceding subject identification of surface boundary position was measured and recorded. Because learning during the course of the experiment was believed to be a possible source of error (in that some subjects may learn to perform better as the experiment progressed), the sequence in which the surface pairs were presented was randomized for each subject. For the same reason, the actual position of the surface boundary was randomly varied between 40 and 70 degrees with respect to the fully

extended finger position for trials throughout the experiment. This range of motion was selected as that frequently used in human grasp motions.

One additional parameter measured was the maximum finger velocity prior to contact with the virtual surface. Because this measure would be difficult to control by subject instruction, it was measured as a blind variable, wherein the subjects were not given any instruction as to how fast to move their finger, but rather the actual maximum speed at which they retracted their finger was recorded without subjects' knowledge. The finger velocity prior to contact was believed to be a factor that may contribute (as an input variable) to the level of penetration into the virtual surface before application of any force, as discussed in the mathematical modeling section of Chapter 2. Thus, a higher velocity before contact is expected to result in a higher degree of instability, and a lower degree of accuracy in surface edge detection.

The DECAFF system implementation for the experiment was identical to that described in chapter 3 for a single finger device. The pre-contact distance offset (α^*) was set at 30 degrees. Unobstructed motion contact drum lead (α_{\max}) was set at 50 degrees. The traditional control system was implemented with the same hardware, but had a modified control algorithm to model a traditional design (described in Chapter 1). The haptic PC algorithm for the traditional control model controlled the contact drum as follows:

1. During operator finger motion while the slave is not in contact with any slave environment objects, the contact drum is position controlled to follow the replicated finger position, offset by 0 to 1 degrees ($0 < \alpha < 1$). This is done to simulate an actual

physical coupling between the contact drum and the replicated finger as would be required by a traditional approach to haptic display design for a system similar to the one under investigation. The coupling of the two components was done via control method rather than by physical means to permit rapid changes between traditional control and the proposed DECAFF system during experimentation.

2. When contact is made with a virtual object, the contact drum is immediately force controlled to provide a force given by $F = Kx + Bx'$ [EQ. (1.1)]. It is worthy to note that there is no pre-contact distance sensing used in this algorithm, and there is no position control of the contact drum while the slave finger is in contact with the virtual surface.

In the experiments, the twelve subjects were each presented with eight surface models for a traditional control algorithm, and eight surface models for the proposed DECAFF control system. The eight surfaces were defined by both a high and a low level for each of three variables expected to contribute to the perceptual experience of the operators. The variables included surface stiffness (K), surface damping constant (B), and rate of communication (S) between the haptic control PC and the VR PC. Table 4.1 shows the approximate values for high and low levels of the surface variables. The actual stiffness and damping coefficient experienced by the operators depends on the length of their knuckle to fingertip vector and their finger velocity at surface contact (due to step response in reading of fingertip position). Because the damping coefficient is dependent on the communication rate, two values are given for damping coefficients. The higher value is that associated with the low communication rate while the low damping coefficient value

is associated with the higher communication rate. In the actual implementation, the high value of K and B are chosen such that a single calculation cycle results in a change from 0% to 100% force application while crossing the surface boundary under moderate to high finger velocity. Because the communication rate (S) is the largest time lag in the system, this value is a good *approximation* of system bandwidth. The subjects were presented surfaces of matching K, B, and S in pairs for both the traditional control and DECAFF system.

Stiffness (K) (N/m)	Damping Coeff. (B) (N/m sec.)	Com. Rate (S) (Hz)
High 7142	High 650 / 246	High 29
Low 71.42	Low 6.5 / 2.46	Low 11

Table 4.1 Experiment Variable High and Low Values

For each pair of surfaces, subjects were asked to report which surface felt more like a “wall” or “rigid body”. This was a forced choice response where the subjects could choose first, second or same as a reply. Subjects were given ample time to repeatedly touch each surface prior to selecting which was more “wall-like”. Subjects were allowed to comment on the feeling of each surface, and their responses were recorded. Secondly, for each surface, the subjects were asked to indicate the location where they thought the surface began, or the finger position at which they made initial contact with the surface. To accomplish this task, the subjects were asked to completely extend their finger and then

retract it until they “felt” contact with the virtual surface. As there was no visual or audio indication of contact available to the subjects, they had to rely solely on their haptic sense to report the initial contact position. The ability to identify the precise location of the surface provides a good indication of the sensitivity of the haptic interface when displaying low stiffness surfaces and a good indication of the stability of the interface when displaying rigid bodies. In order to quantify the stability of each surface, the amplitude of oscillation of the prior 10 finger positions was recorded at the time the subject identified the location of the surface. Because finger velocity was believed to affect surface position perception, the maximum finger velocity was recorded for each surface trial.

4.3 Experimental Results

The primary goal of the human perception experiment was to determine to whether the DECAFF system provided improvement in effectiveness, compared with traditional methods of design and control and if it was more effective, to what level. The effectiveness can be measured by subjects’ perception of rigid surfaces, sensitivity in detection of surface boundaries, and the stability of surfaces. The results of these measurements of system effectiveness for both the proposed DECAFF and traditional design and control methods are presented in this section.

4.3.1 Perceptual Comparison to Real Surfaces

In this section the results to the force-choice response experiment are presented. In this experiment subjects were to choose which surface felt more like a real wall or rigid surface, when presented with a pair of surfaces of the same K , B , and S , but under varying

control methods. Figure 4.1 shows the perception of subjects as the number reporting which control method felt more like wall, based on surface model variables. For trials using surfaces with high stiffness (K) levels, subjects overwhelmingly (92% of the 48 trials) chose the DECAFF system as that which was more like a wall, while in only 6% they reported each had the same wall-likeness. In only 2 % of the trials subjects selected a traditional control system surface with a high stiffness as that most like a wall. Subjects described the traditional control high stiffness surfaces with terms such as “active”, “bumpy”, “bouncy”, “jumpy”, “difficult to detect edge”, and “resonating”. In contrast subjects described the DECAFF high stiffness surfaces as “solid”, “more secure”, “stable”, “hard like desk”, and “more comfortable”. Of those surfaces with a low stiffness, the DECAFF system again proved to provide a perception of more wall like, with respondents choosing the DECAFF surfaces in 44% of the trials. By comparison subjects in 15% of the trials chose the traditional control surface and in 42% reported that both surfaces were the same. Subject descriptions of low stiffness surfaces were highly dependent on the level of damping present. For low K, high B surfaces descriptions of traditional control and DECAFF surfaces were similar to those of high stiffness. Of the surfaces with a high level of damping, in 63% of the trials DECAFF was chosen, in 6% traditional was chosen as that most like a wall, while in 33% of the trials subjects could not distinguish between the two control methods. For surfaces with low damping in 73% of the trails subjects chose DECAFF, in 15% same, and in 13% subjects chose traditional as that which most felt like a wall. Subject descriptions of low stiffness and low damping surfaces under traditional control included statements such as “softer”, “moving”, “too soft to detect”, and “less

firm". By comparison, the low K and low B surfaces under DECAFF control were described as "strong sponge", "soft", "more comfortable", and "viscous like pushing a fluid". For high speed control, in 73% of the trials subjects chose DECAFF as most wall-like, in 6% traditional control was chosen, and in 21% of trials subjects reported the same sensation. Finally for low speed control in 63% of trials DECAFF was chosen, in 27% same was chosen and in 10% traditional was indicated as that most like a wall. Subject comments did not change significantly when comparing traditional and DECAFF controlled surfaces on the basis of control speed. It should be clear from the above results that the DECAFF system consistently was reported to be more like a real surface (more "wall-like") than those presented under traditional control methods. Further, the improvement while extraordinary for surfaces of high stiffness, was repeatedly cited for all surface parameter variables.

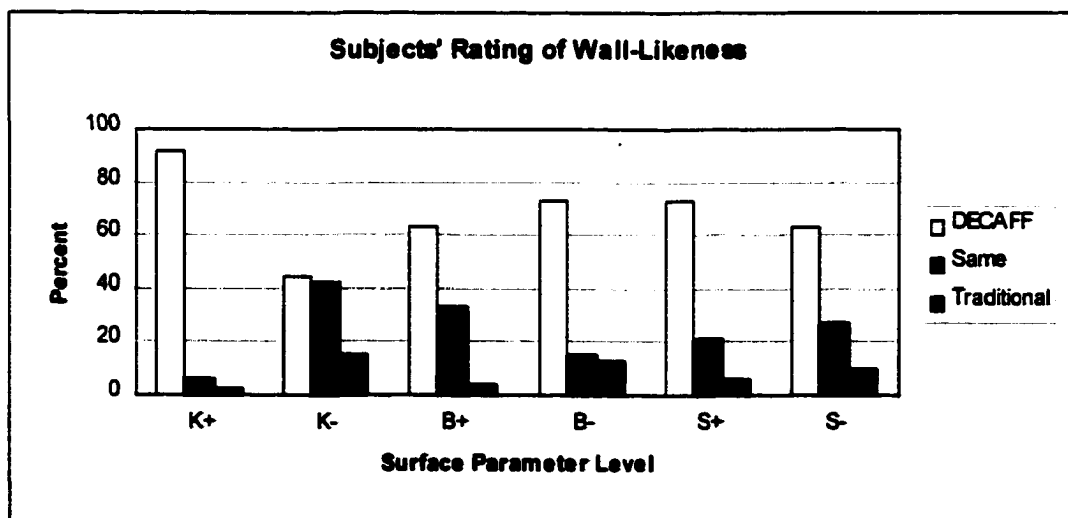


Figure 4.1 Subjects' Response to Which is more "wall-like"?

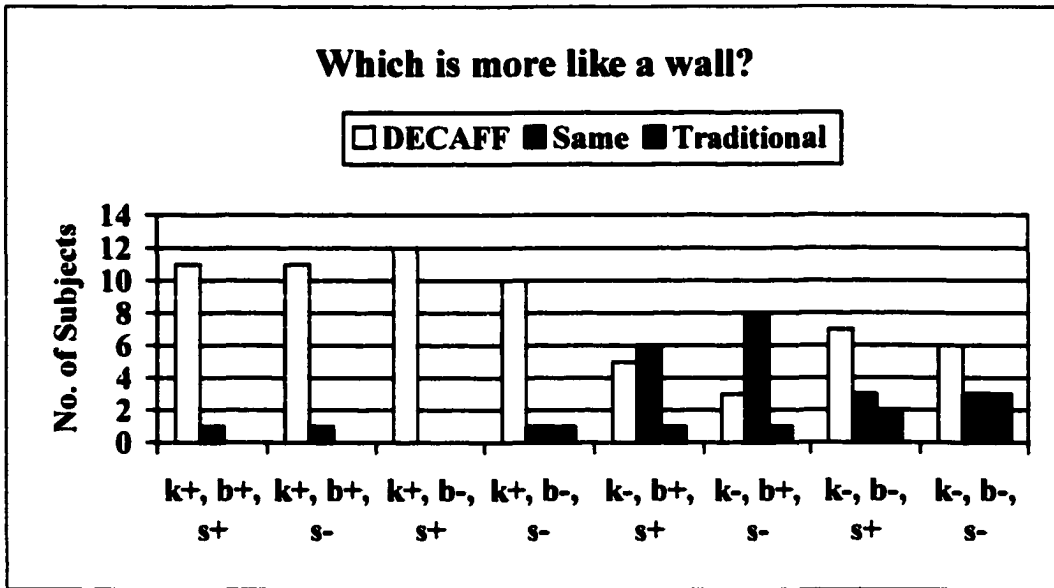


Figure 4.2 Subjects' Response to Which is more "wall-like"? (Raw Data)

Figure 4.2 shows the raw data for subjects' response to the question "Which is more wall-like?" From this figure it is evident that all surfaces carrying a high stiffness, regardless of the magnitude of damping and/or control speed, appear to the subjects to much more like an actual "real" rigid object when controlled by the proposed DECAFF method.

4.3.2 Haptic Perceptual Accuracy in Location of Surface Boundaries

Another measure of haptic system effectiveness is the operator's ability to accurately determine the boundary location of surfaces presented. To quantify the effectiveness of the proposed system in comparison to traditional control methods, the subjects were asked to identify the finger position at which they perceived the surface boundary. For this measure of performance, the difference between the actual surface edge position with respect to a fully extended finger (i.e. 0 degrees) and the subjects' perception of the edge position with respect to the same datum was defined as an error. The average (mean) errors in surface

location as reported by the subjects for both DECAFF and traditional control systems are shown in figure 4.3. The overall average error in surface edge location across all subjects was 7.26 degrees for traditional control and 4.51 degrees for DECAFF. From the figure it is clear that there was a high degree of variability between subjects, yet only one subject was less accurate in determination of the surface edge location while using the DECAFF system.

In FIG. 4.3 the error bars indicate the mean standard deviation per subject across all surface models (i.e. k+, k-, b+, b-, s+, s-).

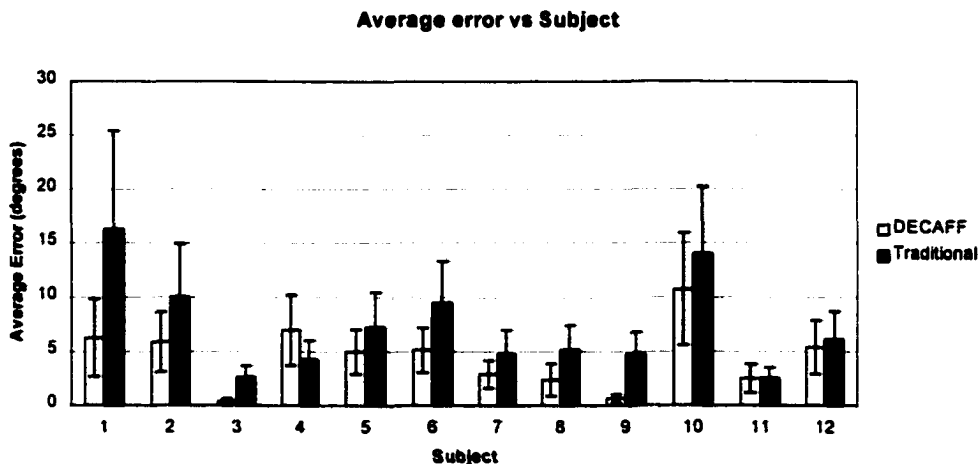


Figure 4.3 Average Error in Boundary Detection by Subject

The mean standard deviation is calculated (Holman, 1984) by:

$$\sigma_m = 1 / n^{1/2} (\sum (y_i - y_m)^2 / (n - 1))^{1/2} \quad [4.1]$$

where y_i is a raw data point, y_m is the average of the data (mean) and n is the number of trials. Because it is expected that these parameters will effect the error values, higher

variability is also expected in the by subject average, across all surfaces data. The dependency of the error magnitude for each control method upon the surface model parameters is shown in figure 4.4. The data represents an average across all 12 subjects, each having 4 trials at the high and low levels for each surface variable. Here one can see that regardless of surface model, the DECAFF system showed lower errors in surface edge detection. In this figure error bars provide the mean standard deviation across all subjects for a given surface model variable. Here the variability and magnitude of the mean standard deviations indicated by the error bars is notably lower than that of figure 4.3.

To further quantify the difference in sensitivity of perception of position the difference between the error in surface boundary detection with traditional control and that with DECAFF was calculated. Figure 4.5 shows the average error reduction across all surface models. The overall average error reduction for all subjects across all surface models while using the DECAFF system was 2.75 degrees or 38%.

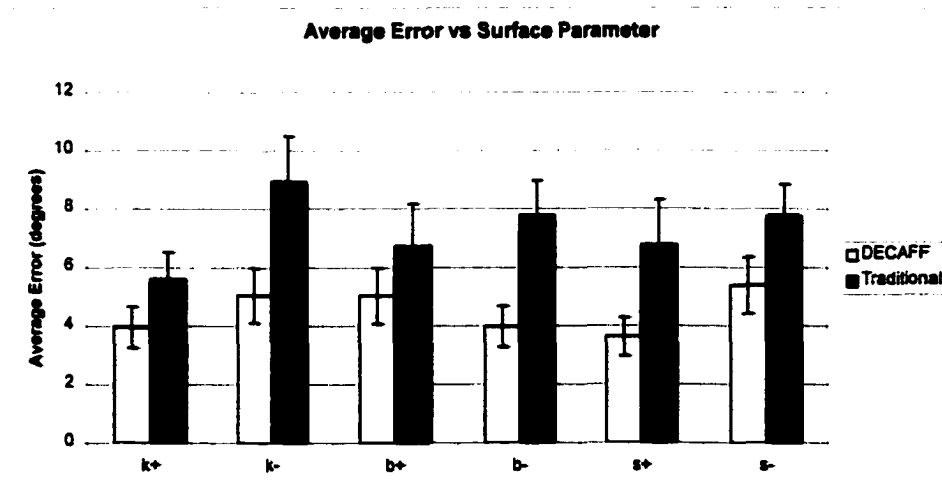


Figure 4.4 Average Error in Detection by Surface Variable

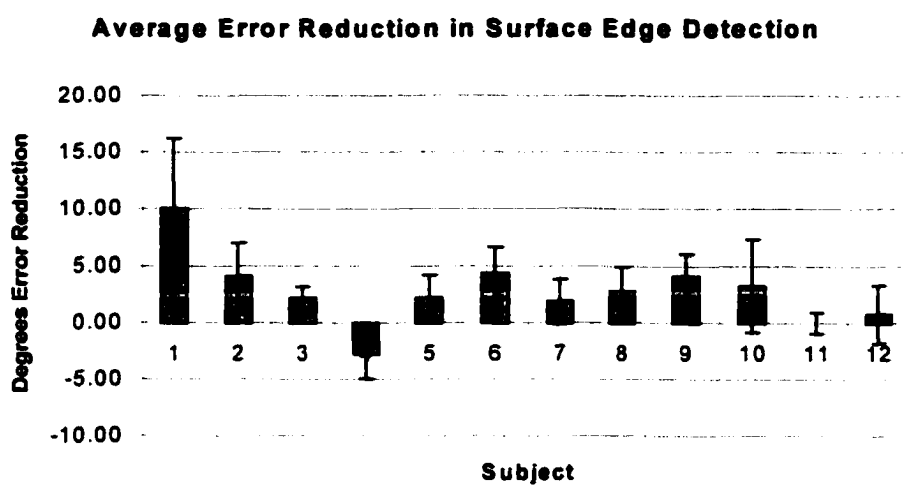


Figure 4.5 Average Error Reduction in Edge Detection (Degrees)

Some subjects demonstrated an exceptionally higher sensitivity than others did in their ability to accurately identify the surface locations for both control methods. These subjects (e.g. 3 and 9) also demonstrated the highest accuracy percentage improvement (over 85%) as shown in FIG. 4.6.

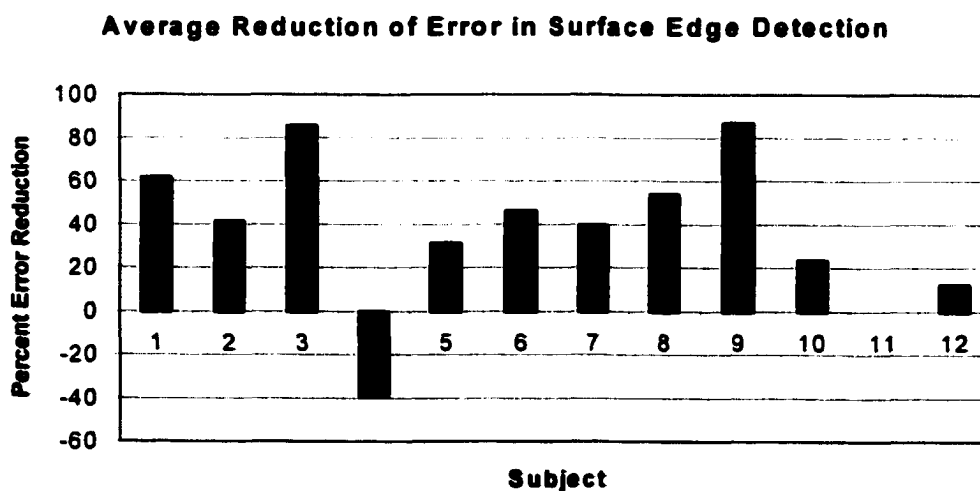


Figure 4.6 Average Error Reduction in Edge Detection (Percent)

Only two of the twelve subjects (on average) did not show an improvement with their accuracy in surface edge locations. Subject 11 was able to equally accurately detect surface locations for both control methods, while subject 4 was able to more accurately detect locations while using the traditional control.

To evaluate the effect of surface model parameters on the accuracy improvement in surface location detection, figures 4.7, 4.8, and 4.9 provide an average across all subjects for high and low levels of stiffness, damping, and communication rate. The mean error reduction for all high stiffness surfaces was 1.66 degrees, while for low stiffness this value was 3.85 degrees.

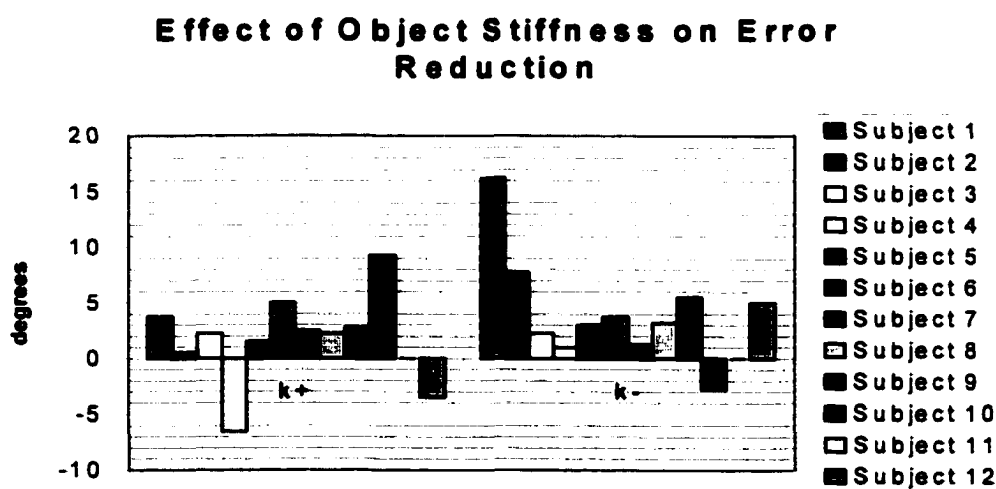


Figure 4.8 Effect of Surface Stiffness on Error Reduction

For high and low damping coefficient surfaces, the mean error reduction of the DECAFF system was 1.71 degrees and 3.79 degrees, respectively. The greater improvement in accuracy for DECAFF surfaces on low stiffness, and low damping surfaces may provide an indication of improved transparency and fidelity of the proposed system. For these

surfaces, the improved accuracy reflects an improvement in the ability to sense a transition from a simulated free motion to a simulated very low magnitude force.

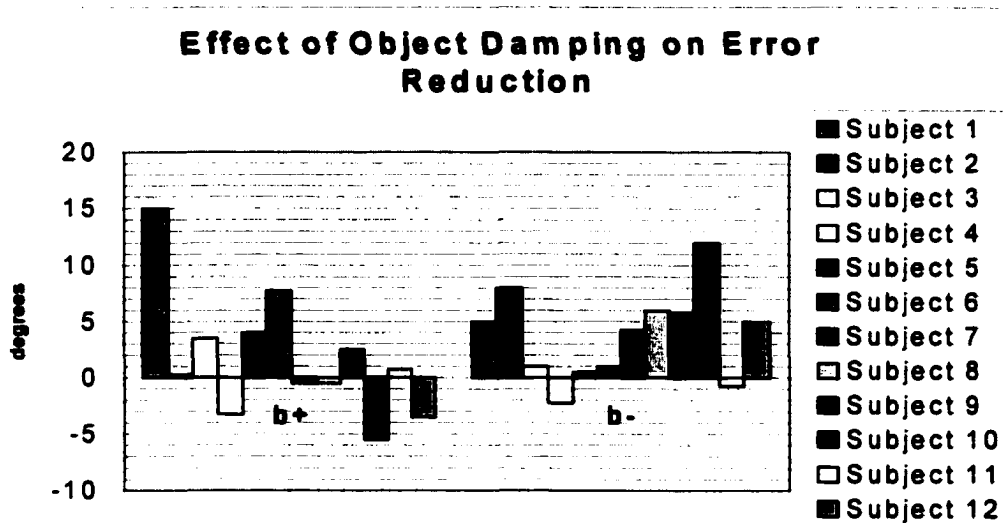


Figure 4.9 Effect of Damping Coefficient Value on Error Reduction

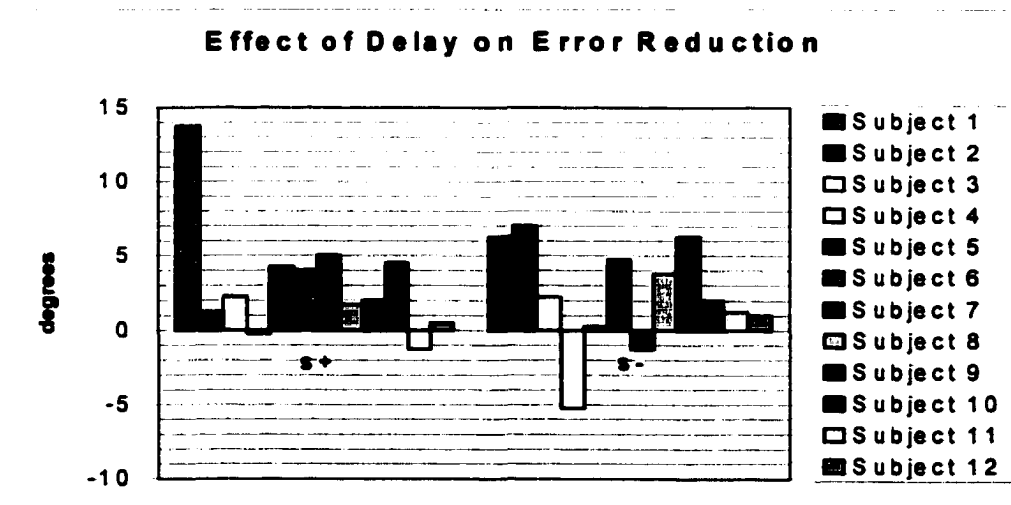


Figure 4.10 Effect of Delay on Error Reduction

The error reduction of the proposed system was somewhat greater under high speed communication, as shown in figure 4.10. Here the average improvements in surface

position detection accuracy offered by the DECAFF method were 3.14 degrees for high speed communication and 2.35 degrees for low speed communication.

Figure 4.11 shows the dependency of improvement in accuracy on surface model parameters averaged across all subjects, given as a percentage error reduction achieved by subjects using the DECAFF system. It can be seen from the figure that a low damping value leads to the highest improvement of 49%, and that a low stiffness value provides an improvement of 43%. The result clearly demonstrates the subjects increased ability to detect initial contact with the DECAFF system while interacting with “soft” surfaces which are characterized by low stiffness and damping.

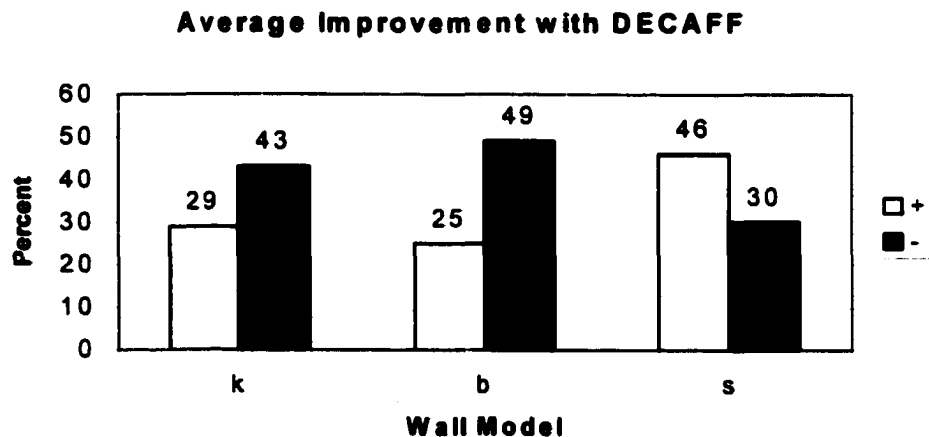


Figure 4.11 Average Accuracy Improvement with DECAFF

4.3.3 Stability and Oscillation Amplitudes

Another measure of haptic interface effectiveness is the stability of surfaces touched. In order to comparatively evaluate the proposed DECAFF system in the measure of stability,

the amplitude of oscillation was recorded. The amplitude was calculated as the difference between the maximum and the minimum finger bend angle (in degrees) of the most recent 10 calculation cycles prior to identification of the surface boundary. The stability of surfaces presented was improved considerably for 9 of the 12 subjects, as measured by the amplitude of oscillation. Figure 4.12 shows the average amplitude for each subject. One interesting observation is that some subjects (e.g. 1, 5, and 10) were able to consistently stabilize the oscillatory surfaces, regardless of stiffness and damping coefficient values. In Figure 4.13 the average amplitude of oscillation is presented as a function of surface parameter. Here one can see that improvements in stability of the DECAFF system are consistent across all surface parameter values. It should be noted that for “harder” surfaces, under traditional control, with high K and/or B subjects often reported surface felt like it was moving or vibrating. For the “softer” surfaces, under traditional control, with low K and/or B subjects often repeatedly moved their finger across the surface boundary in an effort to ascertain its location. This repeated crossing appears as an oscillation, although the surface did not vibrate in an unstable manner, as did the harder surfaces. Subjects generally did not use this repeated crossing strategy while operating under DECAFF control as evidenced by the lower average amplitude data shown in figures 4.12 and 4.13. This provides a good indication of the improved perceptual quality of the proposed system and is consistent with subjects’ comments about traditionally controlled low stiffness and damping surfaces, referring to a “moving surface” or one for which it was “difficult to determine the position of”. Across all subjects and all surfaces the average amplitude for the traditional control method was 8.34 degrees, while the average amplitude for the

DECAFF system was 1.85 degrees. These values indicate an immense improvement in stability of 78%.

In figures 4.12 and 4.13, the error bars indicate the mean standard deviations. One observation here similar to that of the haptic perceptual accuracy experiment is that the standard deviations (and thus variability) for data presented by subject across all surfaces are notably higher than that averaged across all subjects for a given surface parameter. This result holds for both the DECAFF and traditional control methods. The average of mean standard deviations for figure 4.12 data are 0.92 for DECAFF and 3.74 for traditional. If we consider the ratio of the average mean standard deviations to the overall average amplitude as a normalized measure of variability, we have a variability of $0.92/1.85 \cong 50\%$ for DECAFF and $3.74/8.34 \cong 45\%$ for traditional control in the by subject data analysis (figure 4.12). For the by surface parameter data of figure 4.13, the average of the mean standard deviations are 0.44 for DECAFF and 1.71 for traditional. Considering the ratio as above we arrive at normalized variability of $0.44/1.84 \cong 24\%$ for DECAFF and $1.71/8.34 \cong 21\%$ for traditional control, approximately one half of that calculated for the data of figure 4.12. This result indicates the significantly lower variability between subjects when all subjects are given the same surface than the variability for a given subject across all various surfaces.

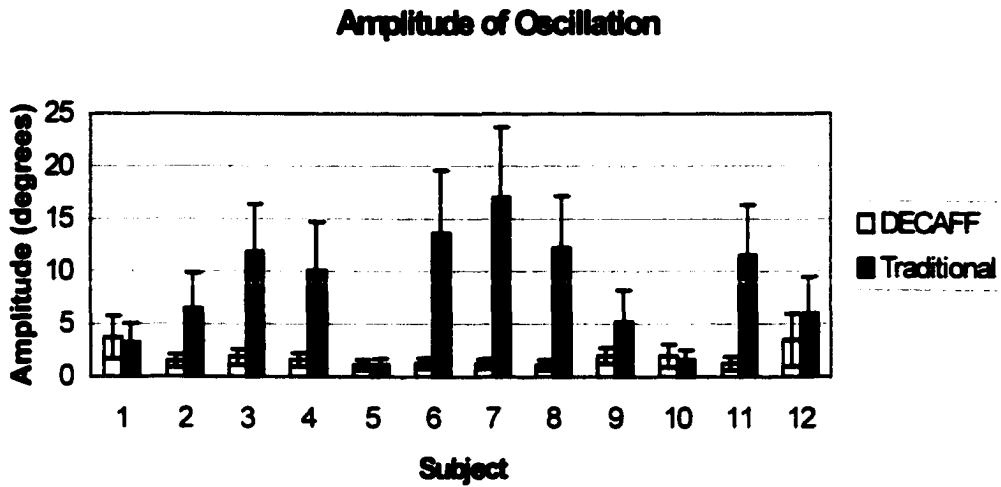


Figure 4.12 Amplitude of Oscillation (by Subject)

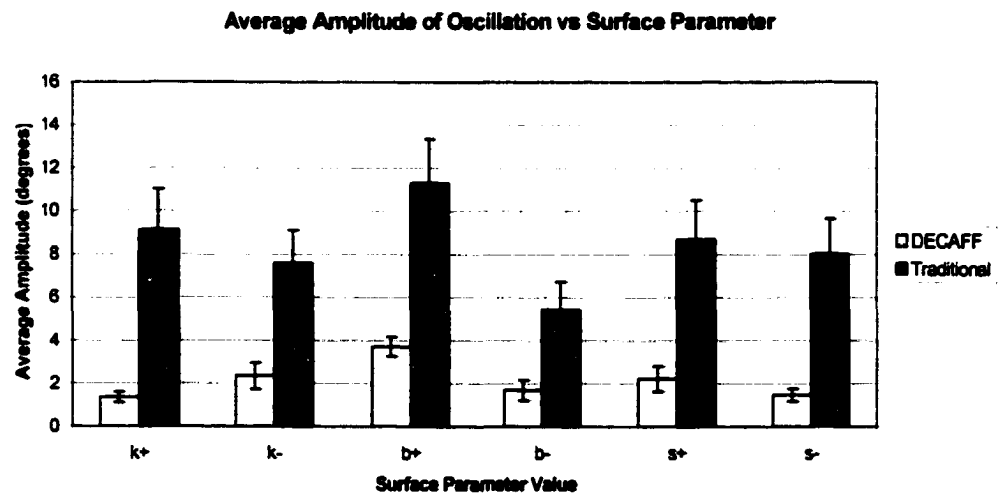


Figure 4.13 Amplitude of Oscillation (by Surface Parameter)

4.3.4 Effects of Pre-Contact Velocity on Perceptual Accuracy

The effect of finger velocity on error in surface position detection was found to be less significant than expected and is shown in figures 4.14 and 4.15. This may be a result of

the relatively small number of high velocity data points. Hasser, (1995) reports maximum finger velocities of up to 17 radians/sec. (974 degrees/sec.), while the test data reports very few points above 500 degrees/sec. The lower range of velocities recorded is attributable to the blind measurement of this variable without instruction for subjects to attempt high (or low) speed finger retraction. Nonetheless the magnitudes while operating under traditional control initiate at and reach a higher value than those of DECAFF control. The slope (by least squares fit) of the data trend line increases by approximately 35% for traditional control compared to DECAFF. This indicates that while neither system showed an enormous dependency on finger velocity in the velocity ranges recorded, there is some evidence of a higher dependency on finger velocity for accuracy while using traditional control than that of DECAFF control. This result supports the analysis of Chapter 2.

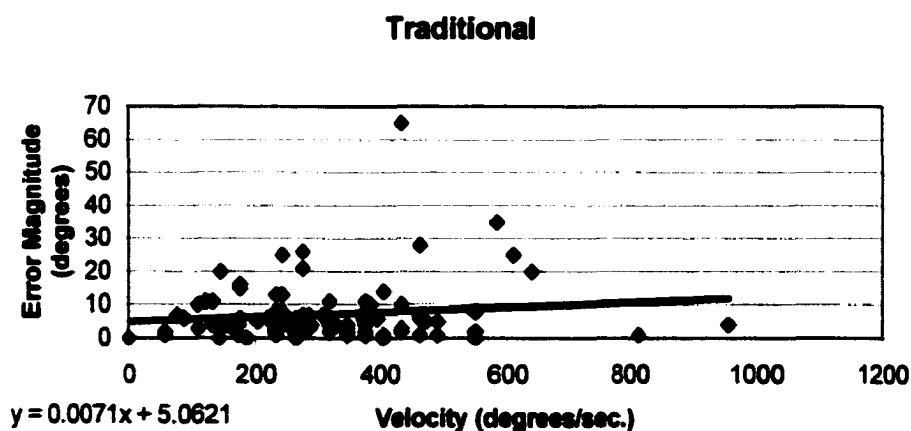


Figure 4.14 Error Magnitude vs Velocity with Traditional System

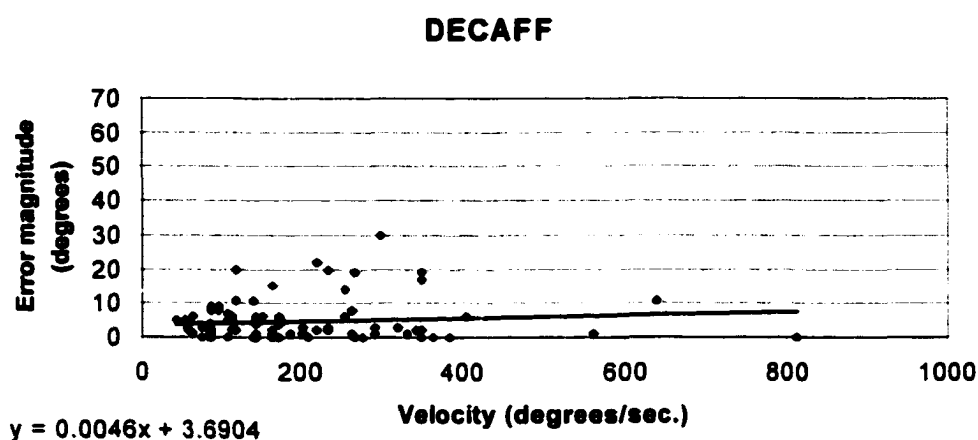


Figure 4.15 Error Magnitude vs Velocity with DECAFF

4.3.5 Statistical Analysis of Accuracy Experiments

There were two sets of numerical response data collected for the experimentation conducted that are subject to statistical analysis in this section; position perceptual accuracy and amplitude of oscillation. In this section all statistical analysis for the accuracy experiments is presented, and all statistical analysis for the amplitude experiments is presented in section 4.3.6. Because the experiment was designed as a pair of two-level three variable (2^3) factorial designs, the results of the experiment for each of the responses may be analyzed in several different ways. First a traditional analysis of effects and development of a predictive model can be done for both the DECAFF system and the traditional control experiments as separate 2^3 factorial design experiments. Secondly a similar analysis can be done for a two-level four variable a (2^4) factorial design using the paired results, considering the control method (DECAFF or traditional) as a fourth variable.

Following the procedures outlined by DeVor, Chang, and Sutherland, (1992) the effects of the variables for a 2^n factorial design experiment without replication are calculated as follows:

$$E(i) = (2/n) \Sigma (+/- y_i) \text{ for } i = 1 \text{ to } n \quad [4.2]$$

Where $+y_i$ indicates the measured response or error magnitude for this section, (averaged across all subjects) for trial with variable x_i at the high level, and $-y_i$ indicates the error or amplitude magnitude for trials with variable x_i at the low level. The number of tests conducted is n , which equals 8 when traditional and DECAFF control methods are considered as separate experiments for analysis. When the results of both control methods are analyzed as a combined experiment n is 16. The relative magnitudes of the effects estimates for each input variable (and interactions) provide a good indication as to which input variables dominated the experimental response, in this case the position perceptual error.

In order to judge the significance of the effects estimates, a variance for the data is calculated based on the “sparsity of effects principle” that states main effects and low-order interactions dominate the system. Thus relatively low magnitude higher order effects are assumed to be negligible and are used to estimate the variance and the standard error. While this method is recommended for 2^4 and higher unreplicated factorial designs, it should be appreciated that due to the relatively small number of higher order interactions only an approximate indication of the statistical significance of the unreplicated 2^3 factorial designs will result (Montgomery, 1991). Again following

the methods suggested by DeVor, et.al, (1992), the standard error and confidence interval calculations were performed as follows. The standard error (s.e.) of an effect was calculated by

$$\text{s.e.} = (\sum_N [(E_i - \mu_{Ei})^2 / N])^{1/2} \quad [4.3]$$

where E_i are the higher order effects assumed to be negligible and N is the number of higher order effects considered negligible. A value of zero is substituted for the true mean effect (μ_{Ei} in the above equation), which is assumed to be known. The confidence interval for the effects estimates are calculated as the product of the standard error and the student's distribution t values associated with the number of degrees of freedom present in EQ. 4.3 and the confidence interval. Using the above referenced calculation method, the effects estimates for the accuracy experiment while operating under traditional control are given as follows:

$$E(K) = -3.125$$

$$E(B) = -1.02$$

$$E(S) = -0.979$$

$$E(KB) = -0.271$$

$$E(KS) = -0.396$$

$$E(BS) = +1.98$$

$$E(KBS) = +0.0208$$

Where E indicates the effect associated with the variable or interaction of variables inside the parenthesis and the variables are coded as follows:

K = stiffness

B = damping coefficient

S = speed, or communication rate

The standard error of an effect was calculated to be 0.277, leading to an effect estimate $E(i) \pm 0.882$ at a 95% confidence interval. Applying this value to the calculated effects given above, the communication rate (S), the surface stiffness (K), the surface damping (B), and the interaction of damping and communication rate (BS) were found to significantly affect the error in surface boundary location perception, while using a traditional design and control approach. This result, identifying K, B, and S as significantly affecting the error magnitude in surface edge detection, supports the results given by the mathematical modeling and simulations given in Chapter 2 for traditionally controlled surfaces. Further, assuming a proportional relationship between accuracy of detection and stability, this result concurs with those presented by Love and Book, (1996), identifying the same variables as those affecting the stability of haptic interfaces.

Using the effects found to be significant a predictive model for the expected error in surface edge perception using traditional control is given by:

$$y = 7.26 - 1.56 x_1 - 0.51 x_2 - 0.49 x_3 + 0.99 x_2 x_3 \quad [4.4]$$

Where the values of x_j are given by the following transformation from coded to variable space:

$$x_j = [r - (r_{-j} + r_{+j}) / 2] / [(r_{+j} - r_{-j}) / 2] \quad [4.5]$$

where r_{-j} = the low value of variable j ,

and r_{+j} = the high value of variable j .

A similar analysis of the data was done considering the DECAFF data as a 2^3 factorial design experiment without replication. The effects of the variables were calculated as follows:

$$E(K) = -1.1$$

$$E(B) = +1.06$$

$$E(S) = -1.77$$

$$E(KB) = -1.23$$

$$E(KS) = -0.56$$

$$E(BS) = -0.81$$

$$E(KBS) = +0.73$$

The standard error of an effect was calculated to be 0.868, leading to an effect estimate $E(i) \pm 2.41$ at a 95% confidence interval. Applying this value to the calculated effects given above no effects were found to be statistically significant, regarding the DECAFF data for error in perception of surface boundary location. From this result we can conclude that due to the nature of pre-contact position control that switches to force control after contact, neither stiffness, damping, or communication rate within the range tested provide a significant effect to 95% confidence as to the accuracy at which an operator can detect surface positions. Thus one would expect that any combination of

these parameters with the test range would not alter the location detection ability of an operator of a haptic interface designed with the DECAFF system. This result, identifying no K, B, and S levels or combinations as significantly affecting the error in surface location detection, supports the results given by the mathematical modeling and simulations given in Chapter 2 for DECAFF controlled surfaces.

Combining the DECAFF data and that of traditional control, a four variable two level experiment without replication was analyzed. The effect estimates arrived at for this analysis are:

$$E(C) = -2.75$$

$$E(K) = -1.60$$

$$E(B) = +0.21$$

$$E(S) = -1.38$$

$$E(CK) = +0.58$$

$$E(CB) = -0.48$$

$$E(CS) = -0.40$$

$$E(KB) = -0.75$$

$$E(KS) = +1.04$$

$$E(BS) = +1.10$$

$$E(CKB) = -0.35$$

$$E(CKS) = +1.40$$

$$E(CBS) = +0.08$$

$$E(KBS) = +0.48$$

$$E(\text{CKBS}) = +0.38$$

From which a standard error of 0.708 was calculated, leading to an effect error estimate at the 95% confidence interval of:

$$E(i) + / - 1.80$$

At the 95% confidence interval the effects of control method was found to be significant at the value indicated below.

$$E(C) = -2.75 + / - 1.80$$

Thus we can conclude that the control method does in fact significantly affect the error in surface location perception, and we can be 95% sure that when using the DECAFF system, errors in perceived edge location will be reduced, compared to haptic interface traditional control systems. Thus, the surface location perception experiment has provided a strong confirmation of the predictions set forth in the Chapter 2 analysis.

The mean response of the perceptual position accuracy experiments can also be evaluated by statistical hypothesis testing. Our problem formulation for this analysis is to state a null hypothesis that is to be tested. The null hypothesis is that the mean values for both DECAFF and traditional control methods is the same, or in mathematical terms:

$$H_0: \mu_d = \mu_t \quad [4.6]$$

Where μ_d is the population mean positional accuracy for a DECAFF controlled finger bend haptic interface and μ_t is the population mean positional accuracy for a traditionally

controlled finger bend haptic interface. In this statistical test we are concerned with two main issues. The first concern is to establish a probability with which we can reject the null hypothesis. This probability is called the significance level of the test, usually denoted by α . In human factors research a value of $\alpha = 0.05$ is conventionally accepted (Franklin, et. al. 1996). At the $\alpha = 0.05$ significance level there is a 95% statistical significance between the mean errors in position detection and the null hypothesis is rejected. Because the mean error of the proposed system is lower we conclude that there is in fact an improvement in the position detection ability when using the proposed DECAFF system. This evaluation was completed when the two control methods were compared above for the 2^4 factorial design analysis and resulted in a 95% confidence that the null hypothesis is false. The second concern is that we may fail to reject the null hypothesis, when it is in fact false. This is known as a Type II error. The probability of making a Type II is often denoted as β . The power of a test of significance is defined as:

$$\text{Power} = (1 - \beta) \quad [4.7]$$

And can be considered the probability that the null hypothesis will be rejected (i.e. statistical significance will be obtained), when it is in fact false and there is a real difference between the mean values of position detection error for the two haptic displays systems tested (Bausel, 1986). For a given value of α , increasing the number of subjects tested will increase the power of an experiment. For human subject research, a power of 0.80 is generally considered desirable (Franklin, et. al., 1996). The value of β is calculated by (Montgomery, 1991):

$$\beta = \Phi [Z_{\alpha/2} - (\delta n^{1/2})/\sigma] - \Phi [-Z_{\alpha/2} - (\delta n^{1/2})/\sigma] \quad [4.8]$$

where $Z_{\alpha/2}$ is the percentage point of the normal distribution such that the probability

$$P \{ Z \geq Z_{\alpha/2} \} = \alpha/2 \text{ and } Z_{\alpha/2} = Z_{0.05/2} = Z_{0.025} = 1.96$$

and $\Phi []$ is the cumulative distribution function of the standard normal distribution. The value for δ is the difference between the mean values for each haptic display system (that negates the null hypothesis) and for the accuracy experiment δ is given by $7.26 - 4.51 = 2.75$ degrees. The standard deviation is σ , which is unknown for this calculation and thus it will be approximated by the pooled sample standard deviation (s_p). The pooled sample standard deviation is given by taking the square root of the pooled variance (s_p^2) for the data of both the DECAFF and traditional control experimental responses, which is given by:

$$s_p^2 = [(n_1 - 1) s_1^2 + (n_2 - 1) s_2^2] / (n_1 + n_2 - 2) \quad [4.9]$$

where s_1^2 , s_2^2 are the sample variances for The DECAFF and traditional control accuracy response data. The sample variance is calculated as:

$$s^2 = \sum (y_i - y_m)^2 / (n - 1) \quad [4.10]$$

where y_i represents the individual data points (mean accuracy data across all surfaces for a single subject in this calculation) and y_m represents the overall mean for each control method, thus y_m for the DECAFF control is 4.51 degrees and y_m for the traditional control method is 7.51 degrees. The value of $n = n_1 = n_2$ is 12, indicating the number of subjects

(and data points) for each control method. Applying equations 4.10 and 4.9 to the data for the accuracy experiment we have $s_p = 3.724$. Then substituting the appropriate values into equation 4.8, we arrive at a value of:

$$\beta = \Phi [1.96 - (2.75)(12^{1/2})/3.724] - \Phi [-1.96 - (2.75)(12^{1/2})/3.724] = 0.274$$

leading to a power of $(1 - \beta) = 0.726$. The power of 0.726 indicates we have a 72.6% chance of finding an effect when the effect actually exists under the test conditions utilized. The power value found for this experiment, being slightly lower than the desired 0.80 could have been improved by having more subjects perform the accuracy experiment.

4.3.6 Statistical Analysis of Amplitude Experiments

An analysis of the amplitude data similar to that of the accuracy data can also be done to determine the effects of the various experimental input variables on the resulting degree of stability (as measured by the amplitude of oscillation). Following the methods used for the error in perception of position, a similar analysis of the amplitude of oscillation is presented as follows. First considering the experiment as a two-level, three-variable for traditional design and control method, we arrive at effects of the variables as:

$$E(K) = +1.52$$

$$E(B) = +5.85$$

$$E(S) = +0.66$$

$$E(KB) = -4.40$$

$$E(KS) = +0.19$$

$$E(BS) = +1.90$$

$$E(KBS) = +0.73$$

The standard error of an effect was calculated to be 0.279, leading to an effect estimate $E(i) \pm 0.89$ at a 95% confidence interval. From this result we can conclude for the traditional control, damping coefficient magnitude, spring constant, the interaction of damping and control speed, and the combination of stiffness and damping are significant factors in the stability of contact to the 95% confidence interval. This result, identifying K, B, and combinations of KB, and BS as significantly affecting the amplitude of oscillation, supports the results given by the mathematical modeling and simulations given in Chapter 2 for traditionally controlled surfaces. Further, assuming a proportional relationship between amplitude of oscillation and stability, this result concurs with those presented by Love and Book, (1996), identifying the same variables (K, B, and S) as those affecting the stability of haptic interfaces. The analysis of Love and Book however does not specifically identify any combined effects, although this is implied by their analysis results.

Secondly considering the experiment as a two-level, three-variable for the DECAFF design and control method, we arrive at effects of the variables as:

$$E(K) = +0.79$$

$$E(B) = +0.33$$

$$E(S) = +0.75$$

$$E(KB) = -0.46$$

$$E(KS) = -0.71$$

$$E(BS) = +0.12$$

$$E(KBS) = -0.083$$

The standard error of an effect was calculated to be 0.429, leading to an effect estimate $E(i) \pm 1.19$ at a 95% confidence interval. Applying this value to the calculated effects given above no effects were found to be statistically significant, regarding the DECAFF data for amplitudes of oscillation. From this result we can conclude that due to the nature of pre-contact position control that switches to force control after contact, neither stiffness, damping, or communication rate within the range tested provide a significant effect to 95% confidence as to stability while in contact with virtual surfaces. Thus one would expect that any combination of these parameters within the test range would not alter the stability of an operator of a haptic interface designed with the DECAFF system. This result, identifying no K, B, and S levels or combinations as significantly affecting the amplitude of oscillation, supports the results given by the mathematical modeling and simulations given in Chapter 2 for DECAFF controlled surfaces.

Combining the DECAFF data and that of traditional control, a four variable two level experiment without replication was analyzed. The effect estimates for amplitude of oscillation as the response arrived at for this analysis are:

$$E(C) = -6.49$$

$$E(K) = +0.26$$

$$E(B) = +3.09$$

$$E(S) = +0.70$$

$$E(\text{CK}) = +1.01$$

$$E(\text{CB}) = +0.094$$

$$E(\text{CS}) = +0.052$$

$$E(\text{KB}) = -2.43$$

$$E(\text{KS}) = -2.76$$

$$E(\text{BS}) = -1.26$$

$$E(\text{CKB}) = -0.32$$

$$E(\text{CKS}) = +0.89$$

$$E(\text{CBS}) = +0.26$$

$$E(\text{KBS}) = +0.32$$

$$E(\text{CKBS}) = -0.41$$

From which a standard error of 0.497 was calculated, leading to an effect error estimate at the 95% confidence interval of:

$$E(i) + / - 1.29$$

At the 95% confidence interval the effects of control method, stiffness, communication rate, and the interaction of control, stiffness and communication rate were found to be significant at the values indicated below.

$$E(\text{C}) = -6.49 + / - 1.29$$

$$E(\text{B}) = +3.09 + / - 1.29$$

$$E(\text{KB}) = -2.43 + / - 1.29$$

$$E(\text{KS}) = -2.76 + / - 1.29$$

These variables are also significant to the 99% confidence level.

$$99\% \text{ C.I. } \quad E(i) + / - 2.00$$

$$E(C) = + 6.49 + / - 2.00$$

$$E(B) = +3.09 + / - 2.00$$

$$E(KB) = -2.43 + / - 2.00$$

$$E(KS) = -2.76 + / - 2.00$$

The control method remains significant to the 99.9% confidence level.

$$99.9\% \text{ C.I. } \quad E(i) + / - 3.41$$

$$E(C) = + 6.49 + / - 3.41$$

Thus we can conclude that the control method does in fact significantly affect the amplitude of oscillation, and we can be 99.9% sure that when using the DECAFF system the stability will be improved, compared to haptic interface traditional control systems. Thus, the stability experiment with amplitude of oscillation as the measured response has confirmed the predictions set forth in the Chapter 2 analysis to a 99.9% confidence level.

A power analysis similar to that done for the position discrimination experiment is presented here for the oscillation amplitude response experiment. For the amplitude data, the pooled sample standard deviation was calculated as 3.65. The δ value is given by the difference in the overall mean amplitudes for each control method, or $\delta = 8.34 - 1.85 = 6.49$ degrees. Again the number of subjects n is 12. Then the probability of a Type II error β is given by:

$$\beta = \Phi [1.96 - (6.49)(12^{1/2})/3.65] - \Phi [-1.96 - (6.49)(12^{1/2})/3.65] \approx 0.0000$$

resulting in a power of $(1 - \beta) \approx 1.000$. Having a power of approximately one indicates we are nearly 100% certain to find an effect at the 95% confidence interval, if the effect actually exists.

4.4. Conclusions of Experimental Investigation

In this chapter the design, procedure, and results of an experimental investigation as to the effectiveness of the proposed approach to haptic interface design has been discussed. The proposed DECAFF system was tested in a side by side comparison with one having mechanical design and control performance limitations imposed by the traditional approach to haptic interface design. That is to design the interface with an actuator that is directly coupled to the human operator during use and to control the force display such that after the slave entity has penetrated a virtual surface, or contacted a physical object, output a force to the actuator. Conversely, the DECAFF design and control method, calls for an actuator that is de-coupled from the operator and controlled to provide a first condition of pre-contact where human motion is unobstructed by the actuator with the actuator being position controlled and a second condition of post-contact force control. In this side by side comparison, the DECAFF method was shown to provide superior perceptual experiences for the human operators in areas of discrimination of slave object position, perception of slave object characteristics, and in the stability of virtual slave surfaces. The proposed system was shown to perform dramatically better in performance measures of perceptual quality of surfaces defined by both high and low levels of stiffness and damping. We traditionally would describe such surfaces as being on the high and low spectrums of hardness or

rigidity. Although the experimentation utilized a small number of subjects, the improvements in both of these areas has been shown to be statistically significant beyond a 95% confidence level with a statistical power near the target typically used in human subject research. By reduction of time delays and elimination of the need for wall penetration in the proposed approach, the new approach is able to more accurately represent initial contact with rigid and non-rigid objects. Consequently, the DECAFF method has been demonstrated as a viable solution to an important problem in the haptic display research area, significantly improving virtual wall rendering.

Chapter 5

Extensions, Contributions and Conclusions

5.1 Introduction

This section concisely outlines the work that has been completed and discusses application issues for future implementations of the technology developed in the course of this research program. Opportunities for further improvements in system performance upon further design iterations are identified. Conclusions of the research completed are also presented. The primary and fundamental contribution of a general design and control system based on the DECAFF paradigm has been proposed, analyzed, implemented, and tested on human subjects. Through this analysis and testing several measures of haptic interface performance have been demonstrated to improve when using the proposed DECAFF system. The proposed system provides a significantly better perception of the haptic rendering of rigid bodies in virtual environments, an important problem in the haptics research field. The proposed system has shown to greatly improve the stability of both hard and soft surfaces, and has maintained this performance improvement even when operating at a lower control speed. A measure of haptic perceptual accuracy or position discrimination of initial contact has been introduced, and the proposed system has demonstrated significant improvements in this area as well. A complete design has been established as discussed in the previous sections of this report. Mechanical and electrical systems have been constructed for complete measurement and display for two fingers, while hand mounted mechanical linkages have been constructed for four fingers. Control algorithms have

been implemented for one finger and require slight modifications to establish computer based control for the remaining digits. Communication between the haptic control PC and a virtual finger control computer has been implemented. A virtual test bed environment has been developed that presents a graphical display of a virtual finger which can interact with a virtual surface. The virtual finger (slave) replicates the positions of the master finger attached to the haptic interface. The virtual test bed also includes a virtual surface that has a programmable position, spring constant, and damping coefficient. Thus a wide variety of forces can be calculated as a function of virtual surface penetration distance and/or virtual finger velocity. The force magnitudes calculated in the virtual environment are forwarded to the haptic control PC for subsequent display to the operator. The virtual environment test bed, in combination with the haptic controller and interface provide a real time position measurement system and force display of sufficiently detailed implementation to permit scientific evaluation of the performance improvements offered by the DECAFF design and control method proposed in this research.

The complete system implemented to date can perform the following functions for evaluation purposes:

- (1) Finger bend position calibration and motor position mapping for a single finger is complete and user friendly (for a text based interface). For any operator and range of finger motions, the system can be easily calibrated to reflect the range of motion from a fully extended finger (0°) to a fully retracted finger (180°). The operator may initiate the routine, and repeatedly extend and retract finger as often as desired to

record the maximum and minimum values of motion, striking enter to finish. Then the operator fully retracts the finger, and strikes another key to permit the actuator to slowly extend his or her finger. After this routine, the system will continuously display the finger position as a degree of bend ranging from 0° to 180°.

- (2) Haptic rendering of contact with a virtual wall at any prescribed degree of finger bend can be simulated, as described in chapter 3. The user enters a surface position through a text based interface, and when retracting finger, the user feels the virtual wall as a “crisp” contact sensation. Further finger bend retraction motion is restricted upon contact with the virtual wall, by replicated finger interference with the contact drum. The operator is free to move the finger away from and up to the virtual wall as often and as quickly as desired, without penetrating the virtual wall.
- (3) Variable force display for a single finger is simulated by an implementation of the PWM force control algorithm described in chapter 3. Upon contact with the virtual surface the operator feels a force that is calculated within the virtual reality slave control computer. The force magnitude is controlled to provide a magnitude given by the sum of a user specified stiffness value multiplied by the virtual surface penetration distance and a user specified damping value multiplied by the velocity of the finger while within the virtual surface. The force magnitude (F) is thus controlled by: $F = Kx + Bx'$.
- (4) A virtual finger graphic display is implemented to execute on a separate computer (VR PC) from that of the haptic control algorithm. The virtual display consists of a

rendering of a human finger that is position controlled to reflect the position of the haptic interface operator's finger in real time. For example as the operator moves their finger from a fully extended 0 degree position to a 45 degree position, the virtual finger moves from a 0 degree position to a 45 degree position. This mapping is done continuously as long as both the haptic control and virtual finger programs are running. The virtual finger program also contains an algorithm that permits display of a virtual surface at a user selected position, within the virtual finger's coordinate system. The surface is programmable not only in position, but also in the stiffness and damping it will display upon interference with the virtual finger. These virtual surface variables are controlled as described in item 4 above.

- (5) Communication between the virtual slave controller and the haptic control computer is implemented as a custom serial communication algorithm, designed to encode, transmit, and receive the necessary control data in its smallest form. The haptic control computer sends finger position as an angle value between 0 and 180 degrees to the virtual control computer, while the virtual controller sends distance between the finger and the surface, or a force to display value. The distance between the virtual finger and virtual surface assumes a value between 1 and 50 degrees, and when this value is less than 1, the force to display is sent instead. The communication routine is programmable in the frequency at which communication between the two computers takes place. To control this variable, the operator enters a frequency value (f), such that the serial communication will occur after the entered value (f) number of position measurement and motor control calculation cycles.

(6) A traditional haptic control algorithm has been implemented. This algorithm controls the DECAFF single finger hardware to operate as though the actuator and operator's finger were mechanically coupled, as they would be in a traditionally designed haptic interface. This algorithm is useful for comparatively evaluating the two design and control paradigms.

The above implementation provides a complete test bed for evaluation of the haptic display system performance in terms of comparison between a traditional control method and the proposed DECAFF design and control method. While the above simulations represent an implementation of the novel concepts presented in this research, it is also desirable to permit application of the technology developed in the course of this research to both complete tele-robotic and VR applications. The detailed implementation in these two application domains is not necessarily novel, yet requires a significant effort and resources for each domain. Some important issues involved in these applications as well as application of the DECAFF method to general multiple degree of freedom haptic interfaces is discussed in the following sections.

5.2 Applications and Extensions of the Research

In this section some application issues for the technology developed in this research program are addressed. The first issue addressed is that of pre-contact distance sensing computation requirements for VR applications. Utilizing a slight modification of the control algorithm described in chapter 3, which is discussed below, reduces the computation requirements for VR applications. A second issue addressed is that of

extensions of the DECAFF technology to multi-degree of freedom haptic interface designs. The technology has been developed and tested for a unilateral single degree of freedom per finger actuator. In section 5.2.2, the DECAFF technology is first applied to bilateral prismatic joint design as one may see on a Cartesian coordinate system haptic interface, and then applied to revolute joint design as one would expect to see on serial link design.

5.2.1 Reducing Computation Load for VR Applications

For implementation in a three-dimensional virtual reality modeling computer, there is some question as to the computation load of the virtual reality modeling computer imposed by the system as described thus far. The basic concern is whether the computation requirements for determination of pre-contact distance are too taxing for a VR application. Should this computation load be too great, it can be greatly reduced by implementing a slight variation of the control algorithm designated as DECAFF-B (Binary feed forward). In the DECAFF-B modification, continuous analog feed-forward pre-contact distance data is replaced by a pre-contact condition that is represented in a binary format. This format of pre-contact condition uses information readily available from a bounding box collision detection routine commonly implemented in virtual reality codes. The bounding box for this implementation is attached to the outer surface of the virtual finger adjacent to the distal pad of the fingertip as shown in figure 5.1. The distance from the virtual finger to the outer surface of the bounding box is defined as a constant α^* (eg. $\alpha^* = 10$ degrees) as shown in figure 5.2.

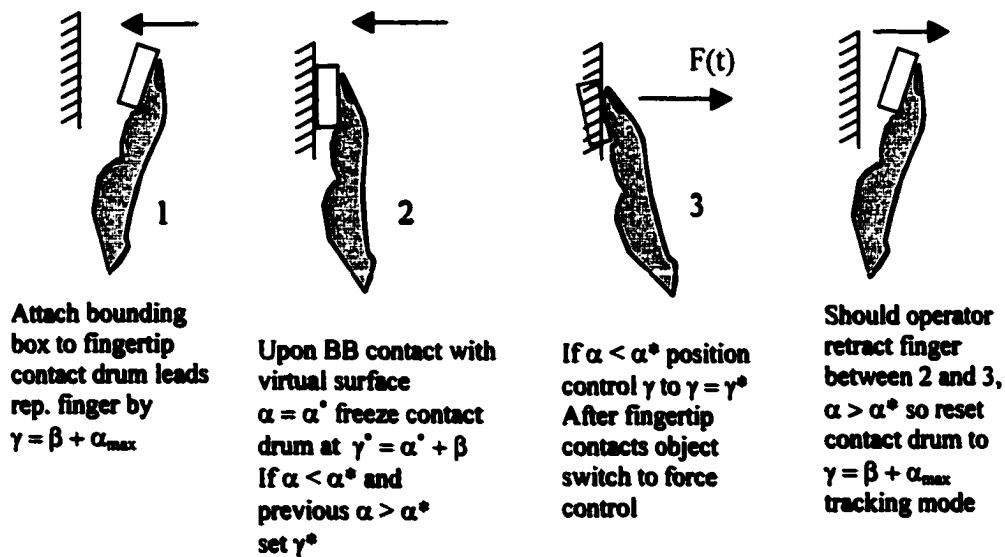


Figure 5.1 Bounding Box Concept for DECAFF-B (Binary Feed Forward)

The virtual reality computer then need only send to the haptic controller as pre-contact close proximity information a code indicating whether there is an object inside the bounding box or not. If there is no object inside the bounding box, the contact drum of the haptic interface is controlled to offset track the position of the replicated finger by a maximum value of α_{\max} (eg. $\alpha_{\max} = 50$ degrees), and a pre-contact condition of 0 is assigned to α . In this case the contact drum is commanded to maintain a position of:

$$\gamma = \beta + \alpha_{\max} \quad [5.1]$$

If the virtual finger approaches an object in the virtual space, such that the object interferes with the bounding box, the haptic control PC defines a fixed contact drum position:

$$\gamma^* = \beta + \alpha^* \quad [5.2]$$

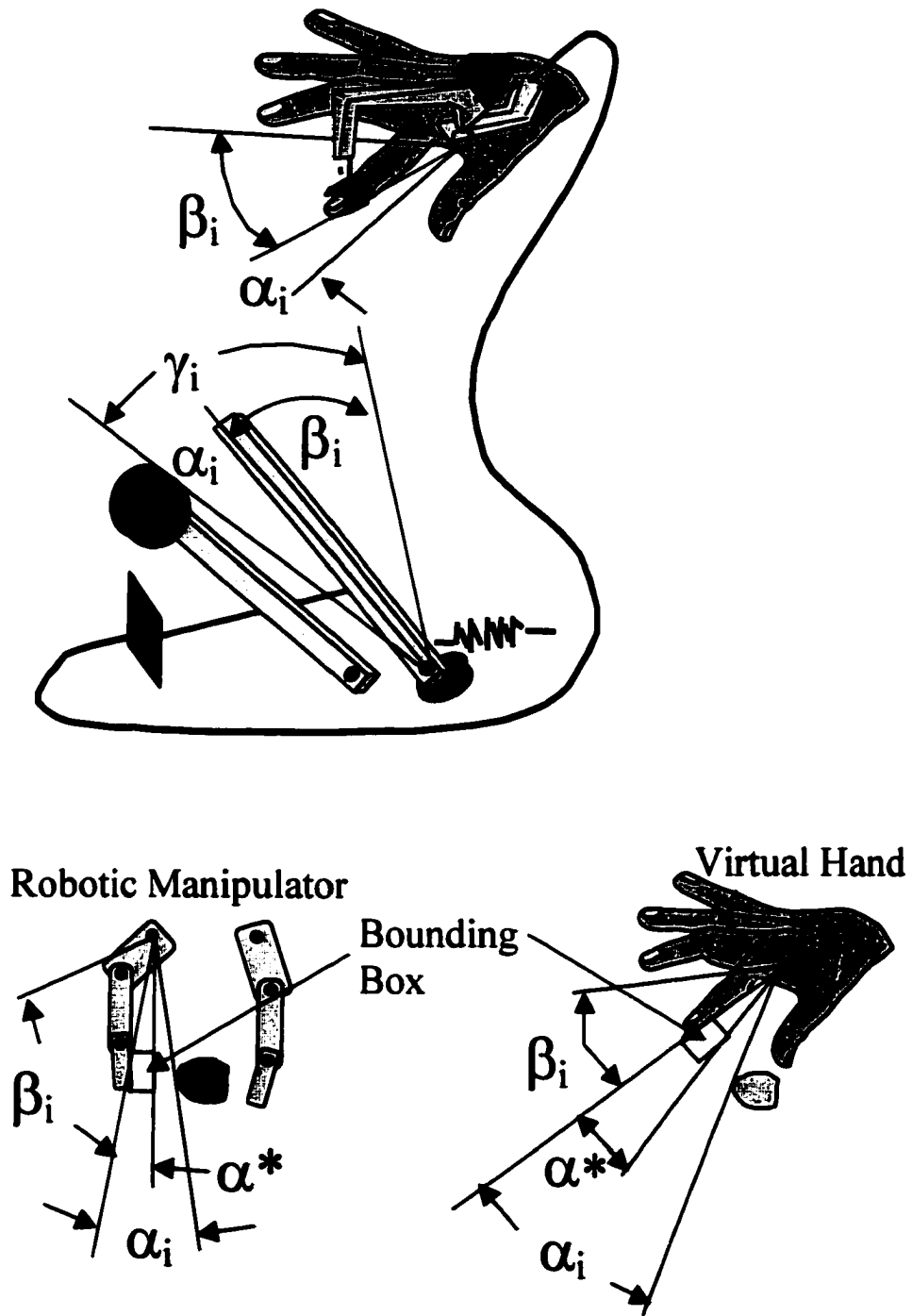


Figure 5.2 Control with Bounding Box by DECAFF-B

The contact drum position γ^* is defined when the bounding box makes contact with an object and the pre-contact condition changes from $\alpha = 0$ to $\alpha = 1$. The contact drum remains at γ^* as long as the object remains in the box and the force is at the 0% or 100% magnitude level (i.e. $\alpha = 1$). Should the object be removed from the box due to virtual finger motion away from the object, or object motion away from the virtual finger, the pre-contact condition changes from $\alpha = 1$ to $\alpha = 0$ and the contact drum returns to position control of EQ. [5.1]. Should the virtual finger position change so as to contact an object in the virtual space, the control of the haptic PC switches to force control mode and provides a variable magnitude force to the operator as commanded by the virtual reality computer (e.g. $F = Kx + Bx'$). In this case as with the DECAFF-A (Analog feed forward) control algorithm described in chapter 3, the force control can be implemented by a PWM algorithm. Similarly the conditions of switching to force control are repeated as:

$$\text{Force Control} \quad \text{if} \quad 0\% < F < 100\% \quad [5.3]$$

$$\text{Position Control} \quad \text{if} \quad F = 100\% \quad \text{OR} \quad F = 0\% \quad [5.4]$$

By EQ. [5.4] position control is maintained for contact with surfaces of high stiffness such that the force (F) makes a step response from 0% to 100% at the first sampling cycle that indicates contact. This implementation takes full advantage of the benefits afforded by the DECAFF-A method for haptic display of rigid surfaces with the exception of a somewhat lower positional accuracy. While the positional accuracy of DECAFF-B is lower than that of DECAFF-A, the accuracy still exceeds that offered by

traditional control methods employed in haptic display for a given surface model and system bandwidth. The reduced accuracy of the DECAFF-B as compared with the DECAFF-A is a result of discrete time sampling of the pre-contact condition of intersection between a slave object and the bounding box. For a finger velocity of β' , the maximum contact drum positional error is achieved when a bounding box and slave object intersection occurs immediately following a slave intersection sample. Then the maximum contact drum error (δ) is given by the product of the finger velocity and the sample period (T):

$$\delta = \beta' * T \quad [5.5]$$

since $\beta' = d\beta/dt$ [5.6]

and $\delta = d\beta$ [5.7]

and $T = dt$ [5.8]

It should be noted that while the above described sampling position error exists, all delay errors that would result (in traditional design haptic interfaces) due to actuator response and force calculations are eliminated. If desired, the magnitude of the maximum positional error can be reduced by accounting for the error in the determination of contact drum position. The reduced error formulation is given by a modification of EQ. [5.2] as:

$$\gamma^* = \beta + \alpha^* - (\beta' * T)/2 \quad [5.9]$$

Where the maximum positional error magnitude of the contact drum controlled by EQ. [5.9] is one half that possible with contact drum control by EQ. [5.2].

A similar simplified algorithm can be effective for reduced sensor requirements in the tele-operation application domain as shown in figure 5.2. Here the distance sensor implemented need only measure whether or not an object is within a preset distance from the robotic finger (indicated by the bounding box in figure 5.2). If there is an object present within the prescribed proximity distance, the haptic interface contact drum is controlled to maintain a position defined by γ^* . Similar to the VR implementation, γ^* is defined by the sum of the position of the replicated finger (β) at the time the robotic sensor changed from a non-contact to a contact condition and a preset sensor range distance (e.g. $\alpha^* = 10$ degrees). If the robotic sensor senses no object, the contact drum traces the replicated finger motion, offset by α_{\max} (eg. $\alpha_{\max} = 50$ degrees). If the robotic finger is in contact with an object, the haptic interface is commanded to provide a variable force signal to the operator, proportional to the force measured by the robotic finger force sensor. Using this system as the operator (when moving at a high rate of speed) initiates a grasp motion, experiences a restriction to continued finger retraction until such a time when the robotic finger would actually be in contact with the grasped object. Thus, (subject to robot bandwidth limitations) human finger position can be used to directly control the robotic finger position, and robotic force sensor data can be directly used to control the reflected force magnitude. This can be done as described above using the DECAFF technology developed in this research, and permit real time simplified tele-robotic control, without system imposed

velocity constraints, and without extreme forces of contact at the robotic finger (due to system time lags in robotic finger tracking of the human finger). Sensors used for this simplified implementation need not present pre-contact *distance* to the haptic controller PC, but rather need only provide an on/off *binary* signal indicating whether or not the robotic finger is in close proximity to an object in the slave environment. Because of the need only to communicate a binary condition, an appropriate sensor could be realized physically by a system of inexpensive whisker switches or proximity sensors.

5.2.2 Application of DECAFF to General Haptic Interface Design

Although the DECAFF design and control method presented in this research has been implemented on a unilateral single DOF per finger grasping system, the significant improvements in human haptic performance demonstrated here are directly applicable to general haptic interface design and control. The results shown in this research would likely be repeated by implementation of the DECAFF paradigm in other haptic interface configurations (e.g. joystick type haptic interfaces). While the complete design of other types of haptic interfaces utilizing the DECAFF technology is beyond the scope of this report, conceptual designs of prismatic and revolute joints necessary for such implementations of the technology are presented in this section. Having general revolute and prismatic joint designs that apply the DECAFF technology in a bilateral manner provides a solid basis for future designs utilizing the DECAFF methods. For VR applications, three dimensional pre-contact information can be provided by a bounding cube or sphere using the DECAFF-B control described above, while for robotic applications multiple distance sensors would be employed.

A prismatic joint implementation can be achieved (for example in a Cartesian coordinate system device) as shown in figure 5.3. In this figure, a replicated pointer (analogous to the replicated finger) traces the motion of the operator's hand. The position (along the x direction) is measured by the position measurement potentiometer, via a cable (shown in dotted lines) fixed to the replicated pointer and routed between two pulleys. The motor drive uses a similar pulley arrangement with a second cable (shown in phantom lines) that freely passes through holes (not shown) in the replicated pointer. Fixed to the motor drive cable are left and right contact stops (analogous to the contact drum) that may selectively assume a position of contact or non-contact with the replicated pointer. From the figure it should be apparent that contact stops can be controlled by a pre-contact position control switching to force control algorithm, just as has been described for the grasping device implementation of the present device. For bi-directional control, two stops are shown, thus permitting a controlled choice for which stop to use (left or right), depending upon the direction of the velocity (dx/dt) of the pointer. The left contact stop B is used when motion is toward the left and dx/dt is less than zero. Then the position of the motor drive is controlled by G_x such that:

$$G_x = B_x - dx_B - d \quad \text{for } B_x' < 0 \quad [5.10]$$

and $G_x = B_x + dx_A + d - D_x \quad \text{for } B_x' > 0 \quad [5.11]$

Where G_x is analogous to γ_i , B_x is analogous to β_i , dx_B is analogous to α_i , while d and D_x are geometric constants as depicted in FIG. 5.3. Because dx_B and dx_A are analogous to α_i they are controlled in a similar manner to assume either a maximum value for

offset tracking when no object is within the bounding entity or a bounding magnitude when remote objects enter the bounding volume for DECAFF-B (binary) control. Alternatively for DECAFF-A (analog) implementation, dx_B and dx_A contain instantaneous pre-contact distances each in the appropriate direction, depending on velocity direction of the pointer. This type of implementation shown for the x-axis could obviously be repeated for the y and z axes in 3-D space, and simply represents another application of the fundamental technology developed and demonstrated in this research. For a three prismatic joint system (3P), the pre-contact conditions (dx_A , dy_A , dz_A) or (dx_B , dy_B , dz_B) could be represented by a bounding cube of dimensions ($2dx$, $2dy$, $2dz$) or by a bounding sphere of radius $r = [dx^2 + dy^2 + dz^2]^{0.5}$.

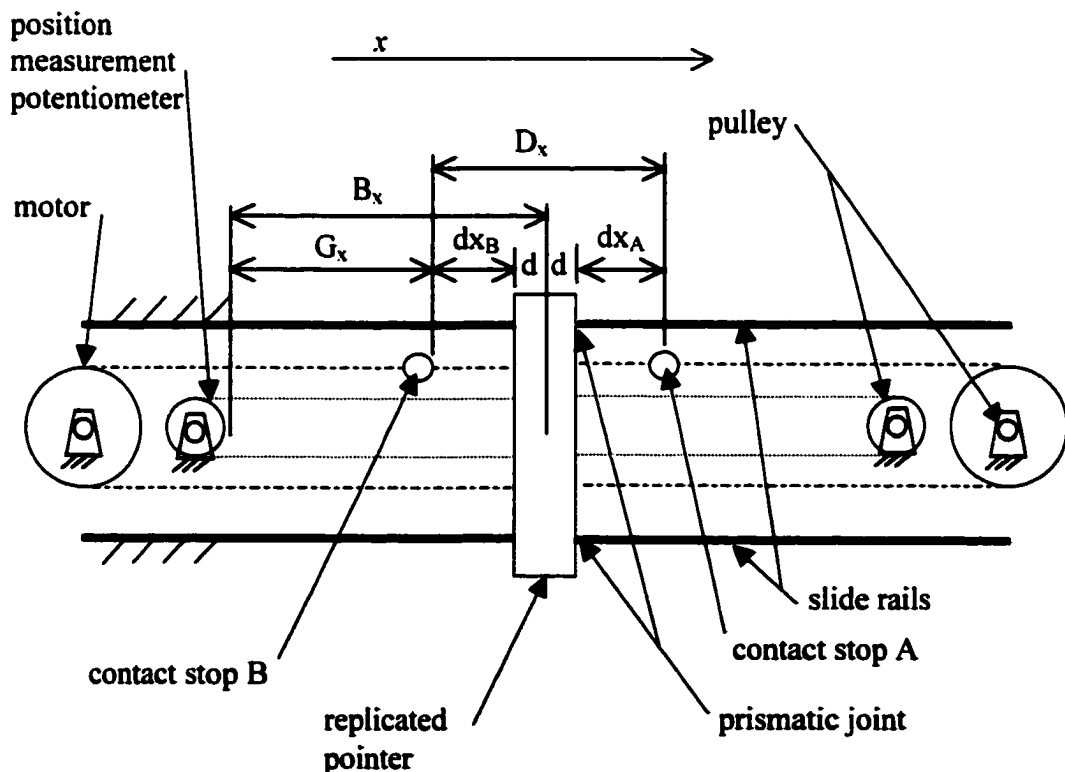


Figure 5.3 – Conceptual Design of Prismatic Joint with DECAFF Technology

Similar to the prismatic joint, a concept design for a bilateral revolute joint for use in haptic interfaces that utilize the DECAFF technology is given in FIG. 5.4. In this figure the active link is given a resistance to motion by the contact disc, via interference between the link and one of the contact drums. Contact drum A is used for resistance to counter-clockwise motion, while contact drum B is used to provide resistance to clockwise motion. The active link is fixed to the shaft, while the contact disc is constructed to freely rotate about the shaft, resulting in selective contact between the motor driven contact disc and the active link.

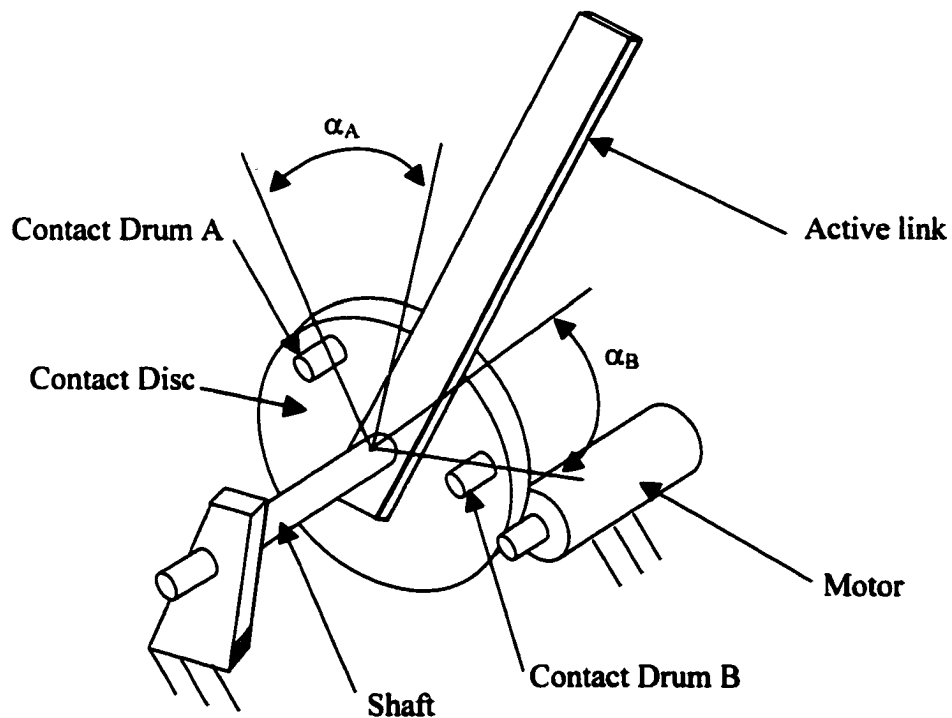


Figure 5.4 – Conceptual Design of Revolute Joint with DECAFF Technology

The angular position of the active link is measured by shaft rotation, while the contact disc position is measured independently, (because it freely rotates about the shaft). Both the motor and the shaft bearing are fixed to the ground or adjacent proximal link, as indicated in the schematic. Control variables α_A and α_B are used to indicate pre-contact conditions for CCW and CW rotation, respectively. As can best be seen in figure 5.5, the control of the bilateral contact disc is accomplished in a manner similar to that of the unilateral rotation of the implemented replicated finger discussed in chapter 3. In the general revolute joint, the link angular position is defined as β . The geometric constant angular distance between the two contact drums A and B is defined as θ , and the angular (constant) difference between the active link defining position and the line of contact between the contact drums is denoted as δ .

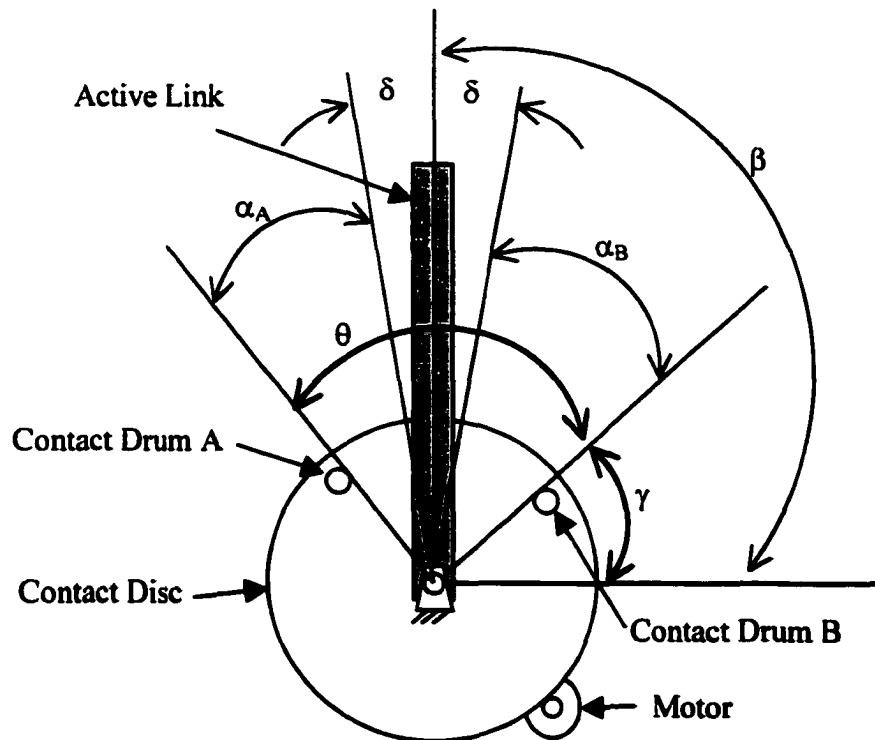


Figure 5.5 – Control of Revolute Joint with DECAFF Technology

Similar to the contact drum of the finger mechanism described in chapter 3, the contact disc is position controlled by angular position γ such that:

$$\gamma = \beta + \delta + \alpha_A - \theta \quad \text{For } \beta' > 0 \quad [5.12]$$

$$\text{Or} \quad \gamma = \beta - \delta - \alpha_B \quad \text{For } \beta' < 0 \quad [5.13]$$

Where EQ. [5.12] is used for counter clockwise motion and $\beta' > 0$ and EQ. [5.13] is used for clockwise motion when $\beta' < 0$. When operating under analog DECAFF-A control the pre-contact angle α_A and α_B are calculated by either solution of the inverse kinematics of the haptic interface (given $x + dx, y + dy, z + dz$; find α), or by evaluation of the expressions for $(x + dx, y + dy, z + dz)$. Where (x, y, z) are the coordinates of the slave and (dx, dy, dz) represent the slave pre-contact distances along the x, y, and z directions.

As an illustrative example, we shall consider a three revolute joint (RRR) haptic interface, similar to the Phantom (Massie and Salisbury, 1994). The example interface has the kinematic structure given in FIG. 5.6. For the example design β_2 is calculated from the measured joint angle β_{2M} by:

$$\beta_2 = 360^\circ - \beta_{2M} + \beta_1 \quad [5.14]$$

Then the forward kinematics of the three DOF system are given by:

$$z = r_1 \sin \beta_1 + r_2 \sin \beta_2 \quad [5.15]$$

$$y = (r_1 \cos \beta_1 + r_2 \cos \beta_2) \sin \beta_3 \quad [5.16]$$

$$x = (r_1 \cos \beta_1 + r_2 \cos \beta_2) \cos \beta_3 \quad [5.17]$$

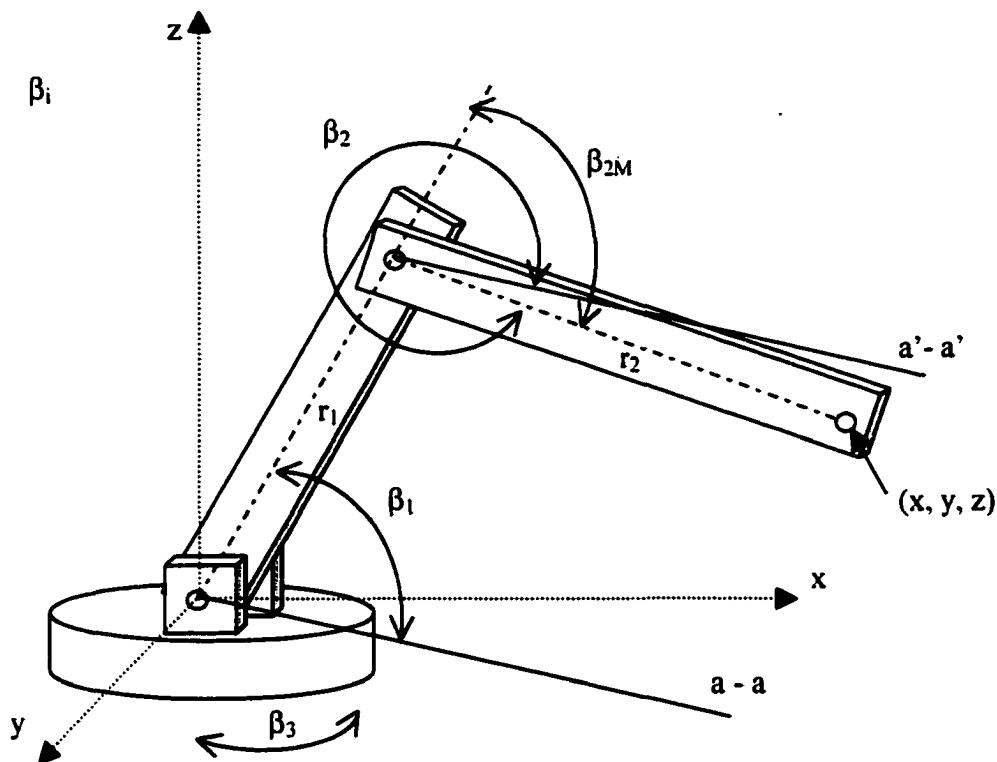


Figure 5.6 – Example RRR Design Haptic Interface Schematic

Then in order to determine the pre-contact angles α_{Ai} and α_{Bi} for each joint ($i = 1, 2, 3$), we are presented with a problem statement of:

Given: $x, y, z, dx, dy, dz, \beta_1, \beta_2, \beta_3, \beta_1', \beta_2', \beta_3'$

Find: α_{A1} or α_{B1}, α_{A2} or α_{B2}, α_{A3} or α_{B3}

First we can determine whether we need to find α_{Ai} or α_{Bi} , based on the sign of the most recent β_i , and γ_i will be determined as the contact disc control variable by EQS. [5.12-5.13] as discussed earlier. Then the solution for α_{Ai} or α_{Bi} is as follows. Considering the slave object edge position as having coordinates of $(x + dx, y + dy, z + dz)$, we can describe each coordinate by:

$$z + dz = r_1 \sin(\beta_1 + \alpha_1) + r_2 \sin(\beta_2 + \alpha_2) \quad [5.18]$$

$$y + dy = (r_1 \cos(\beta_1 + \alpha_1) + r_2 \cos(\beta_2 + \alpha_2)) \sin(\beta_3 + \alpha_3) \quad [5.19]$$

$$x + dx = (r_1 \cos(\beta_1 + \alpha_1) + r_2 \cos(\beta_2 + \alpha_2)) \cos(\beta_3 + \alpha_3) \quad [5.20]$$

EQ. [5.18] expands to:

$$\begin{aligned} z + dz = r_1 [(\sin \beta_1)(\cos \alpha_1) + (\cos \beta_1)(\sin \alpha_1)] \\ + r_2 [(\sin \beta_2)(\cos \alpha_2) + (\cos \beta_2)(\sin \alpha_2)] \end{aligned} \quad [5.21]$$

Because dx , dy , and dz are small displacements, α_1 , α_2 , and α_3 are small angles, thus it is reasonable to assume $\cos \alpha \cong 1$ and $\sin \alpha \cong \alpha$ (in radians), (see Paul, 1983). Making this substitution we arrive at:

$$z + dz = r_1 (\sin \beta_1) + r_2 (\sin \beta_2) + \alpha_1 r_1 (\cos \beta_1) + \alpha_2 r_2 (\cos \beta_2) \quad [5.22]$$

From which we can subtract z from the left side and the expression for z from the right side resulting in:

$$dz = \alpha_1 r_1 (\cos \beta_1) + \alpha_2 r_2 (\cos \beta_2) \quad [5.23]$$

Which can be rearranged as:

$$\alpha_1 = [dz - \alpha_2 r_2 (\cos \beta_2)] / [r_1 (\cos \beta_1)] \quad [5.24]$$

Dividing EQ. [5.19] by EQ. [5.20] we arrive at:

$$[(y + dy) / (x + dx)] = [\sin (\beta_3 + \alpha_3)] / [\cos (\beta_3 + \alpha_3)] \quad [5.25]$$

That can be routinely solved for:

$$\alpha_3 = \tan^{-1} [(y + dy) / (x + dx)] - \beta_3 \quad [5.26]$$

Expanding EQ. [5.20] we have:

$$\begin{aligned} x + dx &= [(r_1 \cos \beta_1) \cos \alpha_1 - (r_1 \sin \beta_1) \sin \alpha_1] \cos(\beta_3 + \alpha_3) \\ &+ [r_2(\cos\beta_2) \cos \alpha_2 - r_2(\sin\beta_2) \sin \alpha_2] \cos(\beta_3 + \alpha_3) \quad [5.27] \end{aligned}$$

Again making the substitution of $\cos \alpha \cong 1$ and $\sin \alpha \cong \alpha$, we have:

$$\begin{aligned} x + dx &= [(r_1 \cos \beta_1) - (r_1 \sin \beta_1)\alpha_1] \cos(\beta_3 + \alpha_3) \\ &+ [r_2(\cos\beta_2) - r_2(\sin\beta_2) \alpha_2] \cos(\beta_3 + \alpha_3) \quad [5.28] \end{aligned}$$

Which can be rearranged to:

$$\alpha_1 = [-1 / (r_1 \sin \beta_1)] \{ [(x + dx) / (\cos(\beta_3 + \alpha_3))] \}$$

$$- [(r_1 \cos \beta_1) + r_2(\cos\beta_2)] - [r_2(\sin\beta_2) \alpha_2] \} \quad [5.29]$$

Equating EQ. [5.24] and EQ. [5.29] we can solve for:

$$\alpha_2 = \{ [-(r_1 \cos \beta_1)(x + dx)] / [\cos(\beta_3 + \alpha_3)] \\ + [(r_1 \cos \beta_1) + r_2(\cos\beta_2)] (r_1 \cos \beta_1) - [dz (r_1(\sin\beta_1))] \} / \\ \{ r_2(\sin\beta_2) \quad (r_1 \cos \beta_1) - r_2(\cos\beta_2) (r_1 \sin \beta_1) \} \quad [5.30]$$

From which we can then sequentially solve EQ. [5.26] for α_3 then solve EQ. [5.30] for α_2 and then solve EQ. [5.24] for α_1 to arrive at all pre-contact angles α_i . Though EQS. [5.26], [5.30], and [5.24] may appear to be computationally expensive due to the large number of sine and cosine function calls, many of these values are required for the forward kinematics solution and thus need only be calculated once.

Because the control algorithms for both the prismatic and revolute joints call for a control switching methodology, it would also be possible to implement a motor brake (together with the motor), thus permitting extremely high forces of contact with rigid surfaces. The use of a brake would allow for the very high rigid surface contact forces, without adding a risk to the operator (in the event of component failure) as would be present if higher torque motors were implemented to achieve the same result. Brakes can be controlled to engage only under pre-contact conditions described by EQS. [5.10] – [5.13] and such that for example: $G_x = G_x^* = B_x - dx_B^* - d$ and $\gamma = \gamma^* = \beta - \delta - \alpha_B$. For which the error can be controlled by engaging the brake(s) only when both the

above conditions of close proximity pre-contact freeze and the condition of positional error is less than a predetermined amount ϵ . The second condition can be stated as:

$$G_x(t) - G_x(t - 1) < \epsilon$$

or
$$\gamma(t) - \gamma(t - 1) < \epsilon \quad [5.30]$$

5.3 Contributions of the Research

In the interface described thus far, there are several areas of contribution to the field of haptic interface research and design. A most striking contribution area is the introduction of a de-coupled actuator paradigm for increased response speed for grasp tasks and increased stability, especially in representing initial contact with high stiffness real or virtual objects. A method has been proposed that theoretically eliminates the time delay in force presentation associated with human controlled master-slave haptic interface systems. By doing so, slave finger positions can be more precisely controlled, without delivering excessive forces, even during rapid human controlled motion, thus improving existing tele-robotic systems. For VR applications, the proposed systems contributes for the first time in the literature a method to accurately represent rigid body contact, without penetrating the body of interest, this being accomplished in “real time”, that exceeds operator sensory processing speed. While the system was implemented and tested for a unilateral motion, single degree of freedom system for finger grasp forces, in this chapter general joint designs for bilateral

position and force control have been introduced. With the general joint designs, many haptic interface designs utilizing the DECAFF technology can be developed. The DECAFF system also is capable of operating under a more position precise analog mode, or when computation limitations dictate, a faster binary pre-contact condition mode.

In the area of finger force display haptic interface research, the design of the present research provides a solution that may surpass prior approaches in the areas of: (i) the ability to precisely control slave finger contact position, (ii) range of finger motion represented, (iii) weight of mechanism carried by the operator, (iv) maximum force that can be applied, and (v) apparent control bandwidth. The present research introduces for the first time in the literature an approach that employs remote location of both position sensors and haptic display actuators and represents each finger by a single DOF, resulting in an extremely lightweight hand attachment mechanism. In the portable interface area, this research presents an approach that provides a force display to the fingertips in a direction that is substantially normal to the distal finger pad throughout a complete range of finger motion from 0 to 180 degrees. This is a feature that is lacking in all prior haptic interface research of the proposed single degree of freedom/finger platform (Jones, Iwata, RM I, RM II), with the exception of the CyberGrasp commercial haptic interface, which has been developed concurrent with the present research.

5.4 Conclusions

In this paper the previous approaches to haptic interfaces for tele-manipulation and virtual reality systems have been reviewed. Several fundamental limitations that exist in prior force-reflecting haptic interface designs that call for an actuator that is directly physically coupled to the operator during use were identified. Some limitations associated with direct coupled actuators include a requirement for interference between the virtual pointer and virtual objects prior to force display, and actuator response time and computation time requirements are too great to permit simulation of initial contact with slave objects to appear as real time haptic sensations. Because of the above limitations, instability often results when attempts to simulate contact with rigid surfaces are implemented. For robotic applications the result of direct-coupled actuators in haptic display interfaces is that the haptic system must operate at a lower speed and thus natural real time tele-manipulation control is not achieved.

To address the fundamental issues in the design of haptic interfaces, mathematical models of the dynamics of contact were developed and simulations of the equations of motion were used to predict force time response characteristics of real human-object contact and that provided by haptic simulations. From the mathematical modeling it was shown that one method to overcome the limitations present under the traditional haptic interface design paradigm, was to design a haptic interface that could present a position controlled surface prior to and during initial contact.

A new general design paradigm for haptic interfaces was proposed that utilized a decoupled actuator and a feed-forward control algorithm to overcome the limitations set forth by the traditional design methods. The new design method incorporates within the haptic interface a mechanical and control system that can present a position controlled surface that assumes a position with respect to the human master coordinate frame consistent with the slave pointer coordinate frame prior to contact. A detailed design of one embodiment of the proposed haptic interface design paradigm was developed, and a prototype constructed for representation of finger bend motion utilized in human grasping tasks. The prototype design provides additional contributions to the grasp task area of haptic interface research including remote position sensing and actuation and a full 180° range of motion for the finger with a single DOF representation of motion. The prototype also demonstrates a force substantially normal to the fingertip at any fingertip position and a simple design with a large workspace that is lightweight, has low inertia and provides a high degree of transparency. The prototype system was constructed for representation of one finger motion and a complete virtual slave application test bed software package was implemented.

The test bed software and prototype system was used to perform human subject perception experiments designed to determine the effectiveness of the proposed approach as compared with the traditional design and control paradigm for force-reflecting haptic interfaces. The experiments included investigation into the subjects' perception of simulation surfaces, the ability to discriminate the initial contact position of simulated surfaces, and the stability of simulations. A factorial design for the

experimentation permitted statistical significance determination of the effects of surface variables on the relative effectiveness of the proposed approach. The proposed method was shown to reduce the dependence on surface model variables (such as stiffness, damping, and control execution speed) present in traditionally designed haptic interfaces, on the ability to accurately identify surface location in a stable manner. The results of the experimentation included a 99.9% confidence that the proposed system provides improved position discrimination and stability compared with the traditional design paradigm of direct-coupled actuation and post contact force reflection. In the subjective perception of rigid surfaces, the proposed de-coupled actuator and feed forward control system was chosen as that which felt more like a real surface in 92% of the trials.

Finally, the novel concepts of the proposed haptic interface design and control method were expanded from the detailed prototype design for finger bend representation to application to other classes of haptic interface design. The general method of DECAFF design was suggested for prismatic and revolute joints with representative examples of haptic interface system designs and control methods applicable to general three dimensional point representations.

References

1. Adelstein, B., Ho, P., Kazerooni, H., 1996, Kinematic Design of a Three Degree of Freedom Parallel Hand Controller Mechanism, *Proceedings of the 1996 ASME International Mechanical Engineering Congress and Exposition*, DSC-Vol. 58, ASME, New York, NY, pp. 539-546.
2. Ascension Company web page <http://www.ascension-tech.com/>
3. Bausell, R. B., 1986, A Practical Guide to Conducting Empirical Research, Harper & Rowe Publishers, Inc., New York, NY, pp. 46-51.
4. Berkelman, P., Butler, Z., Hollis, R., 1996, Design of a Hemispherical Magnetic Levitation Haptic Interface Device, *Proceedings of the 1996 ASME International Mechanical Engineering Congress and Exposition*, DSC-Vol. 58, ASME, New York, NY, pp. 483-488.
5. Brooks, F., Ouh-Young, M., Batter, J., Jerome, A., 1990, Project GROPE - Haptic Display for Scientific Visualization, *Computer Graphics*, Vol. 24, No. 4, pp. 177-185.
6. Burdea, G., 1996, Force and Touch Feedback for Virtual Reality, John Wiley and Sons, New York, NY, pp. 126-129.
7. Burdea, see ref. 5, pp. 161-165.
8. Burdea, see ref. 5, Zarudiansky pp. 7-9, Hashimoto pp. 94-95.

9. Burdea, see ref. 5, pp. 120-124, 259
10. Buttolo, P., Hannaford, B., 1995, Advantages of Actuator Redundancy for the Design of Haptic Displays, *Proceedings of Virtual Reality Annual International Symposium '95*, IEEE Computer Society Press, Los Alamitos, CA, pp. 623-630.
11. Chen, E., Marcus, B., 1994, EXOS Slip Display Research and Development, *Proceedings of the 1994 ASME Winter Annual Meeting*, DSC-Vol. 49, ASME, New York, NY, pp. 265-270.
12. Chu, P., Dani, T., Gadh, R., 1997, Multisensory Interface for a Virtual Reality Based Computer Aided Design System, *CAD Journal*, accepted May 1997.
13. Colgate, J., Grafing, P., Stanley, C., and Schenkel, G., 1993, Implementation of Stiff Virtual Walls in Force Reflecting Interfaces, *Proceedings of Virtual Reality Annual International Symposium*, IEEE Neural Networks Council, Piscataway, NJ, pp. 202-215.
14. Cutkosky, M. and Howe, R., 1990, "Human Grasp Choice and Robotic Grasp Analysis" in S. Venkataraman and T. Iberall Editors, *Dextrous Robotic Hands*, Springer Verlag, New York, pp. 5-31.
15. CyberTouch Product Literature, 1996, Virtual Technologies, Inc.
16. Dani, T. , Gadh, R., 1997, Creation of Concept Shape Designs via a Virtual Reality Interface, *CAD Journal, Special Issue on VR for Design*, 29 (7), July 1997.

17. DeVor, Chang, and Sutherland, 1992, *Statistical Quality Design and Control*, Macmillian Publishing Company, New York, N. Y., pp 542-605.
18. Ellis, R., Ismaell, O., Liosett, M., 1993, Design and Evaluation of a High Performance Prototype Planar Haptic Interface, *Proceedings of the 1993 ASME Winter Annual Meeting*, DSC-Vol. 49, ASME, New York, NY, pp. 56-64.
19. Ellis, R., Sarkar, N., Jenkins, M., 1997, Numerical Methods of the Force Reflection of Contact, *Transactions of the ASME, Journal of Dynamic Systems, Measurement, and Control*, Vol. 119, pp. 768-774.
20. Ephanov, A., Hurmuzlu, Y., 1996, Implementation of Sensory Feedback and Trajectory Tracking in Active Telemanipulation Systems, *Proceedings of the 1996 ASME International Mechanical Engineering Congress and Exposition*, DSC-Vol. 58, ASME, New York, NY, pp. 503-514.
21. Fifth Dimension web page, <http://www.5dt.com>
22. Franklin, R. D., Allison, D. B., and Gorman, B. S., 1996, Design and Analysis of Single Case Research, Lawrence Erlbaum Associates, Mahwah, NJ, pp. 337-344.
23. Gomez, D. Burdea, G., Lagrana, N., 1995, Integration of the Rutgers Master II in a Virtual Reality Simulation, *Proceedings of Virtual Reality Annual International Symposium '95*, IEEE Computer Society Press, Los Alamitos, CA, pp. 198-202.

24. Hasser, C., 1995, Force Reflecting Anthropomorphic Handmaster Requirements, *Proceedings of the 1995 ASME International Mechanical Engineering Congress and Exposition*, DSC-Vol. 57-2, ASME, New York, NY, pp. 663-674.
25. Hajian, A., and Howe, R., 1994, Identification of the Mechanical Impedance of Human Fingers, *Proceedings of the 1994 ASME Winter Annual Meeting*, DSC-Vol. 55-1, ASME, New York, NY, pp. 319-327.
26. Holman, J. P., 1984, *Experimental Methods for Engineers*, McGraw-Hill, New York, N.Y., pp. 88-89.
27. Howe, R., and Lederman, S., 1996, Introduction to Haptic Interfaces for Virtual Environment and Teleoperator Systems, *Proceedings of the 1996 ASME International Mechanical Engineering Congress and Exposition*, DSC-Vol. 58, ASME, New York, NY, pp. 395.
28. I-CARVE Laboratory home page, <http://icarve.wisc.edu>
29. Ishii, M., Sato, M., 1994, Force Sensations in Pick and Place Tasks, *Proceedings of the 1994 ASME Winter Annual Meeting*, DSC-Vol. 55-1, ASME, New York, NY, pp. 339-344.
30. Iwata, H., Nakagawa, T., Nakashima, T., 1992, Force Display for Presentation of Rigidity of Virtual Objects, *Journal of Robotics and Mechatronics*, Vol.24, No. 1 pp. 39-42.

31. Iwata, H., 1993, Pen-based Haptic Virtual Environment, *Proceedings of Virtual Reality Annual International Symposium*, IEEE Neural Networks Council, Piscataway, NJ, pp. 287-292.
32. Jones, L., Thousand, J., 1966, Servo Controlled Manipulator Device, U. S. Patent No. 3,263,824, USPO.
33. Karson, S., Srinivasan, M., 1995, Passive Human Grasp Control of an Active Instrumented Object, *Proceedings of the 1995 ASME International Mechanical Engineering Congress and Exposition*, DSC-Vol. 57-2, ASME, New York, NY, pp. 641-647.
34. Kazerooni, H., 1993, Human Induced Instability in Haptic Interfaces, *Proceedings of the 1994 ASME Winter Annual Meeting*, DSC-Vol. 49, pp 15-27.
35. Kelley, A., Salcudean, S., 1994, On the Development of a Force-Feedback Mouse and Its Integration into a Graphical User Interface, *Proceedings of the 1994 ASME Winter Annual Meeting*, DSC-Vol. 49, ASME, New York, NY, pp. 287-294.
36. Klatzky, R., Purdy, K., and Lederman, S., 1996, When is Vision Useful During a Familiar Manipulatory Task ?, *Proceedings of the 1996 ASME International Mechanical Engineering Congress and Exposition*, DSC-Vol. 58, ASME, New York, NY, pp. 561-566.

37. Kontarinis, A., Howe, R., 1993, Tactile Display of Contact Shape in Dexterous Telemanipulation, *Proceedings of the 1993 ASME Winter Annual Meeting*, DSC-Vol. 49, ASME, New York, NY, pp. 81-88.
38. Kramer, J., 1993, Force Feedback and Textures Simulating Interface Device, U. S. Patent No. 5,184,319, USPO.
39. Kramer, J., 1997 personal communication, November ICEME of ASME, haptics demonstration in poster session.
40. Lawrence, D, Salada, M., Lucy, P., and Dougherty, A., 1996, Quantitative Experimental Analysis of Transparency and Stability in Haptic Interfaces, *Proceedings of the 1996 ASME International Mechanical Engineering Congress and Exposition*, DSC-Vol. 58, ASME, New York, NY, pp. 441-449.
41. Li, Y., 1996, A Sensor Based Robot Transition Control Strategy, *International Journal of Robotics Research*, Vol. 15, No., 2, April 1996, pp. 128-136.
42. Love, L., and Book, W., 1995, Contact Stability Analysis of Virtual Walls, *Proceedings of the 1995 ASME International Mechanical Engineering Congress and Exposition*, DSC-Vol. 57-2, ASME, New York, NY, pp. 689-694.
43. Luecke, G., Chai, Y., Winkler, J., Edwards, J., 1996, An Arm Exoskeleton Manipulator for Application of Electro-magnetic Virtual Forces, *Proceedings of the 1996 ASME International Mechanical Engineering Congress and Exposition*, DSC-Vol. 58, ASME, New York, NY, pp. 489-494.

44. Massie, T., Salisbury, J., 1994, The Phantom Haptic Interface: A Device for Probing Virtual Objects, *Proceedings of the 1994 ASME Winter Annual Meeting*, DSC-Vol. 49, ASME, New York, NY, pp. 295-299.
45. Millman, P., Stanley, M., Colgate, J. 1993, Design of a High Performance Haptic Interface to Virtual Environments, *Proceedings of Virtual Reality Annual International Symposium*, IEEE Neural Networks Council, Piscataway, NJ, pp. 216-222.
46. Montgomery, D. C., 1991, Introduction to Statistical Quality Control, Second Edition, John Wiley & Sons, New York, NY, pp. 59-92, 501-512.
47. Norton, R., 1999, Design of Machinery, An Introduction to the Synthesis and Analysis of Mechanisms and Machines, Second Edn., McGraw-Hill, New York, NY, pp 500-512.
48. Paul, R. P., 1983, Robotic Manipulators: Mathematics, Programming and Control, MIT Press, Cambridge, MA, pp 85-118.
49. Polhemus web page, <http://www.polhemus.com>
50. Rosenberg, L. and Adelstein, B., 1993, Perceptual Decomposition of Virtual Haptic Surfaces, *Proceedings of IEEE 1993 Symposium on Research Frontiers in Virtual Reality*, San Jose, CA, pp 46-53.

51. Salcudean, S., Vlaar, T., 1994, On the Emulation of Stiff Walls and Static Friction with a Magnetically Levitated Input/Output Device, *Proceedings of the 1994 ASME Winter Annual Meeting*, DSC-Vol. 55-1, ASME, New York, NY, pp. 303-309.
52. Sato, K., Igarashi, E., Kimura, M., 1991, Development of Non-Constrained Arm with Tactile Feedback Device, *Proceedings of the International Conference of Advanced Robotics*, IEEE, New York, NY, pp. 334-338.
53. Schmult, B., Jebens, R., 1993, Application Areas for a Force Feedback Joystick, *Proceedings of the 1993 ASME Winter Annual Meeting*, DSC-Vol. 49, ASME, New York, NY, pp. 47-54.
54. Schulteis, T., Dupont, P., Millman, P., and Howe, R., 1996, Automatic Identification of Remote Environments, , *Proceedings of the 1996 ASME International Mechanical Engineering Congress and Exposition*, DSC-Vol. 58, ASME, New York, NY, pp. 451-458.
55. Shigley, J. E., Uicker, J. J., *Theory of Machines and Mechanisms*, 2nd Edn., McGraw-Hill, Inc., New York, NY, pp. 548-553.
56. Shimoga, K., 1993a, A Survey of Perceptual Feedback Issues in Dextrous Telemanipulation: Part I Finger Force Feedback, *Proceedings of Virtual Reality Annual International Symposium*, IEEE Neural Networks Council, Piscataway, NJ, pp. 263-270.

57. Shimoga, K., 1993b, A Survey of Perceptual Feedback Issues in Dextrous Telemanipulation: Part II Finger Touch Feedback, *Proceedings of Virtual Reality Annual International Symposium*, IEEE Neural Networks Council, Piscataway, NJ, pp. 271-279.
58. Shimoga, K., Murray, A., Khosla, P., 1996, A Touch Display System for Interaction with Remote and Virtual Environments, *Proceedings of the 1996 ASME International Mechanical Engineering Congress and Exposition*, DSC-Vol. 58, ASME, New York, NY, pp. 523-529.
59. Springer, S., Gadh, R., 1996, State-of-the-art Virtual Reality Hardware for Computer-aided-design, *Journal of Intelligent Manufacturing*, Volume 7, pages 457-465, December, 1996.
60. Springer, S., Gadh, R., 1997, Haptic Feedback for Virtual Reality Computer Aided Design, *Presented at the 1997 ASME International Mechanical Engineering Congress and Exposition*, November 1997, Dallas, TX, ASME, New York, NY.
61. Springer, S., 1998, Force Display Master Interface Device for Teleoperation, U. S. Patent Application, U. S. Patent and Trademark Office.
62. Springer, S., Ferrier, N., 1999, Design of a Multi-Finger Haptic Interface for Teleoperational Grasping, *Presented at the 1999 ASME International Mechanical Engineering Congress and Exposition*, November 1999, Nashville, TN, ASME, New York, NY.

63. Springer, S., Ferrier, N., 1999, A New Method for Design and Control of Haptic Interfaces for Display of Rigid Surfaces, *Presented at the 1999 ASME International Mechanical Engineering Congress and Exposition*, November 1999, Nashville, TN, ASME, New York, NY.
64. Springer, S., Ferrier, N., 2000, DECAFF: Experimental Study on Human Haptic Perception, *Submitted to the 2000 ASME International Mechanical Engineering Congress and Exposition*, November 2000, Orlando, FL, ASME, New York, NY.
(to appear)
65. Springer, S., Ferrier, N., 2000, Design and Control of a Force-Reflecting Haptic Interface for Teleoperational Grasping, *Submitted to the ASME Journal of Mechanical Design*, ASME, New York, NY. (to appear)
66. Srinivasan, M., Chen, J., 1993, Human Performance in Controlling Normal forces of Contact with Rigid Objects, *Proceedings of the 1993 ASME Winter Annual Meeting*, DSC-Vol. 49, ASME, New York, NY, pp. 179-125.
67. Stone 1991, Teletact , ARRC/Airmuscle Ltd., reported by Shimoga, K., 1993, *Proceedings of Virtual Reality Annual International Symposium*, IEEE Neural Networks Council, Piscataway, NJ, pp. 263-270.
68. Virtual Technologies, Inc., 1997, company web page <http://www.virtex.com>.
69. Wellman, P., Howe, R., 1995, Towards realistic Vibrotactile Display in Virtual Environments, *Proceedings of the 1995 ASME International Mechanical*

Engineering Congress and Exposition, DSC-Vol. 57-2, ASME, New York, NY, pp. 713-718.

70. Woodworth, R., 1938, *Experimental Psychology*, Henry Holt and Company, New York, NY, pp 455.